In-Plane Deformation of Kōwhaiwhai Auxetic Structure

MASSEY UNIVERSITY
TE KUNENGA KI PŪREHUROA
UNIVERSITY OF NEW ZEALAND

A thesis presented in partial fulfilment

of the requirements for the degree of

Masters

In

Food Technology

At Massey University, Palmerston North, Manawatū, Aotearoa New Zealand

Brayden T. Whitton

2025

Abstract

This thesis explores the development and characterisation of a novel kōwhaiwhai auxetic structure, providing bespoke mechanical functionality. Inspired by traditional Māori art and building on prior work, the research aims to characterise the geometric and mechanical properties of the kōwhaiwhai auxetic structure, with a focus on its Poisson's ratio, tensile behaviour, and performance under varying humidity conditions to be used as a foundation for future packaging solutions involving the auxetic. The research used a combination of experimental testing, finite element modelling, and statistical analysis to understand the auxetic structure. Tensile tests were conducted to determine the Poisson's ratio and stiffness, and FEM was used to simulate the tensile tests as a foundational model for understanding the Poisson's ratio, stiffness, and stress distribution. Uniaxial tensile tests of the structure showed the influence of measurement regions on the apparent Poisson's ratio of the structure and discussed the discrepancy with literature due to this. The trends described experimentally were shown numerically as well, showing the strength of the underlying model. Testing samples conditioned at high humidities showed a significant impact of relative humidity on the fibre-based material but the magnitude of this effect was not influenced by auxetic geometry on the material. Hinge thickness was the most significant parameter affecting stiffness of the kōwhaiwhai auxetic design. In the context of the effect of humidity on the material, this impact could be offset by a parameter change, showing the high tuneability of the auxetic. This research advances the understanding of auxetic materials properties as a foundation for packaging applications, demonstrating the kōwhaiwhai structure's potential for use in diverse environmental conditions. The findings provide a framework for optimising auxetic designs to enhance shock absorption and sustainability in the packaging industry.

Acknowledgements

Firstly, to the creator of this project, Maihi Potaka. His deep knowledge and skill around Māori art and culture helped me to build a connection with a different perspective of the project that was vital to its success.

I'd like to thank my head supervisor, Eli Gray-Stuart, who was able to reliably guide me towards my goals from my often jumbled mess of questions that I would load onto him each week.

To John Bronlund, whose curiosity, critical-thinking, and knowledge (including the often off-topic short-courses on what he discovered that week) has motivated me to be a greater engineer and person through both my bachelor's and master's degrees.

Next, I'd also like to thank the people at SCION who put up with me and made me feel very welcome throughout the year. In particular, my two supervisors Kate Parker and Kelly Wade. Kate, for her energy, technical knowledge, and leadership. To Kelly, for his deep practical knowledge of papermaking that I could lean into that helped greatly across the whole year.

The financial support from MBIE, Massey University, and Scion Research, which made this whole project possible, is greatly appreciated.

A special thanks to my Parents for their continued support and encouragement through my life to anything I set my mind to and shaping me into the person I am today. Lastly, to my amazing fiancée, Lateisha, who has continued to support me through my journey in research.

Table of Contents

List of Tables and Figures

Chapter 1: Overview

1.0: Introduction/Background

Auxetic structures have gained considerable attention in recent years due to their unique mechanical properties that set them apart from traditional materials. These structures exhibit a unique mechanical property that allows them to expand laterally when stretched axially and vice versa, rather than contracting laterally when stretched like most materials. This phenomenon is characterised by a negative Poisson's ratio, the ratio of transverse to longitudinal strain. Auxetics occur across multiple size scales, in engineered lattices at the macro level, or at the micro level in a foam. Auxetic behaviour has also been observed in the natural world, with examples in cat and cow skin (Lees et. al., 1991; Veronda & Westmann, 1970), and tendons (Gatt et. al., 2015).

Auxetic structures are comprised of various units connected by hinges at their vertices. When pulled in one direction, the collective motion of the rotating units induces the material to expand in the transverse direction. This property enables them to exhibit beneficial mechanical performance, such as fracture resistance and energy absorption, which make them attractive for a variety of engineering applications, including in the field of packaging. It has been shown that auxetic behaviour can be induced at multiple levels to tune or improve the performance of the material, examples being multiple size scales of the repeating elements or through the microstructure of the underlying material itself. 2D auxetic structures can be designed and optimised for specific applications and can be fabricated using a range of additive manufacturing, machining or other suitable production techniques. This makes them highly customisable and adaptable to different design requirements.

With greater recycling and sustainability pressures from consumers, cardboard packaging continues to grow and take place of other packaging materials. In some applications replacing plastic packaging with a fibre-based alternative can be straightforward. However, in some instances, where a specialised solution is already in place or where cardboard may not match the original material for all desired mechanical properties, a more novel solution may be required. This highlights the need to improve upon the functionality of paper-based packaging, for example its cushioning

and vibration-dampening properties, while also improving strength-to-weight ratio and simplifying manufacturing processes. This would enable paper-based materials to compete with plastics in addition to pressure from environmental considerations. A means of achieving this could be to apply an auxetic pattern to a corrugated cardboard or laminate paperboard sheet to improve its formability and impart new functionality. This thesis explores the concept using a novel auxetic pattern inspired by traditional Māori design.

The novel auxetic design used in this study was kōwhaiwhai pūtoi koiora (auxetic kōwhaiwhai). The design at its simplest form is a three-pointed star with a mangopare (smooth hammerhead) design which draws from traditional Māori art forms, commonly found carved into canoe paddles and prows or the rafters of wharenui (meetinghouses). The kōwhaiwhai auxetic design has three main tuneable parameters. Scale of the motif, hinge thickness, and radius of the mangopare design. The underlying aim of this thesis was to demonstrate how changes in these parameters affect the properties of the auxetic.

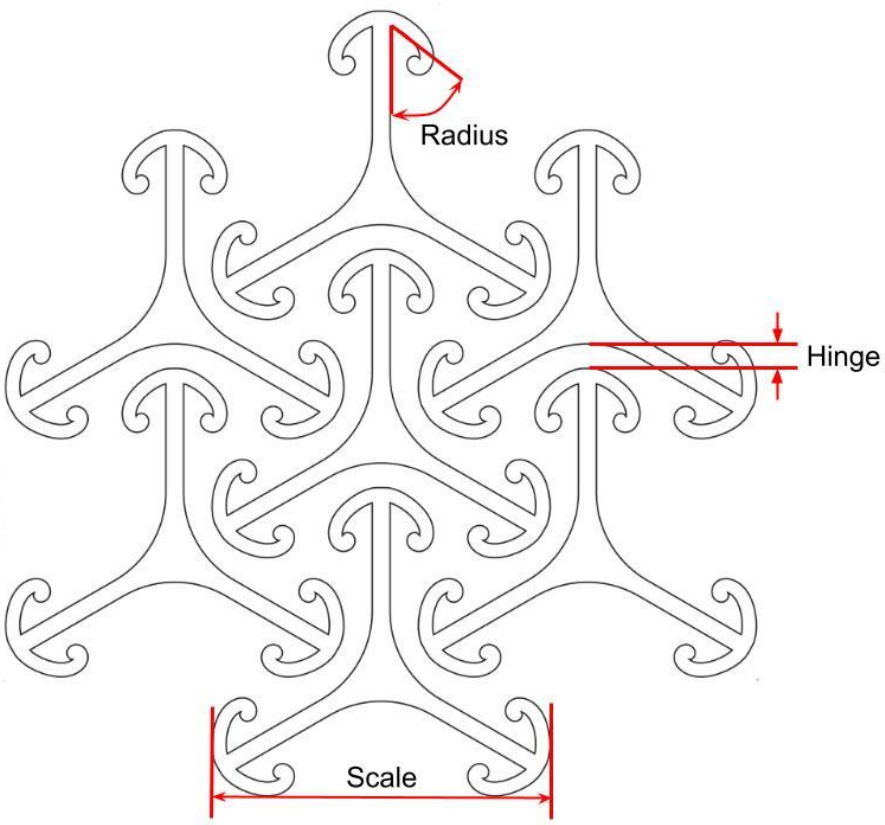

Figure 1 - Kōwhaiwhai pūtoi koiora design showing key parameter changes.

Kōwhaiwhai pūtoi koiora could provide a solution to the removal of the plastic tray from exported Kiwifruit packaging in place of a cardboard tray to improve overall recyclability within the supply chain. The incorporation of the auxetic design into a cardboard tray may be a possible solution to provide beneficial shock absorbing and fracture resistant properties to the cardboard from out-of-plane forces from the fruit during transport.

1.1: Objectives

This thesis presents a kōwhaiwhai auxetic structure, a novel material to be used for a solution to improve out-of-plane shock absorption for fibre-based packaging. This work partially draws inspiration from the work completed by Rafsanjani and Paisini (2016), and Chen et. al. (2021), which investigated a bistable auxetic from ancient geometric motifs to create a surface structure for elastic sheet material. The structure can be flat fabricated from a cardboard paper material and moulded to create a tray of optimised concave holders for the purpose of Kiwifruit transportation. The objective of this thesis is to create a basic understanding for the novel auxetic material presented in the study by characterising basic geometric properties experimentally and numerically. The foundational work here could allow for greater optimisation of the design in future work to enable it to be applied to packaging solutions.

1.2: Thesis Structure

Chapter 1: Introduction to auxetics, objectives of the work, and structure of the report

Chapter 2: Literature review covering auxetics, cardboard, finite element models (FEM), and paper & board testing methods. It outlines each topics relevance to the project and identifies areas needing further clarification or research.

Chapter 3: Foundational work – Explored the method of tensile testing for auxetics and how changes in the method effect the apparent tensile properties.

Chapter 4: Development of a foundational numerical model based on the experimental work in chapter 3 to enable further work on optimising the auxetic design.

Chapter 5: Determine the effect of tuneable parameters of the auxetic and to examine the relationship between the stiffness and elasticity loss, and moisture content of different fibre-based boards under in-plane tension.

Chapter 6: Further work – Closing statements about the thesis and possibilities for potential future work.

Chapter 2: Literature Review

2.1 Auxetics

Auxetic structures are mechanism-based metamaterials that are characterised by a negative Poisson's ratio. This means that they have a property of expanding laterally when stretched, unlike conventional materials which contract in the transverse direction (Saxena et al., 2016). This behaviour of auxetic structures offers advantages such as increased toughness, energy absorption, and impact resistance (Uzun, 2012), making them promising materials for a wide range of engineering applications.

Auxetics are collections of rigid elements or motifs which have a geometric design linked together by flexible hinges allowing for low-energy, free motion within the auxetic state. These elements enable high tunability of the complex motions and properties of the linked elements and allows for careful optimisation of the mechanisms at the element scale to form a part of a complex structure in a wider range of engineered structures, from lightweight deployable structures in complex environments such as space (Balan et al., 2022) and medical (Lvov et al., 2022), to pressure reducing design of athletic shoe midsoles (Zhang, Lu, Yang, et al., 2024; Zhang, Lu, Lin, et al., 2024).

The stresses at the hinge and corner connections of auxetic structures are known high stress points that could lead to failure in the repeated deployment or strain of these structures (Chen et. al., 2021, Khare et. al, 2018). This is an important issue for this project as localised stress on fibre-based materials may lead to adverse microstructural effects at these hinges which would reduce the geometric effect of the auxetic over time more quickly than when using another material (Wang et. al., 2019). The structure can be optimised by changing internal angles or hinge thicknesses (Cheng et. Al., 2019; Gu et. Al., 2020). Additionally, the utilisation of various auxetic designs such as s-shaped hinges (Khare et. al, 2018; Meena & Singamneni, 2019), has yielded various improvements. These changes have helped in decreasing or delocalising the stresses on the structures. It was found that the energy dissipation not only was reduced across each hinge, but also allowed for more even dissipation of the forces between elements within the whole structure, leading to more uniform expansion and contraction. The elements that create

the auxetic mechanisms come in a wide variety of structural designs, each having beneficial properties that enhance the material at which it is created from.

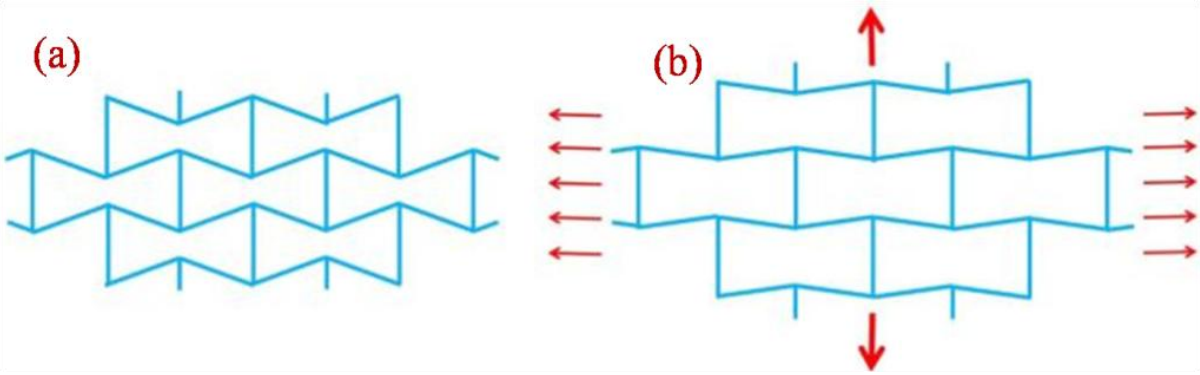

Figure 2 - Expansion of typical re-entrant auxetic structure (Liu & Hu, 2010)

The re-entrant auxetic structure is a commonly used element which is a structure made up of hexagonal units (Figure 3 left image). The interior angles of this design often exceed 180˚and are defined as negative angles in elemental design. The auxetic movement of the elements occurs as follows: when a uniaxial tensile load is applied, the edges of the elements bend and are pulled in unison, resulting in volume expansion in both axial and transverse directions, consistent with auxetic behaviour. Starting from a typical hexagonal shape, various re-entrant-like auxetic elements can be created by altering the number of polygonal edges and adjusting the negative angles. Using these changes, elements like the double arrowhead (Qiao et. al., 2015), three-, four-, and six-star shaped (Saxena et. al., 2016; Grima et. al., 2005; Wang et al., 2018) re-entrant structures can be created (Figure 3 a, b, c, and d respectively). Additionally, re-entrant structures can be tuned within some limits to obtain a desired stiffness and Poisson's ratio. Re-entrant structures are commonly used for their simple structure and ease of implementation. Due to their open cell structure, however, the structures are obtained at the expense of strength and stiffness. It has been shown that these properties can be dramatically improved by implementing augmented cell walls (Li et. al., 2019).

Chiral auxetics are non-superimposable structures that consist of ligaments attached to the tangent of rigid rings. The auxeticity occurs from the rotation of the rings that essentially wind or unwind the ligaments as compressed or expanded (Spadoni, 2011; Spadoni & Ruzzene, 2011). The structures properties are tuneable based on the scale of

the chiral structure, radius of the rigid rings, and the length of the connecting ligaments (Prall & Lakes, 1997).

Figure 3 - Various re-entrant auxetic designs (Z. Wang et al., 2020).

Rotating rigid structures are lattices of rigid geometries connected by hinges on the shapes corners. When stretched, the elements rotate about their hinges, generating the auxetic effect. The variations of the structures are restricted only by variance in geometries. Grima et. Al. (2000; 2004; 2005; 2006; 2007; 2008) studied many types of rotating rigid structures, including square, rectangle, triangle, and rhombi. The tensile properties of these structures are controlled by the rigid shapes side lengths, angle between the rigid shapes, and stiffness constant of the hinges. Gatt et. Al. (2015) then proposed a new class of rigid auxetics that form a hierarchical system (Figure 4) where each level is a larger rotating rigid material made from a smaller grid of rotating rigid structures. It was shown that the Poisson's ratio of the material could be controlled by changing the size of the pores. This was used to have greater control and versatility of rotating rigid elements across larger scales.

Similar to rigid structures, sheets with perforations can also exhibit auxetic behaviour where the edges of perforations in the material act as the hinges compared to most other auxetics. Optimising the properties of perforated sheet auxetics is done by varying the shapes, sizes, and orientation of the slits (Mizzi et al., 2015).

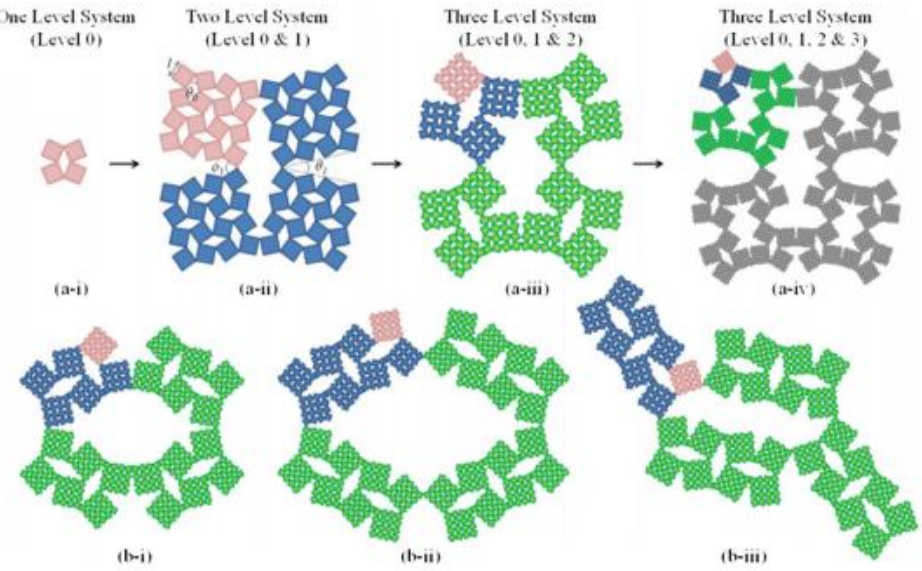

Figure 4 - (Gatt et. Al.,2015) – Hierarchical structures of rotating rigid auxetic structures.

2.2: Auxetics in Paper Based-Materials

The nature of auxetic structures has great potential for the packaging industry as they are highly deformable, which makes them suitable for conforming to irregular shapes and surfaces, providing better protection against impacts and vibrations (Sgobba et al., 2019; Uzun, 2012). A preliminary study that used the out-of-plane forces that a negative Poisson's ratio brings to create self-erecting curved surfaces by unravelling auxetic structures (Attard et al., 2018). The study showed that auxetic structures can be tuned to limit in-plane expansion or contraction under tension while also creating an out-of-plane deformation. Zhang et al. (2022) used a novel 'windmill' shaped auxetic structure to improve energy absorption. It was shown that there were tuneable parameters to optimise Young's modulus, shear modulus, relative density, Poisson's ratio, plateau stress, and specific energy absorption. These studies show the potential for auxetic structures to be used in the packaging industry by allowing for tuneable energy absorption, Young's modulus, and deformation so that the effectiveness of the structures can be characterised in comparison to current packaging methods.

Cardboard is a commonly used packaging material for many reasons including its high strength-to-weight and stiffness-to-weight ratios (Fadiji et al., 2017). It is also of increased interest over the last decade due to its recyclability, and potential for reducing

waste within the supply chain compared to many polymer-based alternatives. Auxetic structures increase toughness, energy absorption, and impact resistance in the material they are applied in (Uzun, 2012). Thus, the use of auxetic structures on cardboard could lead to a simple yet effective method of improving packaging solutions. Studies have shown promising results in energy absorption, stiffness, and synclastic deformation using auxetic cores in cardboard (Peliński et al. 2020; Peliński & Smardzewski, 2020; Peliński & Smardzewski, 2022). Although there are several studies on auxetics, none investigate the efficacy of two-dimensional auxetics cut into cardboard, which could have different behaviour than an auxetic core which has been studied. Additionally, reviews of auxetics in both 2016 and 2020 outlined the need to study auxetics under a wider variety of materials, as many papers investigated the use of auxetics in polymer-based materials (Wang et. Al., 2016, Saxena et. Al.,2020), further showing the gap in the literature around auxetics using corrugated board and other paper/fibre-based materials to help broaden the literature.

2.3: Kowhaiwhai Design, History, and Significance

The novel auxetic design used in this study was kōwhaiwhai pūtoi koiora (auxetic kōwhaiwhai). The kōwhaiwhai design draws from traditional Māori art forms and has become ubiquitous with Aotearoa's graphic identity. The motif of the kōwhaiwhai is drawn from some natural object. The unravelling of fern fronds, flower of the Kowhai ngutukaka (Clianthus puniccus), patiki (flatfish), rautawa (tawa leaf), and mangopare (hammerhead shark) are all associated with elements of kōwhaiwhai design (Hamilton, 1896). The various designs all have coded meanings which reflect the genealogy of the tribe origin and story, leading to site-specific kōwhaiwhai designs that vary between regions (R. Neich, 1993)

The abstract curvilinear patterns have been utilised in various ways over its history. Traditionally, they have appeared carved into canoe paddles and prows as well as to rafters (heke) of meeting houses and in moko (tattoos) (Hamilton, 1896). In recent times, they have become part of the country's global identity, with kōwhaiwhai designs

appearing in wearable art, costumes, and uniform for sports teams, beauty pageants, and national airlines (Groufsky, 2019).

In this thesis, the kōwhaiwhai pūtoi koiora design is brought forward to show a novel auxetic design that has been inspired by traditional Māori art forms. In a similar concept to a study by Rafsanjani & Pasini (2016), inspired by architecture in the Kharraqan twin towers, this is not the first time a geometric art is presented for materials science but is the first to show how kōwhaiwhai can be used in auxetics. The design at its simplest form is a three-pointed star with a mangopare (smooth hammerhead). The kōwhaiwhai auxetic design has three main tuneable parameters. Scale of the motif, hinge thickness, and radius of the mangopare design. These changes are shown in Figure 1. The original design features the standard motif scale (20 mm size); with a hinge thickness of 1.6 mm; and a mangopare radius of 1.1.

2.4: Cardboard and Paper-Based Materials

Cardboard and corrugated fibre-based materials have been a vital part of packaging and protection for over a century. With its first known use as a liner inside tall hats in 1856 to unlined corrugated board used to protect glass and kerosene lamps from 1871 to the first corrugated boxes in 1894 (Fibre Box Association, 1999). The carboard box has been and still is one of the most utilised materials in packaging today with 90 % of all products shipped in cardboard and accounts for the second highest amount of global waste at 17 % after food and green waste according to Business Waste (2024)

As manufacturers optimised for lightweight and high mechanical performance, the design of the corrugated layer was ideal. Over time, further improvement of the material for specific uses has come from changing the corrugation fluting profile, adding layers to the fibreboard to have multiple fluting layers, and incorporating a range of board materials in the cardboard.

2.4.1: Production Process of Cardboard and its Principal Directions

The production of single walled corrugated board involves forming of the corrugated core by preheating and pre-steaming a fibreboard and passing through corrugated rollers, followed by gluing to one board face, then to another. The starch-based adhesive is applied to the flute core tips by applicator rollers and then pressure rollers to secure the glue between the corrugated board and its liners on each side (Kline, 1991)

As a consequence of production, cardboard has its principal material directions. In the x-axis, the machine direction (MD), where the paperboard was manufactured and paper fibres become aligned. The y-axis, the cross direction (CD), is parallel to the corrugated fluting. The z-axis, out-of-plane direction, describes the different layers of the corrugated board.

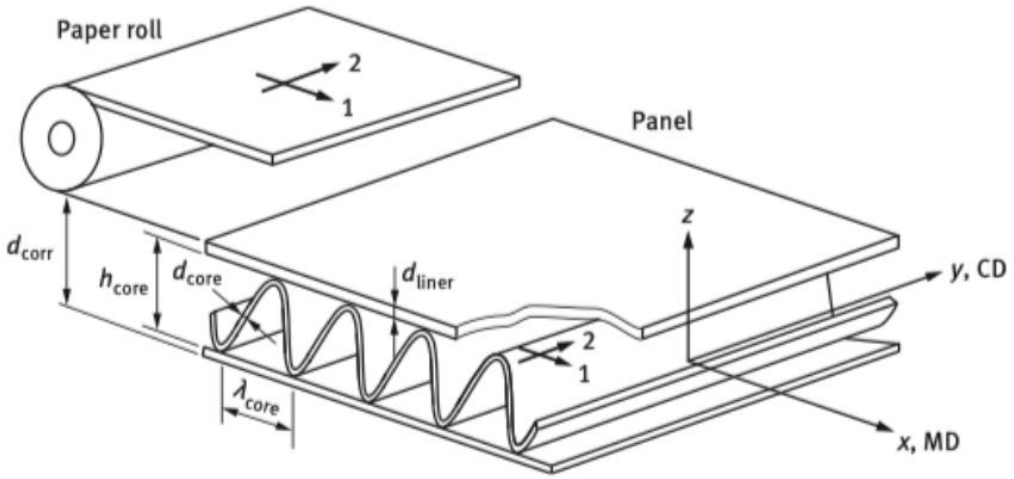

Figure 5 - Key dimensions and orientations of corrugated board (Ostlund, n.d.)

2.4.2: Effect of Humidity on Material Properties

The moisture content of paper-based materials can also affect its mechanical properties, with higher moisture levels leading to decreased strength and stiffness. This is a particular interest for the fruit packaging industry as fresh fruit must be refrigerated for transport in high humidity environments (TIS, 2023a; TIS, 2023b). Research conducted on the mechanical properties of cardboard indicates that it is highly susceptible to elevated

levels of humidity. The elastic properties of the material undergo significant alterations beyond 70 % relative humidity (RH), resulting in a reduction in stiffness of up to 50 % at 90 % RH. The impact of moisture on the failure stress and ultimate strain of the material is even more pronounced (Allaoui et al., 2009; Fadiji et al., 2017). Furthermore, the effect of humidity on the cardboard warps the material under stress (Dano & Bourque, 2009), and once dried, can maintain the deformation. This can have negative effects on the mechanical properties of the cardboard but can be utilised for the design and production of the packaging in processes such as thermoforming.

Although the effect of humidity on fibre-based materials is well documented, it is unknown how this knowledge extends itself to auxetics on these materials. With respect to the auxetic elements cut into the cardboard material, it could be observed that the material has an increased porosity, therefore leading to a greater impact of humidity on the material. On the contrary, the inclusion of the auxetic into the material itself will improve upon certain properties as well, in turn, potentially counteracting the effects of humidity on the material. To what degree at which each side of the equation balances out is unknown, thus highlighting an avenue of knowledge to be acquired to provide a more complete picture of the behaviour of auxetic materials.

2.4.3: Standard Mechanical Testing of Paperboard

There are many published test standards and methods for testing paper and board created by organisations to help ensure that products meet industry recognised best practices. Some of these organisations are Organisation for Standardisation (ISO), American Society for Testing and Materials (ASTM), and Technical Association of the Pulp and Paper Industry (TAPPI). For this thesis, the TAPPI versions of standards have been used as they provide more standards and methods specific to cardboard performance and it is recognised across the industry of corrugated packaging.

2.4.3.1: Conditioning and Sampling

Before testing can occur, it is important to ensure the uniform condition of all specimens by preconditioning them. TAPPI T402 (Technical Association of the Pulp and Paper

Industry [TAPPI], 2021) defines the standard atmospheres for normal preconditioning, conditioning, and testing of paper and paper products of the like. This is described in the standard as the preconditioning of the specimen at 10-35 % relative humidity and 22-40 ºC for 24 hours. The specimens are then conditioned at 50 % ± 2 % relative humidity and 23 °C ± 1 °C for enough time for the specimen to reach satisfactory equilibrium with the atmosphere. This time is usually 5-8 hours for unsealed board boxes and for this work, the samples were left to acclimate for at least 24 hours to ensure this.

The standard sampling TAPPI T400 (2022a) describes the procedure for obtaining a representative sample for testing cardboard. This standard addresses the general considerations to ensure the material used across all testing in the work are consistent to ensure that there are no discrepancies based on manufacturer, batches, or other minor manufacturing changes.

2.4.3.2: Tensile Testing

Mechanical testing of 2D auxetic structures is crucial for understanding their unique mechanical properties and optimising their design for specific applications. Several testing methods have been developed for characterising the mechanical behaviour of 2D auxetic structures, including uniaxial tension and compression, shear, and bending tests. These tests provide valuable information on key parameters that effect Poisson's ratio, Young's modulus, stiffness, and energy absorption, which are essential for optimising the performance of 2D auxetic structures.

Although there are some instances of variations to standard tests for novel structures like auxetics, there is no standard testing method that is currently used for finding tensile properties of auxetics. This investigation will combine concepts from TAPPI T494 (2022b), literature, and novel methods to create an effective method to determine the properties of the novel auxetic used in this study.

Cardboard typically contains small variations when produced, leading to inconsistencies in the output data during testing. Because of this material inhomogeneity, TAPPI 494 (2022b) states to complete at least ten replicates of specimen for standard tensile testing to determine an adequate average in data. Additionally, due to the fluting inside

cardboard, the material direction plays a large role in the material's mechanical properties, leading to a clear difference in strengths of the material between its two in-plane axes (Allaoui et. Al., 2008). Because of this, it is expected that each principal direction is tested for each specimen.

2.5: Measurement of the Poisson's Ratio

The Poisson's ratio (υ) is described as the negative ratio between transverse strain ($\varepsilon_{transverse}$) and axial strain (ε_{axial}):

Equation 1 - The Poisson's ratio

$$\upsilon = -\frac{\varepsilon_{transverse}}{\varepsilon_{axial}}$$

In most materials, when stretched in the longitudinal direction, the material exhibits contraction in the lateral direction. This inverse interaction leads to a positive Poisson's ratio. In auxetic materials, the opposite is seen. The geometrical design is manipulated to cause overall expansion laterally when under longitudinal strain, leading to a negative Poisson's ratio.

The key properties of auxetic materials is the negative Poisson's ratio. Where dimensional changes to auxetics need to be quantified and understanding the distribution of forces, the Poisson ratio is a critical property of an auxetics definition.

The expanding and contracting cell structure of auxetics comes about by the elements connection by hinges at their vertices, leading to their impressive properties but also a complexity of tracking points within the material akin to non-homogeneous solids. Because of this, the task of measuring the Poisson's ratio becomes more complex where standard methods of measuring this property are not as accurate, leading to uncertainty within literature as to the methods by which studies determined the Poisson's ratio of the auxetic material in question.

When researching the Poisson's ratio of other similar two-dimensional auxetics, many studies do not include details on the experimental determination of the auxetics Poisson's ratio. With the knowledge that the material expands and contracts in a non-

uniform manner, there is no specification of measurement points used in the calculations for the property. This lack of information on a two-dimensional property like this is problematic as this is only made more complex in three dimensions.

In a 2022 study, Yolcu and Baba appears to be the only one that has gone into detail about these decisions for a 2D peanut-shaped auxetic in which their goal was to create a blueprint for a standard method for finding the Poisson's ratio. Using a baseline of an ASTM standard test method for honeycomb cores (ASTM D6790/D6790M-16 (American Society for Testing and Materials., 2016) and combining it with the intuition around auxetic material, they were able to show how measurement regions can affect the outcome of the apparent Poisson's ratio.

2.5.1: Typical Poisson's Ratio Measurement

Poisson's ratio is typically determined with the help of finite element models rather than experiments but can be assisted by image analysis when done experimentally. In literature, the geometric analyses used to calculate the PR values based on the geometric model of the repeating units of the auxetic structure where the length and width of the tensile gauge are formulated using these cells. However, where most literature deviates from each other is in the experimental calculation of the PR.

2.5.2: Image Analysis

To understand and analyse the structural changes of the auxetic during testing, it is important to find ways to visualise these changes. Among other methods, simply imaging the area of interest and analysing these changes digitally can is a great way to determine these changes.

Image analysis has been used to understand the mechanics of auxetics at a smaller scale using techniques such as SEM (Hengsbach & Lantada, 2014), as well as on a larger scale to trace the behaviour of an auxetic under tension to determine the Poisson's ratio across different regions of the structure (Yolcu and Baba, 2022). Various programs allow for varying levels of automatic to manual analysis of the imaging taken. ImageJ, Digimizer,

Kinovea, and many other programs are easy to use and often open source and perfect for a quick analysis solution.

In this study, image analysis is used to visualise and measure specimen during tensile testing to measure the resulting Poisson's ratio of the kōwhaiwhai auxetic. The aim of Chapter 3 is to build upon methods used by Yolcu and Baba to measure various measurement regions using Kinovea as a tool for image analysis to determine the Poisson's ratio of the auxetic.

2.6: Finite Element Models (FEM)

The Finite Element Method is one of the most utilised numerical methods in research, with a wide range of analysis capabilities. With the dramatically increased accessibility and reduced costs for both software packages and hardware with greater computational power, FEM has become a more viable method for effectively and efficiently simulating various engineering design problems. These numerical techniques, in combination with validation of the results, helps designers to optimise food packaging (among other fields) without the need for extensive and expensive physical testing.

FEM is used at various scales within paper and fibre materials. These include modelling paper at the fibre scale, at a fibre network scale, sheet scale, and for laminates and corrugated boards. The ability to focus on interactions at the various scales accurately shows the efficacy of models in literature. In auxetics research FEM is also used extensively, from understanding the interactions from changes in auxetic parameters for compressive and tensile strength in 2D and 3D applications (Alomarah et. Al., 2020, Ma, et. Al., 2022, Khare et. Al., 2018, Yolcu and Baba, 2022), to the optimisation of deployable bistable auxetic surface structures (Chen et. Al., 2021).

The modelling of corrugated board material is complex due to raw material variability as it is biologically derived, is a composite structure, is orthotropic, has a non-linear stress-strain relationship, and is sensitive to environmental changes. It has been found that CB can be conveniently modelled as a single lamina with the three orthogonal axes having homogeneous properties rather than creating detailed layers that depict the shape of the corrugation and its bonds to the liners on either side (Kueh et. al., 2012, Garbowski 2025).

Additionally, auxetics drastically change the materials properties that they inhabit, so a convenient model of a single lamina would suffice. However, obtaining a complete picture of the how an auxetic on a fibre-based material remains a challenge.

2.7: Summary

The objectives of this project were presented in Chapter 1, and this chapter was written to identify the available knowledge and tools while developing a foundation of ways to approach the problems of the kōwhaiwhai project. Additionally, this chapter also highlighted potential gaps in literature that could be addressed in this Masters' project.

Section 2.1; provides an overview of auxetics, their beneficial properties and general uses in various studies. It briefly described a point of high stress in most auxetics about their hinges.

Section 2.2; describes the high use of cardboard in the packaging industry and the motivations for higher use of paper-based materials. It discusses the addition of auxetics to paper-based materials to provide the additional benefits associated with the negative Poisson's ratio. It discusses how some studies have used auxetic cores in place of corrugated cores in cardboard. This section highlights how there are little to no studies on auxetics used two-dimensionally, cut into paper-based materials like cardboard, showing a potential gap in understanding of how auxetics affect cardboard properties.

Section 2.3; introduced the novel kōwhaiwhai-inspired auxetic design that is used in this thesis. A brief history and significance of kōwhaiwhai design and Māori traditional art was described.

Section 2.4; presented an overview of the production process and principal directions of cardboard, the effect of moisture on corrugated board, and the standard material testing methods used in this thesis. The effect of moisture on corrugated board was shown to be well documented in literature but is not documented at all for auxetic materials as there is little evidence of auxetic materials in cardboard to begin with. Thus, showing the potential gap in knowledge to explore in the area of humidity effects on corrugated board with auxetics.

Section 2.5; highlighted a key property of auxetics, the Poisson's ratio, and its importance for quantifying auxetic behaviour. The section discussed methods for measuring typical materials for the Poisson's ratio and how this can become more complex for auxetics due to the moving elements and the inhomogeneity of the auxetic itself. There was one key study that has discussed measuring the Poisson's ratio for two-dimensional auxetics and none for three-dimensional auxetics, highlighting the incomplete understanding of this property across literature. This section discusses this particular study's strengths and weaknesses within its analysis of the data obtained and how it could be improved upon to provide a more standardised method for determining the Poisson's ratio for two-dimensional auxetics in the future.

Section 2.6; shows when and how finite element models are used in literature to understand problem at hand without the need for physical experimentation, the time saving this entails, and how computing advancements have allowed for greater accessibility to these programs. It briefly discusses how FEM would be used in this study to validate experimental work and to complete complex parameter sweeps to optimise designs.

Chapter 3: Measurement of the Poisson's Ratio

3.1: Introduction

The negative Poisson's ratio of auxetic structures allows them to have many superior and useful properties. The response of the material can be related to variations in the elements that make up the structure, allowing for engineered structures, such examples and applications include lightweight deployable structures in complex environments such as space (Balan et al., 2022), medical (Lvov et al., 2022), and body armour (Shah et al., 2022).

Due to the complexity of auxetic's movement, with irregularly shaped deformations from the effect of tensile grips, out-of-plane buckling on thinner or more delicate materials (Wang et al., 2019), and non-uniform expansion and contraction of the material under tension dependent on the strain axis (Wang et al., 2014; Yolcu and Baba, 2022), it can be difficult to gain an accurate measurement of the Poisson's ratio numerically through models and experimentally. In literature, the geometric analyses to determine the Poisson's ratio for auxetic materials are based on the geometric model of the repeating units. However, different approaches are used in the experimental determination of the Poisson's ratio. Usually, arbitrarily chosen square or rectangular centremost regions with three or more points are selected to measure the longitudinal and lateral strains (Yolcu and Baba, 2022; Wang et. al., 2022; Razbin et. al., 2021). Zulifqar et al. (2017) measured the Poisson's ratio of specimens using the distance of two reference points on specimens in each direction. Chang and Ma (2018) proposed a method where the middle widths and lengths of the specimens were used to calculate transversal and axial strains. Wang et al. (2014) investigated the deformation behaviours of auxetic spacer fabrics under uniaxial loading using a similar method. They marked nine points on the centre of the specimen where the central point was used as the reference point for describing other points (Figure 6). The dots were paired up so that there were three pairs in the tensile direction and in the transverse direction, only the middle pair of dots was measured because of the boundary effect of two clamped ends. Then, the Poisson ratio of the specimens was calculated by averaging the displacement of three pairs of dots in the axial and transverse directions. Specimens with three different sizes were also tested to

determine the suitable specimen size for measuring Poisson's ratio. Gaspar at al. (2005) operated in a similar manner with eight tracked points marked on the specimen to obtain Poisson's ratio without the centre point. Wang et al. (2019) determined the Poisson's ratio by tracking the longitudinal and transverse displacement of four reference points, where the position changes were used to calculate the Poisson's ratio, which the four points were chosen to keep away from the loaded faces and outer boundaries to minimise the influence of boundary conditions.

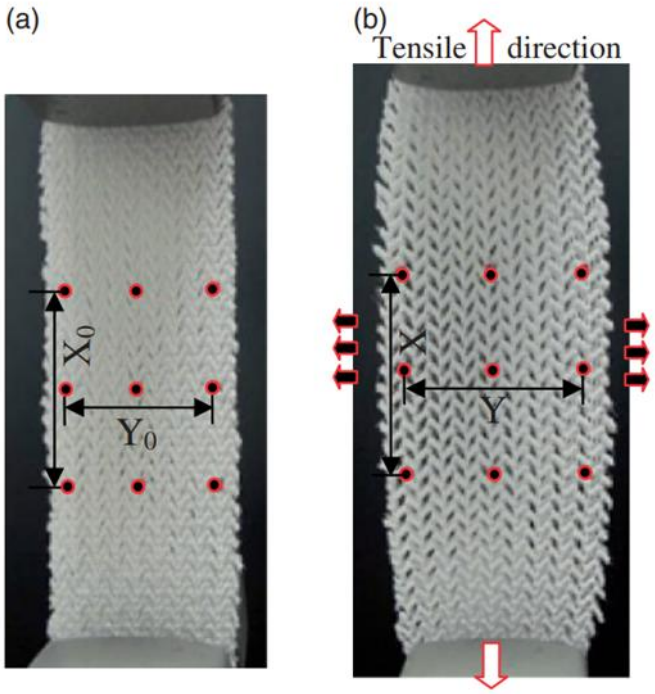

Figure 6 - Experimental image analysis by Wang et. al. (2014) using marked nine points on the auxetic

As discussed above, there are a wide range of methods used to experimentally determine the Poisson's ratio during uniaxial tensile testing. Although they may be accurate for most cases, the expanding and contracting cell structure of auxetics comes about by the unit's connection by hinges at their vertices, leading to the unique properties but also a complexity of tracking points within the material akin to non-homogeneous materials. Because of this, there is uncertainty in determining an accurate Poisson's ratio of auxetics due to their cellular structure necessitating non-standardised methods and therefore, uncertainty in the accuracy of the reported values in literature.

The objective of this work is to use a similar approach used by Yolcu and Baba (2022) and Wang et. al. (2014) to determine the Poisson's ratio of the kōwhaiwhai auxetic unit used in this study. It will extend the concepts described in these papers by justifying what auxetic tensile grid size and rate of separation could be used when testing for auxetics using paper and cardboard materials. This study will investigate the validity of the given Poisson's ratio values described in literature and to develop a standardised method for determining the most accurate measurement of the Poisson's ratio through understanding the deformation behaviours of the auxetic.

3.2: Experimental Method

3.2.1: Kowhaiwhai Pūtoi Koiora Design and Specimen Manufacturing

The auxetic design used in this study was kōwhaiwhai pūtoi koiora (auxetic kōwhaiwhai). The kōwhaiwhai auxetic design has three main characteristics to be varied. Scale of the motif, hinge thickness, and radius of the mangopare (hammerhead shark) design (Figure 7). The original design features the standard motif; 100 % scale; with a hinge thickness of 1.6 mm; and a mangopare radius of 1.1 rad; which will be the 'standard' design used in this chapter to quantify the Poisson's ratio.

The auxetic material used in this study was manufactured from e-flute corrugated board (65E CL) sourced from a local supplier, Oji Fibre Solutions. The auxetic specimen is created through laser cutting the corrugated board using a Makerspace G640L Genesis laser cutter and the corrugated board was cut the materials cross direction with ten replicates each in line with TAPPI T494. Settings for cutting the board were 15 mm/s speed and 45 % power. These settings were chosen for the ability to cut through the cardboard sheets while also maintaining minimal burn marks on the specimen due to the high power of the laser.

Characteristic stress-strain curves show a clear difference in mechanical behaviour of corrugated board in its two in-plane directions (Allaoui et al., 2009) brought on by the impact of the orientation of the corrugation between the boards. However, the auxetic pattern cut into the board greatly changes the behaviour of the material, behaving more as a non-homogeneous material. Because of this large change, the disparity between

board orientation is much less noticeable and thus, the board was only tested in the cross direction.

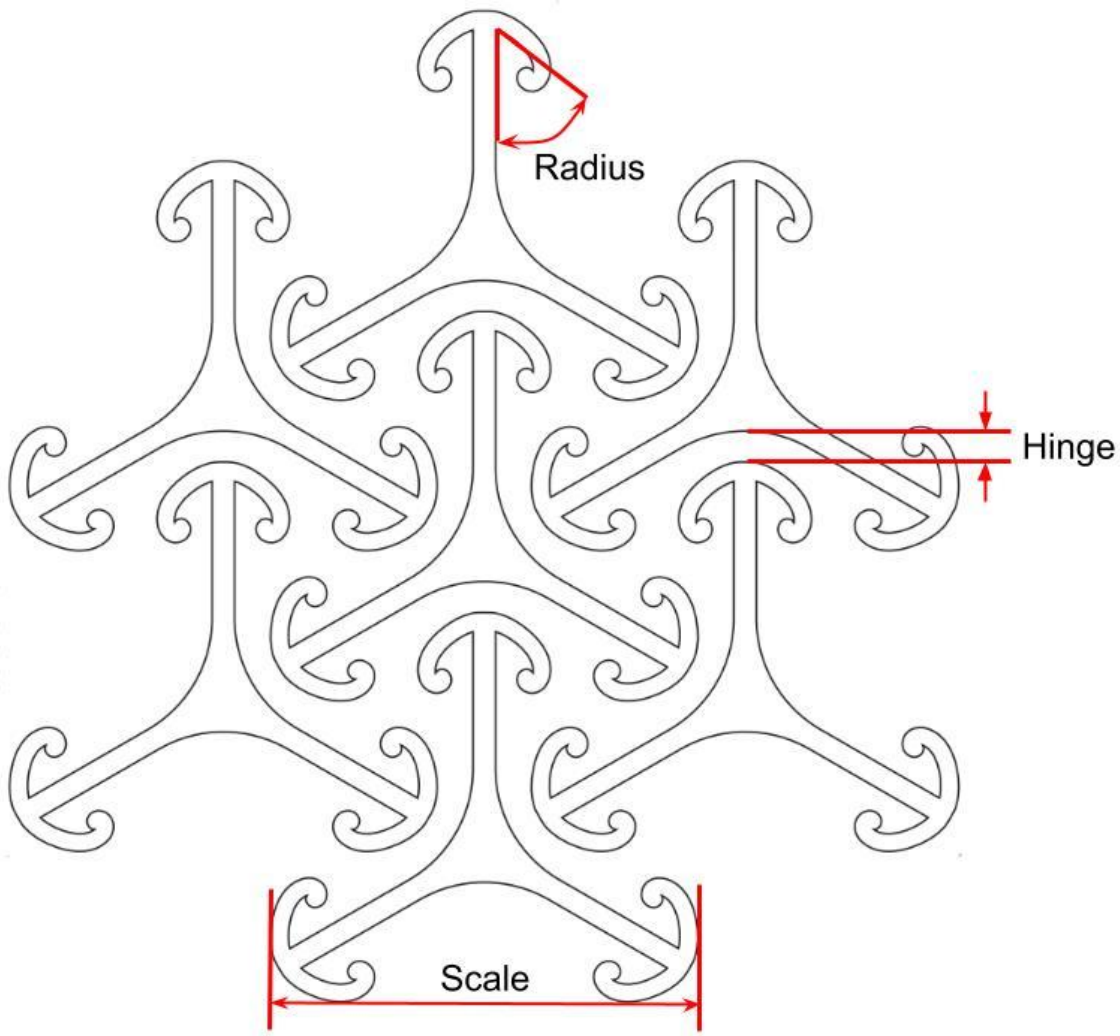

Figure 7 - Kōwhaiwhai auxetic design showing key parameters

3.2.2: Tensile Test

Uniaxial tensile tests were conducted using an Instron 5982 machine equipped with a 500 N load cell. The tensile tests were conducted with the lower specimen clamp fixed and with the top clamp moving at a constant machine crosshead speed of 25 mm/min that was determined in 3.2.2.2. Specimens were loaded until failure, with force displacement data captured during the test along with synchronised video. Figure 8 shows a typical deformation curve for the auxetic and highlights the key points in the

stress-strain relationship of the auxetic, using the 4x8 tensile grid as an example. Between S1 and S2, it shows an initial elastic deformation stage of the auxetic as the hinges of the structure are strained. From S2 to S3 is a plastic deformation plateau where the auxetics hinges are extended beyond their elastic range by the applied load, consequently, these parts of the material begin to lose elasticity and auxeticity is reduced due to the altered material geometry. Past S3 to failure at S4 is then a second elastic stage where the hinges are at their maximum strain and the auxetic grid has fully expanded before the material failure of the specimen at a weak hinge.

Images of the specimen at the ends of each of these key stages (S1-S4) in the stress-strain relationship, as shown in Figure 8, were analysed to determine the Poisson's ratio of the auxetic. This method is outlined in 3.2.3. These points were chosen so the study covers more than the initial elastic stage of the auxetics behaviour and includes non-linear behaviour.

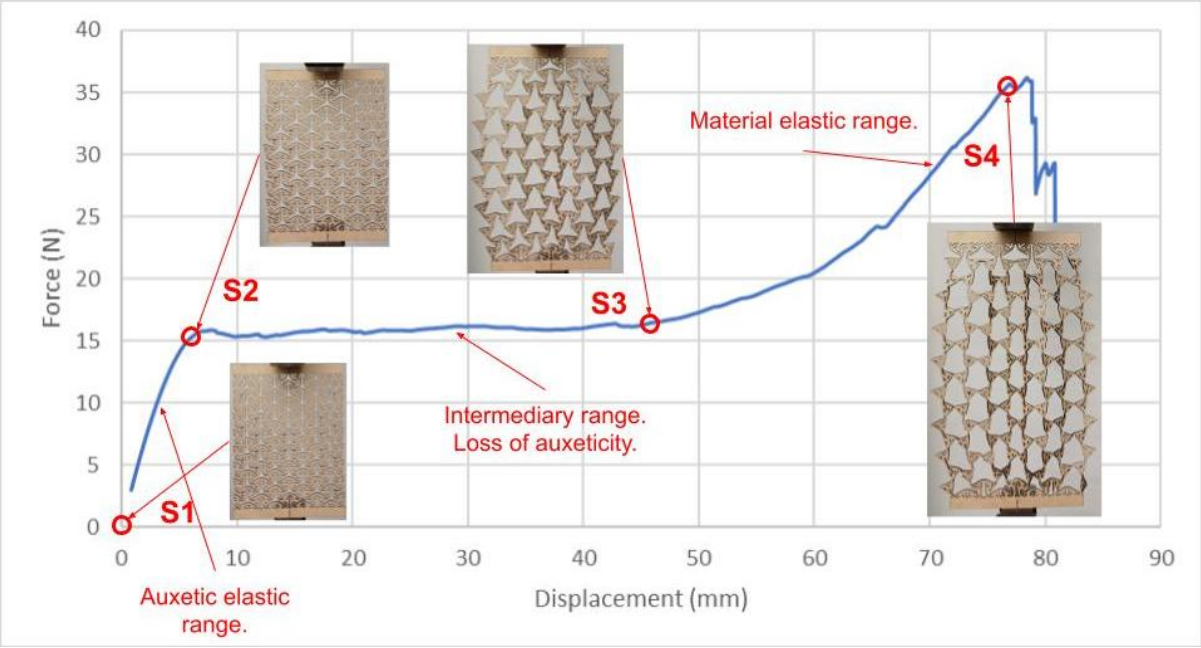

Figure 8 - In-plane changes of the auxetic under tension and the key stages investigated in this study

3.2.2.1: Tensile Grid Selection

As mentioned prior, most research does not describe the details and justifications of the steps taken to determine the Poisson's ratio of an auxetic material. This includes the size of the auxetic grid used to make the tensile specimen. The creation of a specimen used for tensile testing may play a role in the output of the mechanical properties of an auxetic.

Yolcu and Baba (2022) measured the Poisson's ratio of a peanut shaped PLA auxetic in a 8x4 cell array, resulting in an 80 mm x 160 mm tensile specimen. Rafsanjani & Pasini (2016) used a 3x5 auxetic grid while Chen et. al. (2021) used a cell array of 6x10 to conduct their tensile testing of a bistable auxetic with no mention of a rate of displacement for the tests. All these studies used various grid sizes with minimal explanation of the chosen grid size. Wang et. al. (2014) investigated three different specimen sizes to determine the best option for the spacer fabric auxetic used. It was mentioned that theoretically, the specimen size would not influence the apparent Poisson's ratio, however, boundary conditions do affect what is measured as the specimen size increases.

Based on the literature which describes using a range of different tensile grid sizes, three grid sizes were selected for the present study: 3x5, 4x8, and 6x10. Using the base motif design of the auxetic, these grid sizes corresponded to specimen dimensions of 82.0 mm x 83.6 mm for the 3x5, 109.3 mm x 130.9 mm for 4x8, and 164.0 mm x 162.5 mm for the 6x10 grid sizes. These grids were tested to determine if changing the grid shape will affect the resulting auxetics stress-strain curve and Poisson's ratio.

A 10 mm high rectangle along the width of the grid size with a 25 mm x 25 mm square on each side of the auxetic were used to provide an adequate space to clamp the specimen during testing. Additionally, for the larger grid size, 6x10, a 30 mm rectangle of solid board was added to provide support and prevent buckling that may occur during tension. The larger surface area allowed for the clamps to have enough friction to hold the specimen in place without compressing the cardboards fluting during the tensile tests.

3.2.2.2: Rate of Separation

The crosshead displacement rate for the tensile tests on auxetics is another detail that is often left out when discussing the Poisson's ratio of an auxetic. The crosshead rate of the tensile test is an important parameter for cardboard which exhibits time and rate dependent properties that characterise it as a viscoelastic material. Because of this, the rate of separation will have a larger impact on the outcome of the tensile properties of the cardboard based auxetic at a higher rate of separation (Schönwälder & Rots, 2008). Doubling the rate of separation is known to increase the apparent tensile strength and tensile energy absorption for some papers by up to 3 % for the same sized specimen and is stated in TAPPI T494 (2022b) to be accounted for when straying away from the standard method.

TAPPI T494 (2022b) suggests that a rate of separation of 25 mm/min be used to determine tensile properties of paper and board to remain within a typical elastic range. For these experiments, a series of tensile tests using the base motif structure (0.0.0 (scale.hinge.radius (outlined in 3.2.1)) with a central tensile grid of 4x8 was used. Based on TAPPI and ISO standards as a central value, three rates of separation were tested ten times in both MD and CD, 2.5 mm/min, 25 mm/min, and 250 mm/min (International Organisation for Standardisation [ISO], 2008).

The results from this preliminary study are shown in Figure 9. The data does not show any changes in stiffness of the specimen under the different rates of separation. The rate of separation was therefore set at 25 mm/min to remain consistent with standards.

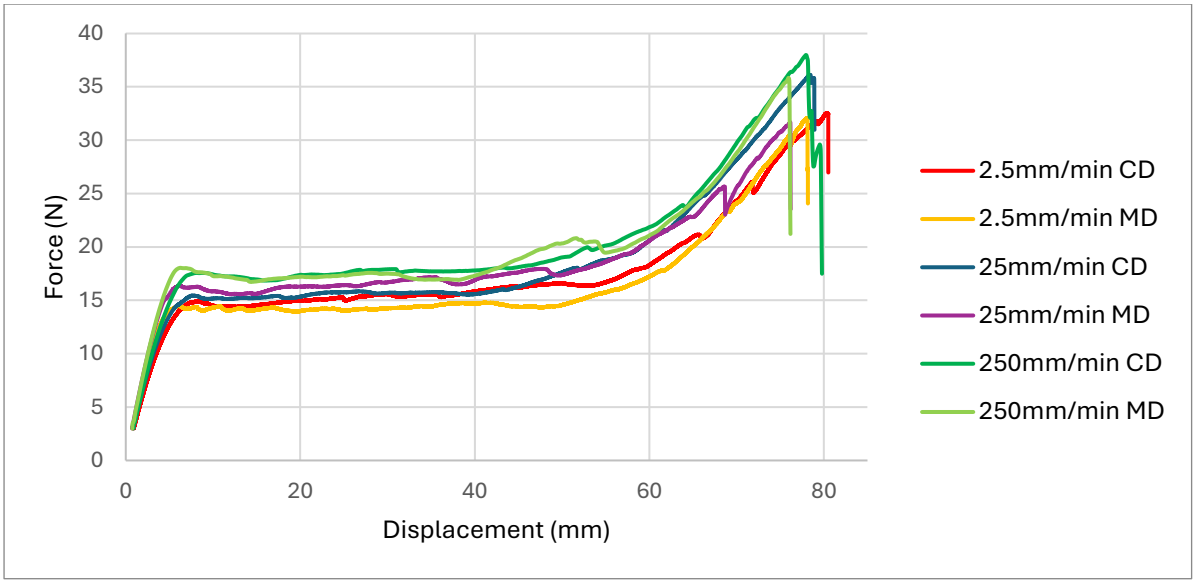

Figure 9 – Effect of separation rate on specimens tested in both machine direction (MD) and cross direction (CD)

3.2.3: Image Processing Analysis

To measure the deformation behaviour of the auxetics to determine the Poisson's ratio, measurement regions, corresponding to those shown by Yolcu and Baba (2022), were determined by starting in the central region of the auxetic and moving outwards to the edges of the auxetic. This created three regions for the 3x5, five for the 4x8, and seven regions for the 6x10 motif tensile grid sizes, shown in Figure 10.

Each of these regions were analysed in terms of displacement at the four key tensile stages to determine the Poisson's ratio using four points per region, each tracking longitudinal and lateral displacement. The four points are each set into two pairs of points in both longitudinal and transverse directions where the Poisson's ratio is then calculated by averaging the distance of the two pairs dots of each direction respectively. Additionally, the Poisson's ratio was tracked over a larger number of points for a few specimens to understand how the Poisson's ratio changes over time. To measure longitudinal and transverse displacements for each specimen, target points were marked and numbered at centrally located measurement regions on the specimen. These key imaging points were chosen to encapsulate a large range of different

measurement points while covering more than the initial elastic stage of the auxetics behaviour.

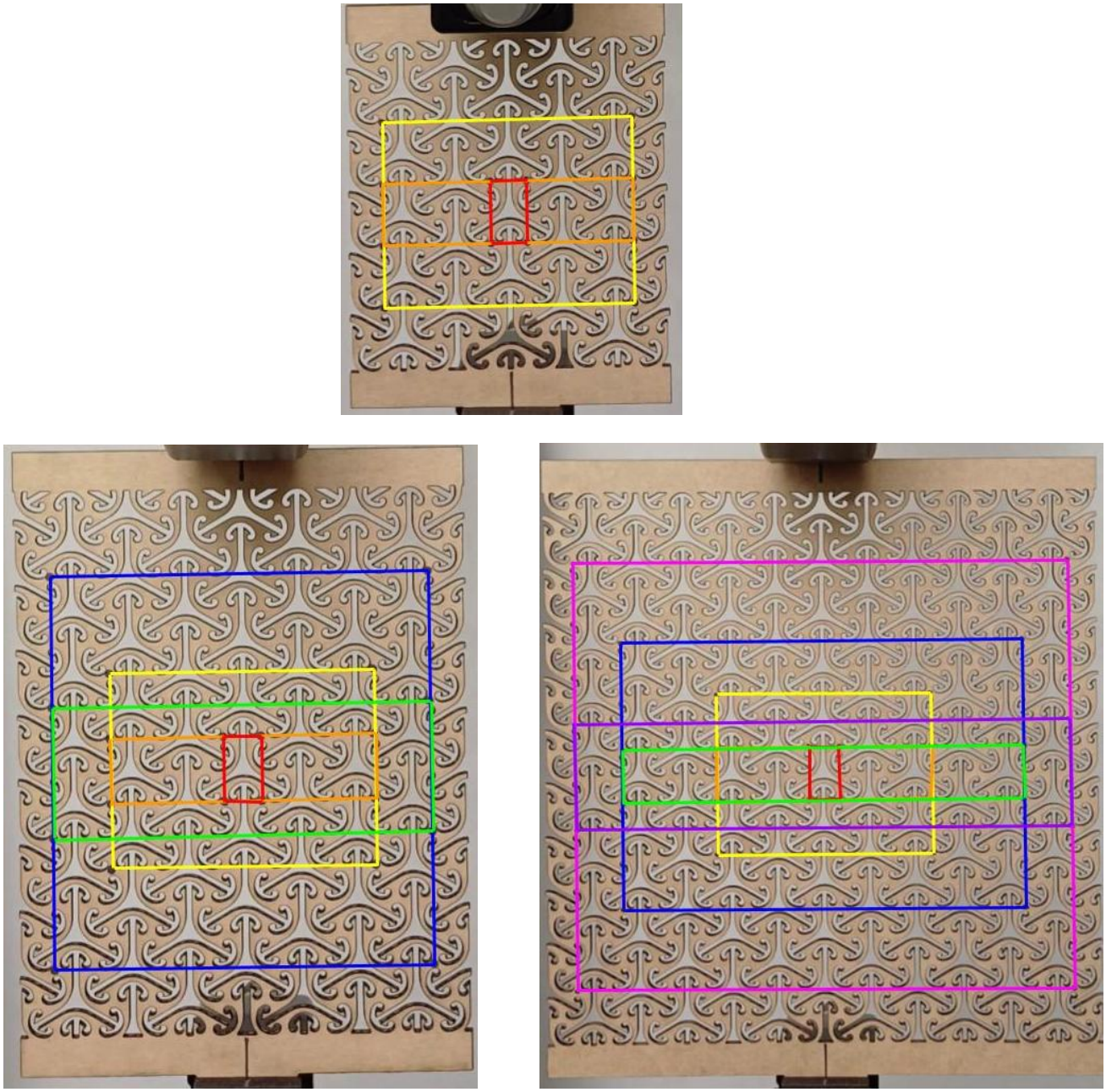

Figure 10 - Three key tensile grid sizes (3x5, 4x8, and 6x10) showing all seven key measurement regions

An image processing method was used to observe dimensional changes that occurred in the specimen during tensile testing. The video (taken using a Samsung Galaxy A34 mobile phone) was screen captured at each key step (S1-S4) to focus on the specimen for determining the Poisson ratio. The images were then transferred to a computer for further imaging analysis using Kinovea 2023.1.2. This software converts a known length to a

certain number of pixels in a frame of a video, such that the marked target points on the specimen can be traced to determine the dimensions for each marked area after testing. Then, by comparing the dimensions of the specimen at each key stage, longitudinal and transverse strains, and the Poisson's ratio were calculated using the equations 1, 2, and 3.

$$\varepsilon_{axial} = \frac{x_{final} - x_{initial}}{x_{initial}}$$

Equation 2

$$\varepsilon_{transverse} = \frac{y_{final} - y_{initial}}{y_{initial}}$$

Equation 3

$$\nu = -\frac{\varepsilon_{transverse}}{\varepsilon_{axial}}$$

Equation 4

3.3: Results & Discussion

3.3.1: Impact of Board Orientation

Figure 11 shows the how board orientation influences the forces at S2 and S4 across each tensile grid size. At the point of failure (S4), board orientation had an insignificant influence on the maximum force across all grid sizes with p-values > 0.05. There is a significant change in force at S2 (p-value << 0.05), at the smallest grid size, 3x5, whereas the force at S2 for the larger two grid sizes are insignificant. This insignificant effect of board orientation on forces on the auxetic is due to the constant twisting of the motifs at their hinges which do not coincide with specific locations of corrugations within the board. This leads to variation of the strengths between each hinge irrespective of board orientation during the production of the auxetic into the cardboard and more down to other factors that would otherwise be less significant in other instances. The smaller grid size begins to have an influence because there is a larger proportion of the material that would remain true to the board's orientation than with the larger grid sizes. Overall, the auxetic pattern cut into the board greatly changes the behaviour of the material, behaving more as a non-homogeneous material. Because of this large change, the disparity between board orientation is much less noticeable.

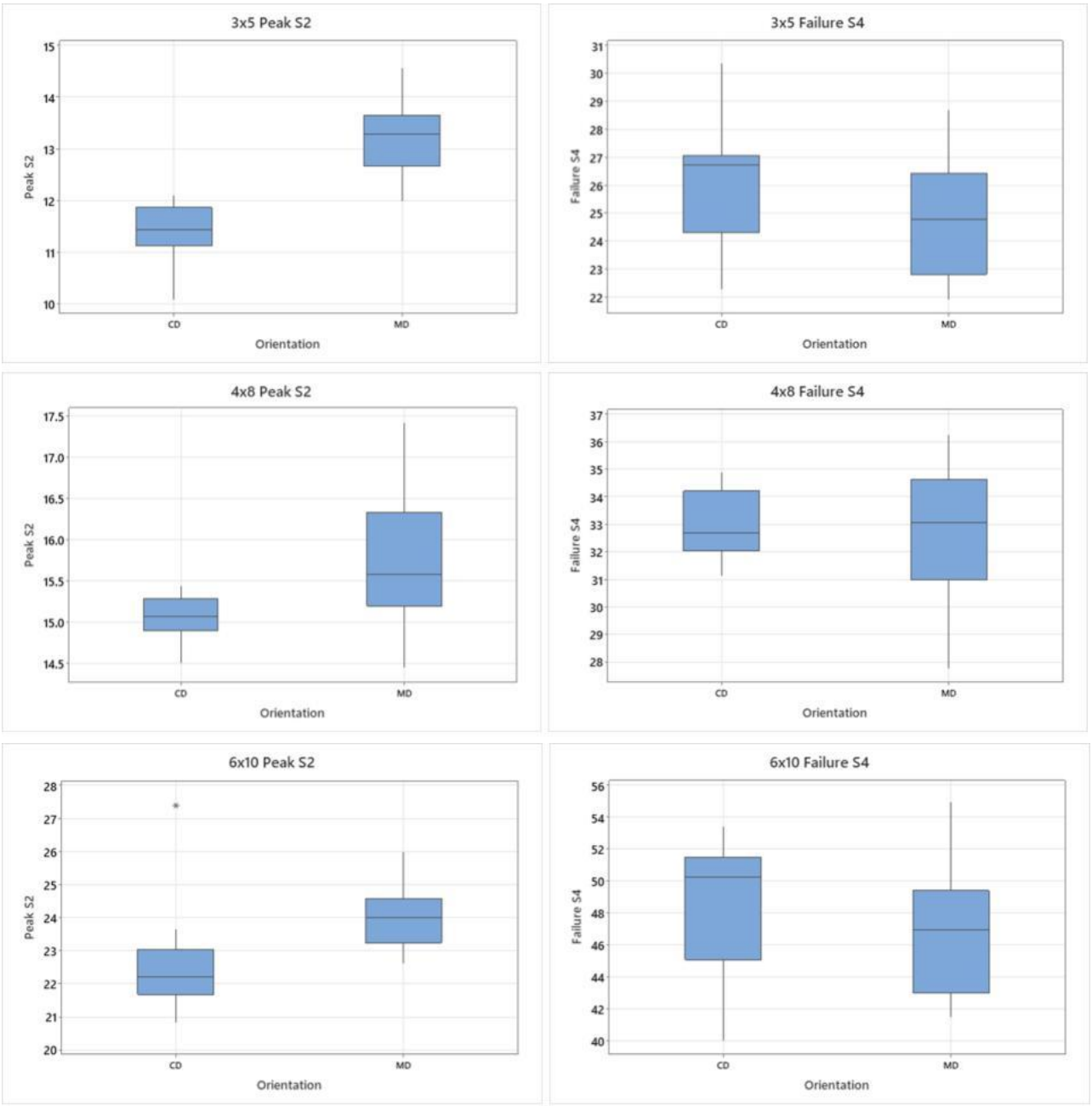

Figure 11 - Boxplots showing influence of board orientation on forces at S2 and S4

3.3.2: How Poisson's Ratio Changes with Measurement Region.

The Poisson's ratios were calculated by determining the different displacements of the specimen between different stages. That is, the Poisson's ratio from S1 to S2 (1-2), S1 to S3 (1-3) and in the second elastic stage S3 to S4 (3-4). Each of the seven regions (for the larger specimens, five for the middle, and three for the smallest) are measured in each of these different stages. Boxplots are shown in Figure 12 to show where the main variances

in the Poisson's ratio occurred. Table 1 below expands from Figure 10 showing the measurement regions and their corresponding colours, shape, and effective placement of the regions on each tensile grid size to assist the discussion.

Table 1 - Measurement regions expanded to show region size, shape, colour, and effective placement among its corresponding tensile grid size.

	3x5 Tensile Grid	4x8 Tensile Grid	6x10 Tensile Grid
1x1 Region. Square-shaped (Red)	Central	Central	Central
3x1 Region. Rod-shaped (Orange)	Edge	Central	Central
3x3 Region. Square-shaped (Yellow)	Edge	Central	Central
5x1 Region. Rod-shaped (Green)	-	Edge	Central
5x5 Region. Square-shaped (Blue)	-	Edge	Central
6x2 Reion. Rod-shaped (Indigo)	-	-	Edge
6x8 Region. Square-shaped (Violet)	-	-	Edge

From these measurement regions, although they cover the same numbers of motifs, the tensile grid sizes change whether these same regions are located near the centre of the specimen or near the edge. For example, the 3x3 measurement region (Yellow coloured region (Figure 10)) is positioned as the outermost region in the 3x5 tensile grid but more central for the 4x8 and 6x10 tensile grid sizes as the number of available motifs for observation increases. This is observed to cause variances in the output Poisson's ratio. For the 3x5 grid size, this is the 1x3 and 3x3 regions (Orange and Yellow regions, respectively), 4x8 grid size is 5x1 and 5x5 (Green and Blue), and 6x10 grid size is 6x2 and 6x8 (Indigo and Violet). The Poisson's ratio calculated using these edge case regions do not match the observed Poisson's ratio for those same regions in larger grid sizes where they are more central in the specimen. The Poisson's ratio appears to be higher (less negative) for these edge cases compared to an observed Poisson's ratio of about -0.4 to -0.5 for the rest of the regions in the S1-S2 stage. This observation is consistent with that of Yolcu and Baba (2022) where between two different Poisson's ratio measurement methods, the only difference is that the measurement method which takes the widest most transverse points to determine the Poisson's ratio led to a reduced (more negative) Poisson's ratio. These edge effects could be due to the triangular motifs not being fully connected on all hinges on the edges, leading to the twisting movement to not be restricted by the boundary provided by other twisting motifs on all sides when more

central. These results overall demonstrate that if the measurement region is not close to the fixed edges of the specimen, the Poisson's ratio remains more consistent. This would also lead to more practical uses of the output Poisson's ratio as 2D designs would more often lead to restricted boundaries on all sides. In situations where the desired design would not be bound on all edges, then observing the edge cases of the auxetic as well could become useful in design optimisation.

Another parameter which varied between each measurement region was the change in longitudinal measurement points. This is where pairs of regions tracked points start along the same transverse widths but different longitudinal heights. These pairs are 1x3 and 3x3, 5x1 and 5x5, and 6x2 and 6x8 where the prior of each pair is more rod-shaped along the transverse direction where the latter of each pair is more square-shaped. A key question in the study was whether the results were consistent with the observations of Yolcu & Baba (2022), where in their study, across the five calculation methods used in each specimen, the methods that took axial measurement points close to the edges are lower (more negative) than the Poisson's ratio calculated using more central points. It was previously suggested that this is because the elongation in the axial direction is greatest through the centre than that of the outermost vertical lines. This phenomenon was also observed in this study although not completely significant in comparison as the boxplots show a visible lower Poisson's ratio for the rod-shaped regions vs square-shaped regions but are still overlapping in quartile ranges. This is because the strain is greatest along the central-most x- and y-directions of the tensile sheet, leading to more expansion along the centre-most points, causing more expansion for the elements in the rod-shaped regions. Thus, the rod-shaped regions are influenced by transverse expansion before square regions, leading to a lower (more negative) Poisson's ratio. It is also noted that the rod-shaped regions were less accurate in measurement, possibly due to reduced numbers of motifs leading to increased potential for error in measurements of the axial strain direction. This higher variance is also observed in the 1x1 measurement region. With fewer motifs and smaller displacements during tension, there is a much smaller margin for error when measuring changes in Poisson's ratio. If the measurement is off by even a couple of pixels during analysis, the Poisson's ratio can vary greatly compared to larger measurement regions. This is also the region of highest volatility

across the five calculation methods seen by Dilek and Buket (2022). For more accurate image analysis or FEM or related techniques, it may be beneficial to take the smallest most central region into account. However, for the most part, this region shows a high amount of variance and likely be too small of a measurement region for accurate measurement of the Poisson's ratio.

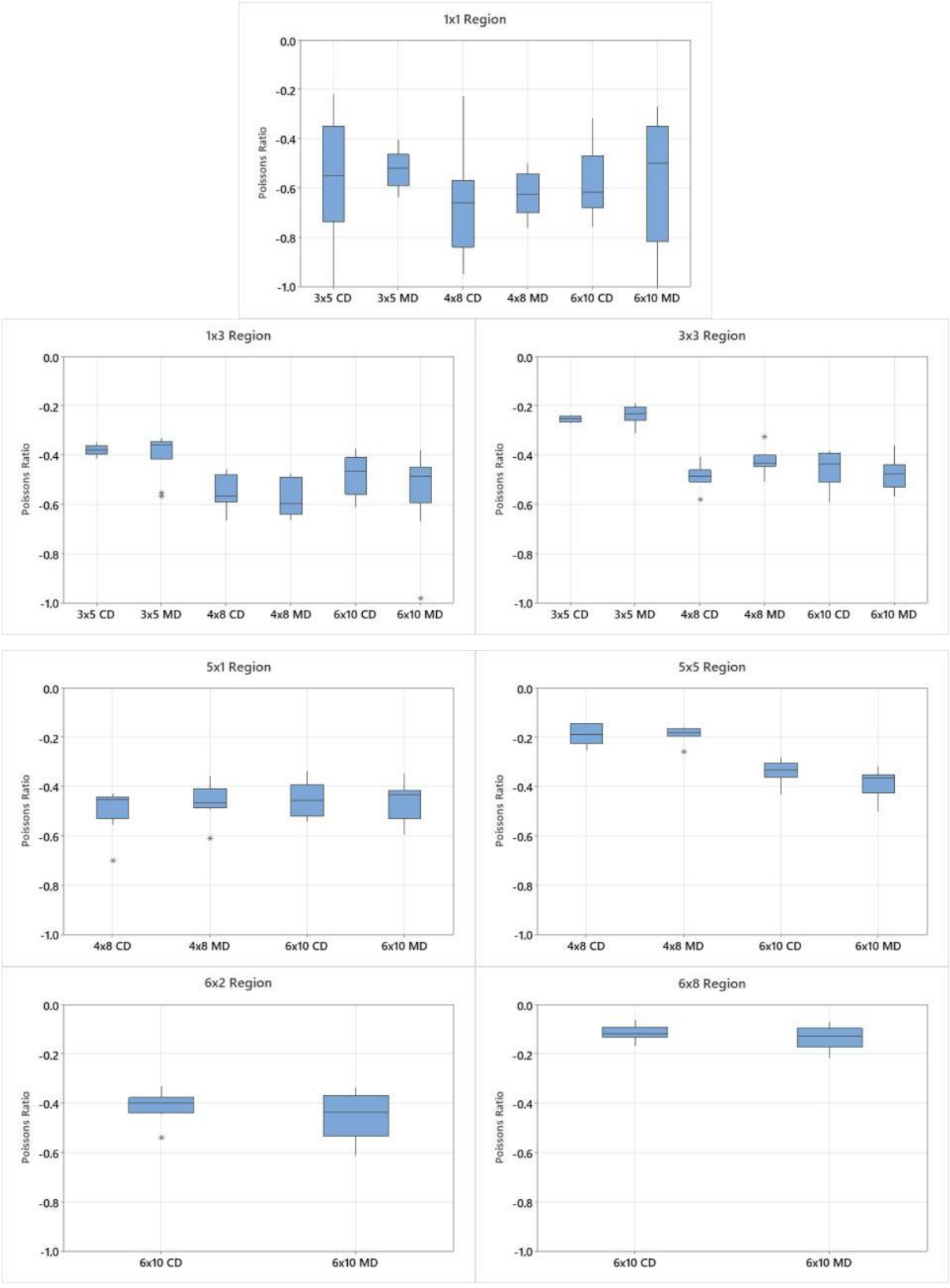

Figure 12 - Boxplots showing how Poisson's ratio changes with measurement region within the auxetic elastic range

3.3.3: Poisson's ratio over time/displacement

To understand how the Poisson's ratio changes over time as the specimen is displaced, a more in-depth analysis of one of each of the tensile grid sizes was conducted. 3.3.2 showed a single measurement from each of the key stages of the auxetic under tension but this section aims to describe the change over smaller increments of displacement. These changes over time are shown in Figure 13, Figure 14, and Figure 15. There are two main pieces of information that can be gathered from these graphs.

Firstly, the Poisson's ratio is seen to slowly increase between S2 and S3 where the stress-strain graph plateaus or slightly decreases. This will be because the motifs within the structure begin to fully extend and become non-auxetic. Past S3, while not a direct focus of the study, the Poisson's ratio will approach and increase past zero until material failure in S4. The Poisson's ratio increasing from its initial value at S2 occurs at different levels of displacement in all different measurement regions. This is because the measured motifs within the smaller regions expand earlier than points further out. This change is best shown in the graph for the 6x10 tensile grid size (Figure 15). The red region increases from S2 first, going above 0 Poisson's ratio from 70 seconds; 1x3 and 3x3 increase from about 60 seconds and plateau just below 0 Poisson's ratio by 130 seconds; 5x1, 5x5, and 2x6 all increasing from about 80 seconds; and the violet region not yet increasing past S3.

The auxetic properties of this depend on the motifs it consists of by twisting. When extension passes S2 and into S3, the material begins to become non-auxetic as the motifs reach a point where they cannot twist any further under the applied load and the hinges break. When discussing how the different regions reach this stage at different points due to more central motifs reaching non-auxeticity, it is noted here that the angles of these hinges between motifs could be related to the point at which that motif becomes non-auxetic, and it follows what could be a relationship between hinge angle and the Poisson's ratio itself. It may become a difficult output to measure due to the out-of-plane twisting of the material as mentioned earlier. This was beyond the scope of the present study but could be a point of further investigation.

The second main takeaway shows that there is large variation in the Poisson's ratio before S2. Initially, it appears to be down to the fact that the error in calculating the Poisson's

ratio is a larger proportion of the total, leading to the volatility. However, past S2, the volatility appears to mostly dissipate, signifying another factor of error. This was confirmed by measuring the 4x8 specimen again, and found that the error is very high in the smallest 1x1 measurement region (Often > 100% error), while the larger 5x5 region had much less error (all < 50 % error, mostly < 10 %) between the measured results by the Kinovea program. Thus, showing that measurement error was not the main issue causing the variation before S2. This error could potentially be due to material inhomogeneity of the cardboard. As the forces are applied and the material is displaced, the structure will always flex along the path of least resistance under tension. This is not always consistent, leading to this variation in results. Once past S2, small changes like inhomogeneity are no longer a big enough factor along with measurement error, the Poisson's ratio stabilises.

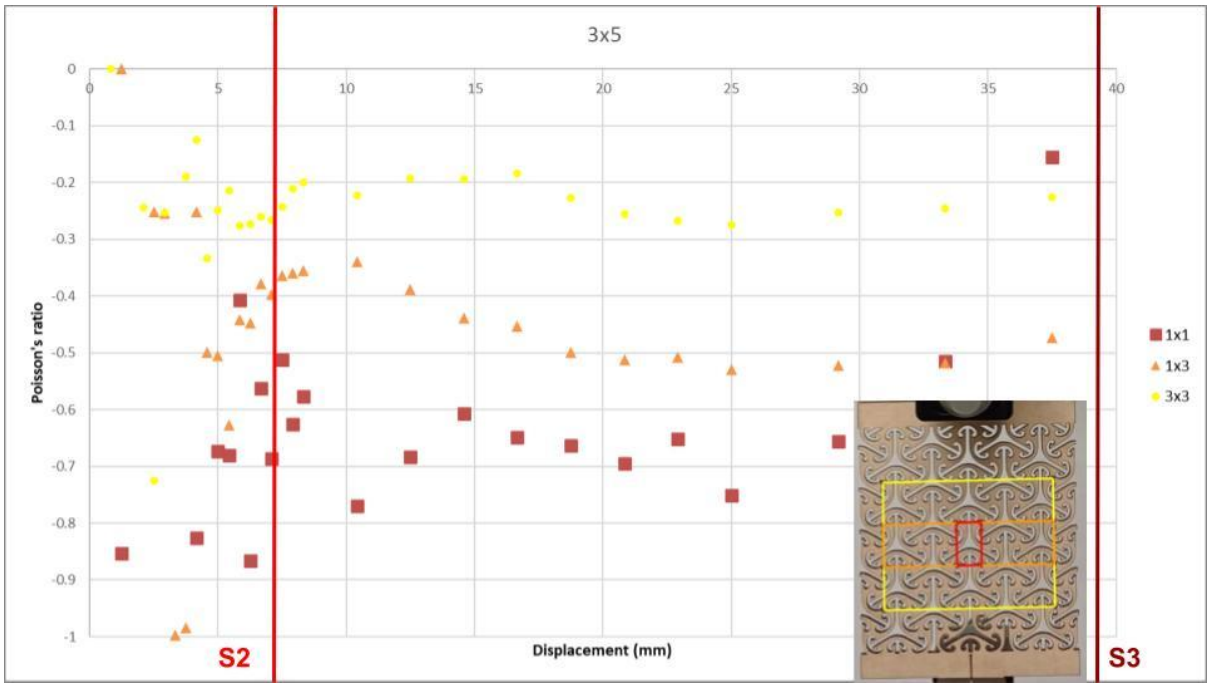

Figure 13 - Poisson's ratio changes over displacement for 3x5 grid size

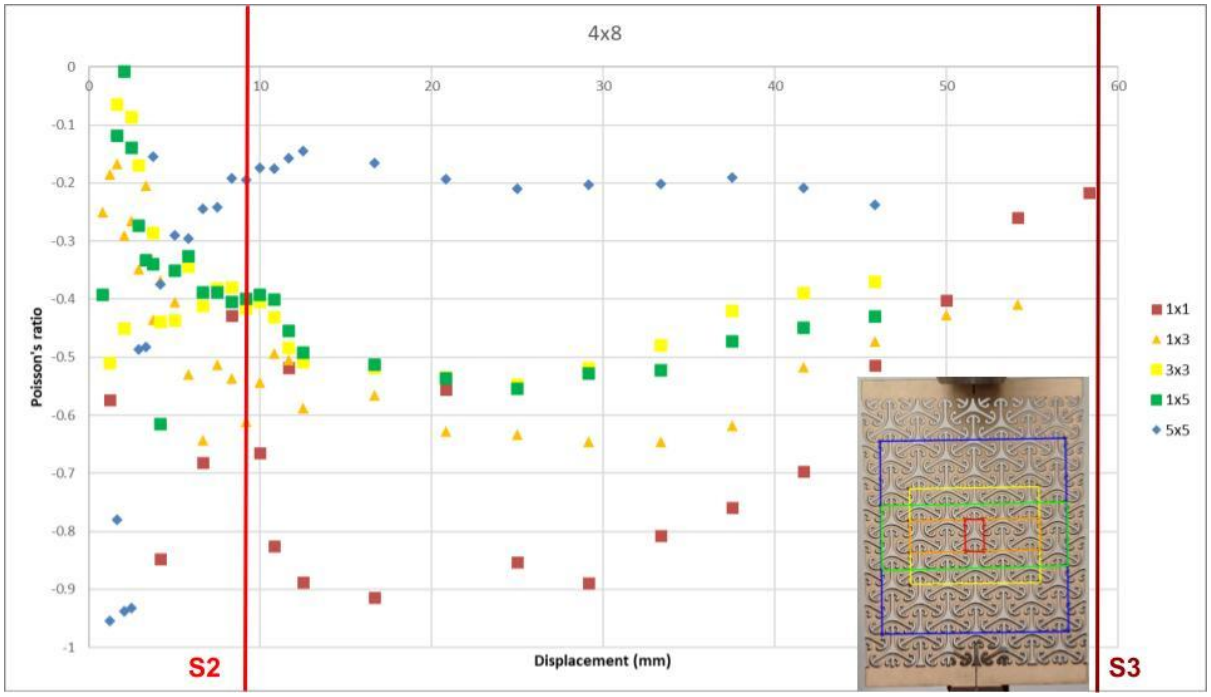

Figure 14 - Poisson's ratio changes over displacement for 4x8 grid size

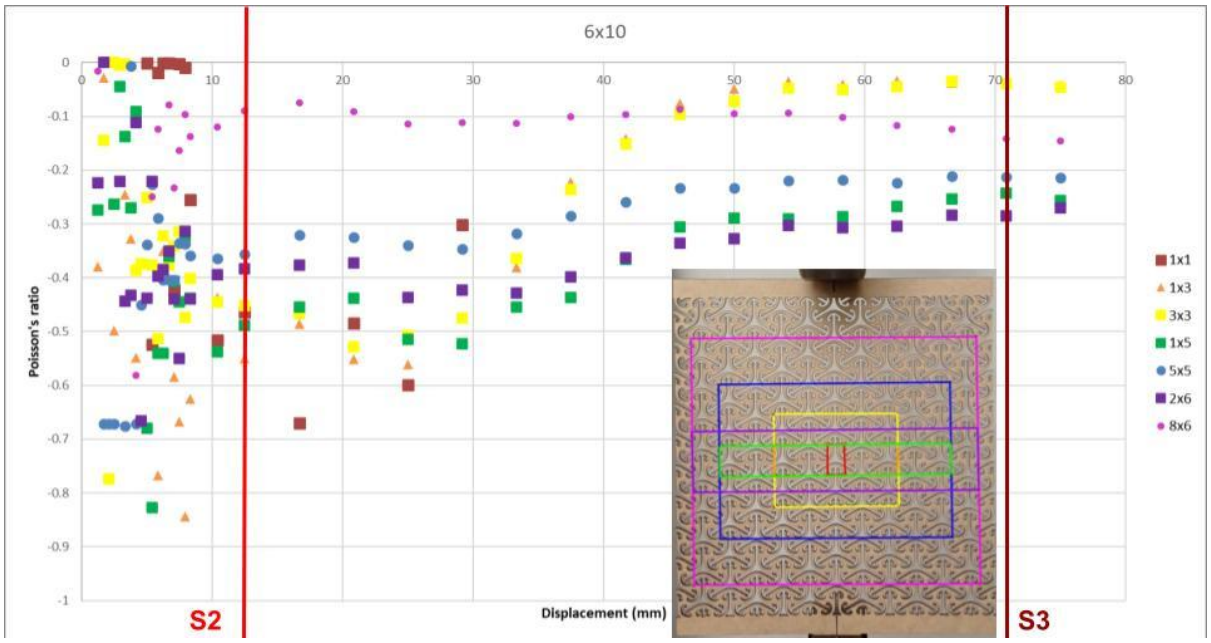

Figure 15 - Poisson's ratio changes over displacement for 6x10 grid size

3.3.4: Validation of the method

Overall, the outcome of the study found that the Poisson's ratio differs between the measurement regions for several reasons: being too close to the edge of the specimen and the unbound motifs, too small of a measurement region, and the region incorporating an uneven number of motifs in either the transverse or axial direction (Figure 12, Section 3.3.2).

Using these key points to find the most accurate Poisson's ratio of a particular auxetic, the desired measurement regions should be the 3x3 and 5x5 regions on the 6x10 tensile grid size. These regions are both away from the edge of the specimen, have a region size greater than one motif, and cover an even number of elements in transverse and axial directions. As the Poisson's ratio is calculated as a ratio of the dimension change within the specimen, the Poisson's ratio should be able to be determined irrespective of material. Thus, to validate the method, the Poisson's ratio will be calculated at S2 using a different material (solid fibre board using the 6x10 grid using the 3x3 and 5x5 regions.

For the comparison of the change in material for the same auxetic size, the Poisson's ratio is similar when comparing the e-flute to the solid board (Figure 16). This shows that the Poisson's ratio of the auxetic is influenced more by the geometry of the elements than the material properties. The results also show the method for finding an accurate Poisson's ratio of the auxetic is repeatable for across a different material.

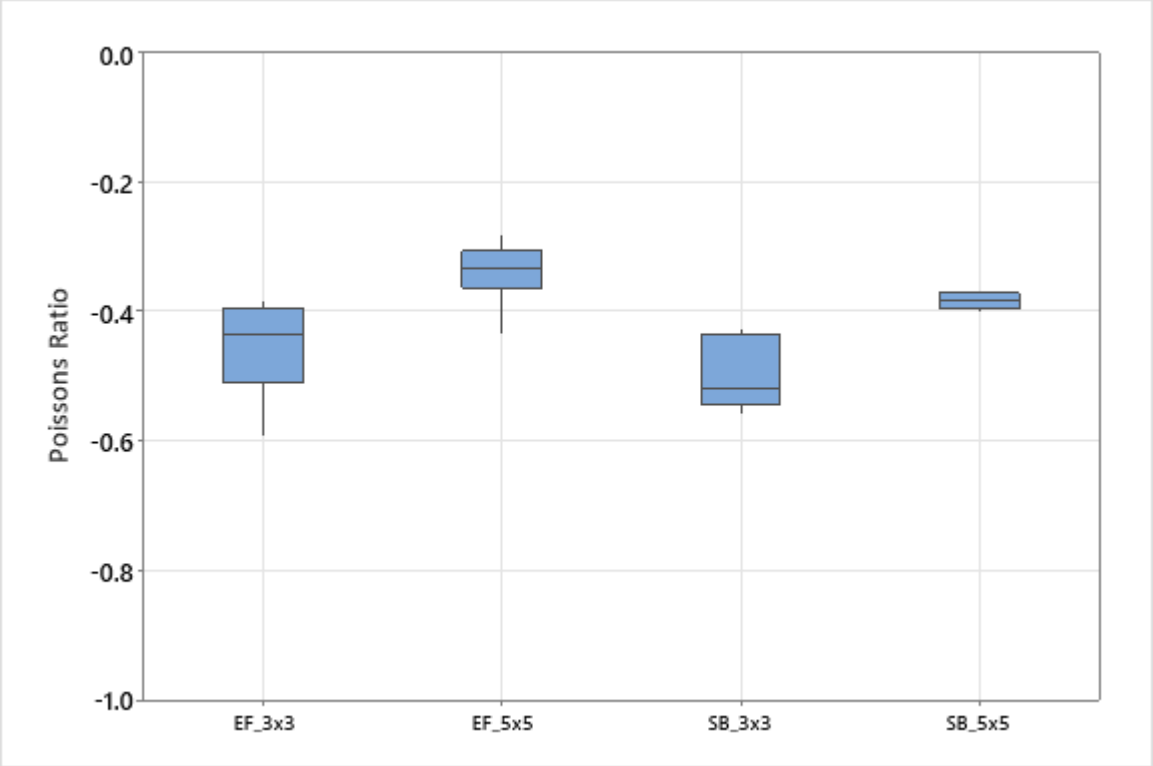

Figure 16 - Figure of the apparent Poisson's ratio of validation comparing materials. SB = Solid Board; EF = E-Flute; 3x3 = 3x3 measurement region; 5x5 = 5x5 measurement region.

3.3.5: Hinge Failure Points

The hinge failure points for each auxetic tensile grid size in Figure 17, Figure 18, and Figure 19 show the number of times the hinge broke across all 20 specimens for each grid size. The numbers located on each hinge in the figures show the first hinge to break for each specimen for all twenty replicates for each tensile grid size. The hinge break points appear to be relatively random in location but slightly away from the central elements. The sample size of 20 per grid size seems to be too low to make any clear conclusions on the main areas of high stress in the tensile specimens. Although the results are inconclusive, the main take away from this is that it shows a genuine failure in the auxetic than an edge case where the tensile grid was not large enough to adequately find a true maximum or a failure point.

Figure 17 - Hinge failure locations of 3x5 grid across twenty test replicates

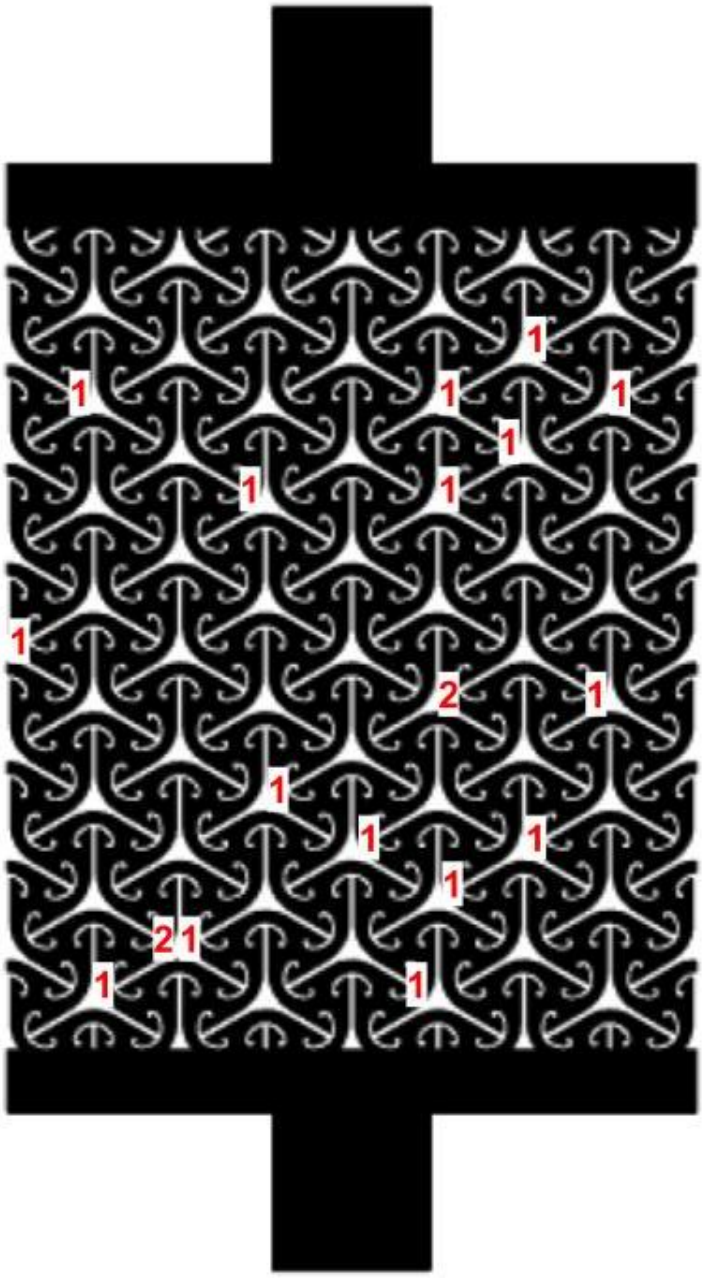

Figure 18 - Hinge failure locations of 4x8 grid across twenty test replicates

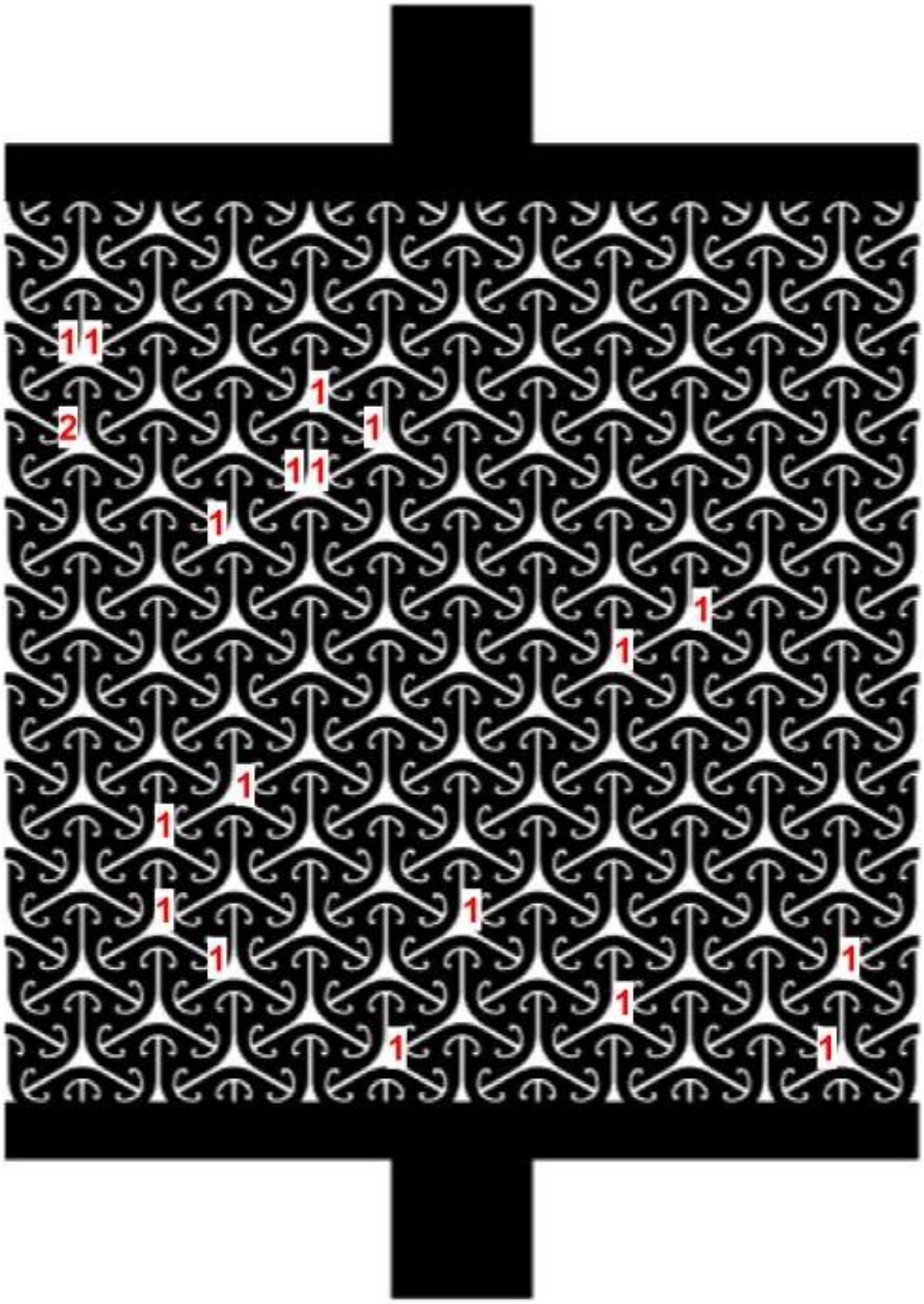

Figure 19 - Hinge failure locations of 6x10 grid across twenty test replicates

3.3.6: Out-of-Plane Behaviour of the Auxetic

The specimens exhibited out-of-plane displacement (Figure 20) during tension. This out-of-plane displacement was uniform and consistent between specimens and was caused by the twisting movement of the motifs. This out-of-plane behaviour begins in the plateau stage after S2 and becomes more apparent up until failure of the structure. It occurs along the central elements as the motifs are more restricted in transverse expansion than on the edge of the specimen, leading to the path of least resistance by the hinges buckling in the out-of-plane direction. This phenomenon was also noted by Wang et al. (2019), where they attributed the out-of-plane behaviour to a lower effective stiffness of the auxetic. This was determined through physical observations of the experimental tensile tests as well as shown by an increase in error between numerical and experimental results for Young's modulus as the effective stiffness decreased. This lower effective stiffness was attributed to auxetic geometric design and the stiffness of the material used. In the case of this study, this out-of-plane buckling is a consequence of a thinner hinge and wider mangopare radius for geometric contribution and the nature of the thin e-flute corrugated board or simply a change of material to the solid fibreboard (Figure 16). Overall, this phenomenon is likely due to the chiral structure of auxetics which allow out-of-plane behaviour when under in-plane tension (Attard et. al., 2018). This behaviour was noted but not fully investigated in this study.

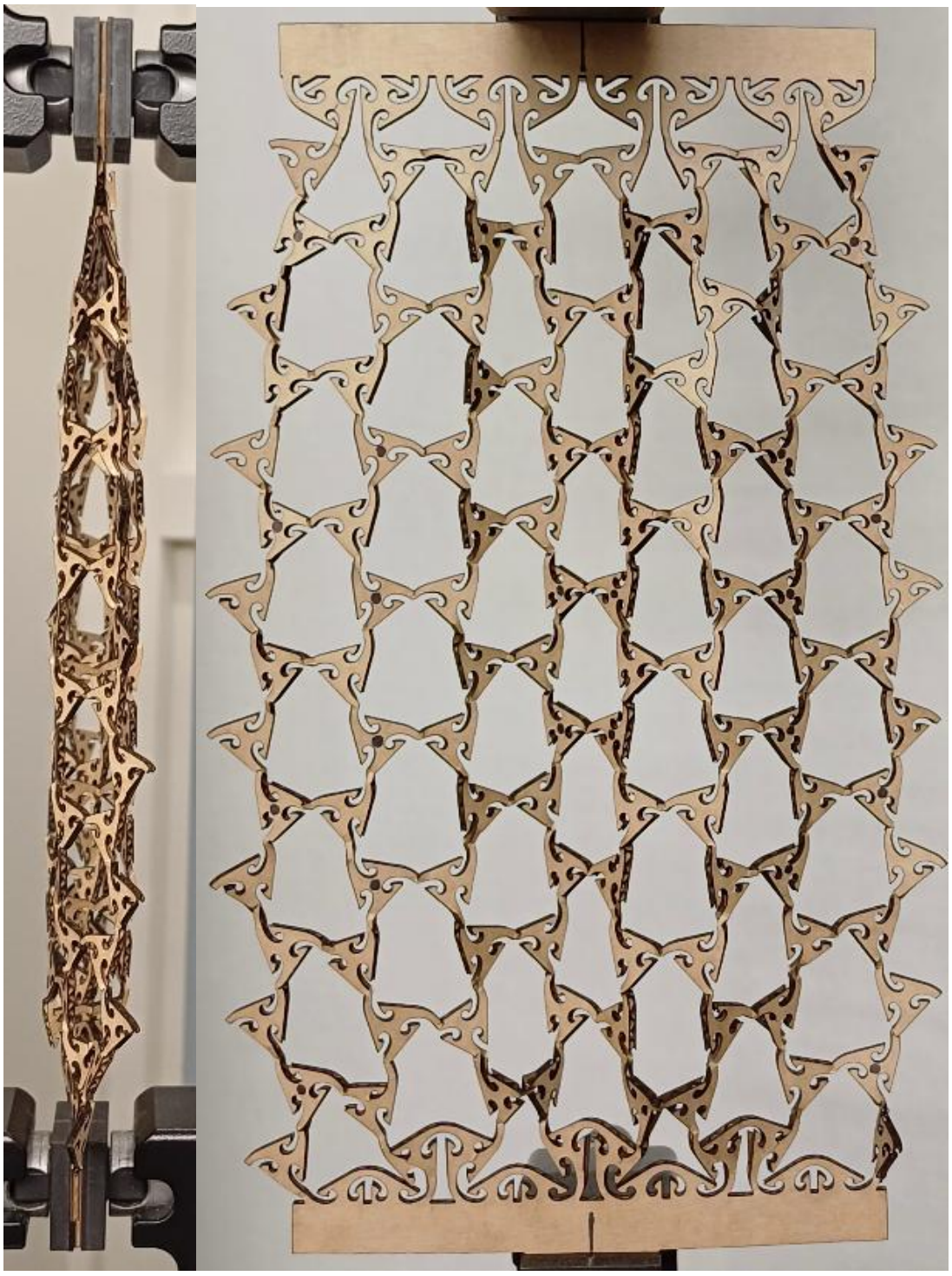

Figure 20 - Out-of-plane behaviour of the auxetic under tension. Side view (Left) and Front view (Right)

3.4: Conclusions

The aim of this chapter was to understand the characteristics of a 2D auxetic structure to help improve the methods used to determine the Poisson's ratio of these materials. It was observed how the Poisson's ratio changed with displacement and with selected measurement regions on the specimen. Several key conclusions can be drawn from the study.

The board orientation, which is often a significant variable in cardboard properties, was found to be an insignificant variable of influence on the stiffness of the board across all stages of the auxetics tensile loading. This is because the stresses within the auxetic are spread across all the hinges which do not coincide with specific locations of corrugations within the board. However, it is noted that E-flute board, the board with the smallest fluting, was investigated as opposed to another grade of corrugated board. A larger fluting such as A, B, C, and D may have a different impact, but was not explored.

The samples exhibited clearly defined stages that signify where the material is auxetic and at what stage the material becomes non-auxetic. This change in auxeticity could also be described by a change in the angle of the auxetics hinges past a certain angle. However, within these stages the Poisson's ratio stays mostly constant and thus leads to consistent identification of the Poisson's ratio within the elastic range of the auxetic.

The Poisson's ratio values of the auxetic varied with the selection of different measurement regions within the specimen. Although there is some general variation from the several regions measured, there are some trends that arise from changes in the regions measured. Regions on the edges that are close to the bound edges at the top and bottom of the tensile specimen yielded a higher (less negative) Poisson's ratio as the motif's hinges were far more restricted in movement. Measurement regions that incorporate an uneven number of motifs in either the lateral or longitudinal direction were also found to affect the apparent Poisson's ratio. This is because the elongation in each direction is greatest along the central axis of the tensile specimen, leading to a lower (more negative) Poisson's ratio when measuring a region that is larger latitudinally and a higher (less negative) Poisson's ratio with more longitudinal motifs.

When the measurement region was very small, there was high variation in results between the specimens. This is partially due to lower margin for error in measurement but could also be related to material inhomogeneity between specimens. Overall, this could still be a viable region size to measure numerically.

Overall, to ensure the accurate measurement of the Poisson's ratio for future literature in two-dimensional auxetic materials, a standardised method is important. For future work, irrespective of the type of 2D auxetic and constituent materials, using the key points determined in this study will help to ensure an accurate Poisson's ratio (3x3 and 5x5 regions). Alternatively, the trends in data observed in both this study and with Yolcu and Baba (2022) can help to show what regions one should measure to determine the most accurate Poisson's ratio for other materials and variations of the auxetic. Beyond the in-plane mechanics, the auxetic design should be tested in the out-of-plane direction to fully characterise the design to be used as a packaging solution.

Chapter 4: Creation of FEM

4.1: Introduction

Finite element models (FEM) are a widely used numerical method in research, offering efficient solutions for complex data calculations that would be time consuming experimentally. Advances in computational power and software have made FEM a practical tool for simulating diverse engineering problems, streamlining experimental validation, and optimising designs.

In pulp and paper research, FEM is applied across multiple scales in fibrous materials, from individual fibres to fibre networks, sheet structures, laminates, and corrugated boards, demonstrating its effectiveness in capturing interactions at various levels. In auxetic materials, FEM is crucial for analysing the impact of auxetic parameters on compressive and tensile strength in 2D and 3D applications (Alomarah et. Al., 2020, Ma, et. Al., 2022, Khare et. Al., 2018, Yolcu and Baba, 2022), as well as optimising deployable bistable structures (Chen et. Al., 2021). FEM enables extensive parameter sweeps to explore input-output relationships, reducing the need for physical testing and facilitating model validation and optimisation. Producing a numerical model involves complexities. Assumptions must be made to decide on the simplicity of the model, which can introduce some error to the model. The modelling of corrugated board material is complex due to raw material variability as it is biologically derived, is a composite structure, is orthotropic, has a non-linear stress-strain relationship, and is sensitive to environmental changes. It has been shown that CB can be conveniently modelled as a single lamina with the three orthogonal axes having homogeneous properties rather than creating detailed layers that depict the shape of the corrugation and its bonds to the liners on either side (Kueh et. al., 2012, Garbowski 2025). Additionally, auxetics drastically change the materials effective properties that they are applied to, so a convenient model of a single lamina would suffice for a simplistic model. Additionally, the complexities of the movement of auxetic structures in the 2D plane and when the material goes out of plane are difficult to compute, where a small error in an auxetic elements movement between experimental and the numerical approach can magnify to a larger change when calculated across a whole structure. Overall, a numerical approach

to auxetics is important to understand the trends in both the individual elements versus the overall movement of the structure.

In this study, the aim is to implement a model using the kōwhaiwhai auxetic design which can simulate the experiments shown in Chapter 3. The model will be used to extract the Poisson's ratio to compare with the experimental result. The overarching aim is to develop a foundational model that can be built on to explore the response of auxetic structures in further detail in terms of changes in the auxetics parameters to enable the optimisation of the kōwhaiwhai auxetic structure for packaging applications.

4.2: Model Development

4.2.1: Geometry and Material Properties

The auxetic design used in this study was kōwhaiwhai pūtoi koiora (auxetic kōwhaiwhai). The original design features the standard motif; 100 % scale; with a hinge thickness of 1.6 mm; and a mangopare radius of 1.1 rad; which will be the 'standard' design used in this chapter to quantify the Poisson's ratio numerically (Figure 7).

The tensile specimen sizes used in this numerical study will be the same as used in Chapter 3. Three different tensile grid specimens were used, 3x5, 4x8, and 6x10, which have dimensions of 82.0 mm x 83.6 mm, 109.3 mm x 130.9 mm, and 164.0 mm x 162.5 mm respectively. These grid sizes were used to show how the tensile model determines how the tensile grid sizes effect the resulting Poisson's ratios.

The material behaviour of the 2D auxetic structure under uniaxial tension was modelled using a linear elastic constitutive model in Comsol Multiphysiscs 6.1. This model assumes a linear relationship between stress and strain and is described by Hooke's law. Experimentally, this is the linear relationship that is observed before S1, as shown in Chapter 3 (Figure 8).

In Comsol, the linear elastic model was implemented by defining the material properties, Young's modulus, and Poisson's ratio in the materials settings (Table 2).

Table 2 - Material properties used in model. Obtained from Jamsari (2020).

Property used	**Value [Units]**
E_x (Young's modulus)	8630 [MPa]
E_y	3330 [MPa]
E_z	43.15 [MPa]
v_{xy} (Poisson's ratio)	0.1500
v_{yz}	0.0210
v_{xz}	0.0100
G_{xy} (Shear modulus)	2075 [MPa]
G_{yz}	95.14 [MPa]
G_{xz}	156.9 [MPa]
Board Thickness	0.0015 [m]
Board Density	780.0 [kg/m^3]

4.2.2: Model Assumptions

To create an efficient but also representative model of the auxetic under uniaxial tension, several assumptions must be made regarding the material behaviour, geometry, loading and boundary conditions, and numerical implementations. The material is considered homogeneous, with linear elastic behaviour through the deformation. The auxetic specimen has no micro defects in the single laminate material, or in the geometry of the auxetic with idealised element geometry. The tensile specimen is a two-dimensional model, neglecting any out-of-plane effects. The model applies a prescribed displacement at the top boundary while keeping the bottom boundary fixed. The stationary solver assumes a state of static equilibrium, meaning time-dependent effects such as inertia and strain rate sensitivity are not considered.

4.2.3: Mesh Generation and Element Selection

The finite element analysis was performed using Comsol Multiphysics 6.1 software to determine the tensile properties and deformation mechanisms of the auxetic with the

various tensile specimen sizes. The 2D geometry is generated using imported dxf files of the auxetic specimen that were used to laser cut the specimens in Chapter 3.

Firstly, convergence analysis was performed for different mesh densities to select the appropriate mesh size. Tetrahedrons elements having an element size greater than 3.4E-5 m were selected and the resulting finite element model for the kōwhaiwhai auxetic specimens consisted of the resulting elements and nodes (Table 3). The mesh study indicated that using finer elements was not consequential to the accuracy of the model, with changes in resulting von Mises stresses (and Poisson's ratio) < 0.5 % while increasing computing time by 34 % for the fine mesh.

Table 3 - Elements and nodes in Comsol models

Grid Size	Elements	Nodes
3x5	75560	43671
4x8	153593	88934
6x10	280459	162494

4.2.4: Tensile Test. Boundary and loading conditions.

Uniaxial tensile tests using Comsol Multiphysics 6.1 were created to mimic the experimental method used in Chapter 3 by simulating using a prescribed displacement method. The numerical study will use a stationary solver as the model assumes static equilibrium, where inertia and time dependent effects are neglected. A displacement controlled test was used in which the specified displacement was chosen to match the measured displacement observed in the auxetic elastic range in Chapter 3. The bottom edge was fully constrained (Figure 21) and the top edge of the specimens were subjected to a prescribed displacement (Figure 22) in the y-axis of 2 mm, 3 mm, and 4 mm, for the 3x5, 4x8, and 6x10 tensile grids, respectively. Past these displacements, is beyond the materials elastic range where the material behaves differently and was therefore not shown as the experimental data does not fit the numerical data past these points. The lateral edges were left free to capture the free lateral expansion of the elements.

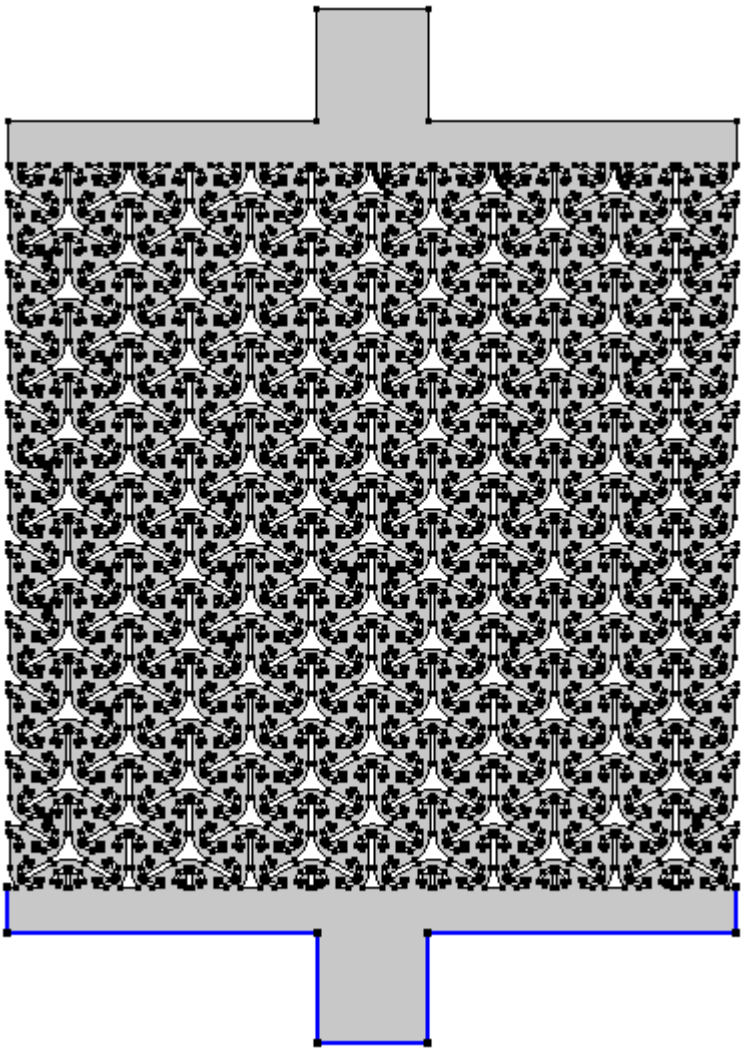

Figure 21 - Fixed constraint on bottom edge of auxetic

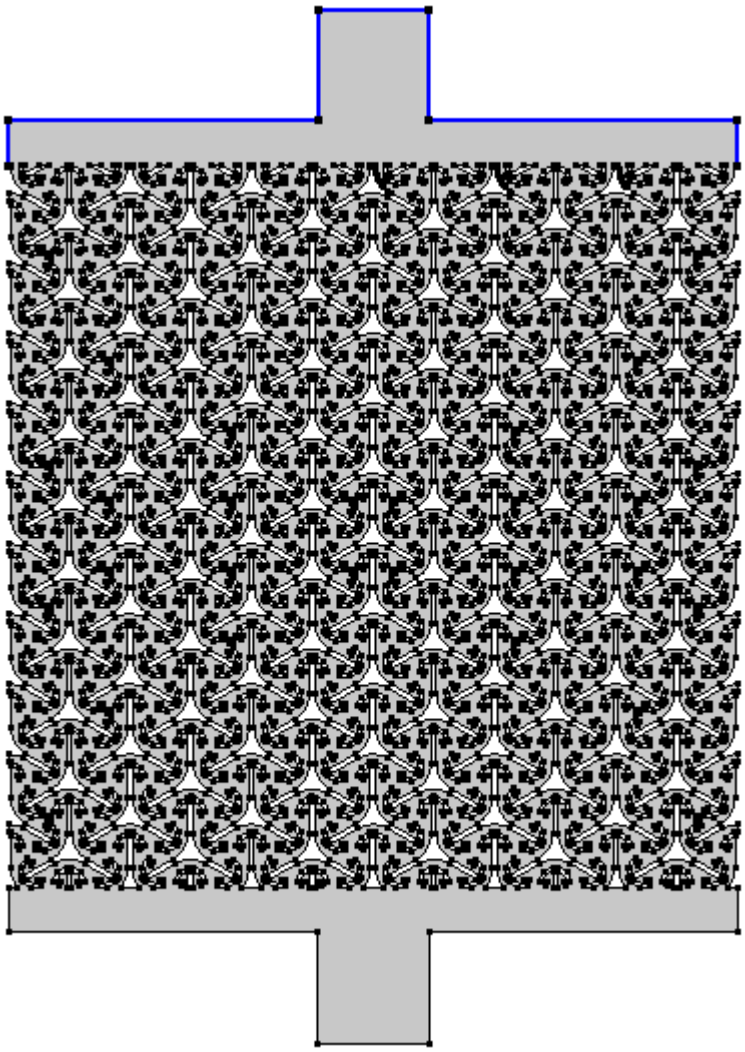

Figure 22 - Prescribed displacement on top edge of auxetic

4.2.5: Numerical solver and convergence

The model output was measured by following the same points as for the experimental setup for each tensile grid size to enable comparison of the Poisson ratio between each method, with three measurement regions for the 3x5, five for the 4x8, and seven for the 6x10 tensile grids. These measurements were determined by the displacement of points on the corners of these regions to then calculate the Poisson's ratio. Coordinates of the Comsol geometry are tracked using point probes that are then exported into a excel file for post-processing. The separated x and y coordinate displacements measured in the model for each point before and after the prescribed displacements to create the measurement regions used in chapter 3. These regions are used to then calculate the

Poisson's ratio values for each region and tensile grid size using Equation 2, Equation 3, and Equation 4.

Images of the auxetic are exported from the model and overlaid with the experimental images at the same displacement. These images can then be compared to assist discussion on the Poisson's ratio values.

For deformation and strain contour visualisation, Comsol's surface strain function will be used to obtain von Mises forces along with visualisation of these forces across the auxetic from the models output.

4.3: Results and Discussion

4.3.1: Predicted Poisson's ratio

The numerical model was created to understand the general trends that the model output when calculating the Poisson's ratio across measurement regions, grid sizes, and with varied material stiffness. Calculated Poisson's ratio data from the model showed a consistent trend with some of the conclusions drawn from the experimental data in chapter 3 which indicates that the model is a good fit to predict behaviour of the auxetic.

The Poison's ratio from the FEM for each region and grid size along with the average experimental results in both board orientations are shown in Figure 23, Figure 24, and Figure 25. The Poisson's ratio steadily increases (becomes less negative) as the region becomes larger. This trend occurs as the measurement region approaches the edge of the tensile specimen where the elements are less restricted in movement, leading to a greatly different Poisson's ratio compared to the same measurement region in a larger grid size, as these elements are now located more centrally and can expand within the structure.

However, for the regions for each grid size where the measured points of the regions are close to the restrained ends of the tensile specimen, the Poisson's ratio increases drastically. This is consistent with the results found in chapter 3, as the restrained ends of the tensile specimen do not allow for full auxetic expansion. This behaviour is also noticeable as the measurement region pairs which has tracked points that start along the same transverse widths but different longitudinal heights (more rod-shaped region than the square region) that are at this unrestrained edge of the auxetic specimen maintain a more consistent Poisson's ratio to the rest of the structure. This is because, as mentioned in the last point, these regions near the unrestrained edge of the specimen are free to expand in the transverse direction, while the largest region, closer to the rigid top and bottom ends of the tensile specimen, does not.

In terms of trends within the model, the central-most measurement region (1x1) shows the most consistency between tensile grid sizes, as well as matching the Poisson's ratio of the experimental results the closest. In comparison to the inconsistency of

experimentally measuring the 1x1 region, an accurate model will be able to predict the Poisson's ratio of the auxetic by using this region instead.

For the 6x10 tensile specimen size, and chosen measurement regions, 3x3 and 5x5, corresponding to the regions chosen in chapter 3, the model slightly underpredicts the expansion of the auxetic (20.5 % and 17.3 % change in Poisson's ratio, respectively), indicating that the model still requires some work to improve accuracy. However, the model matches the experimental data the best across all the measurement regions for the 3x5 tensile grid size (0.10 % to 3.80 % error). This could be due to a compounding effect of smaller errors, including out-of-plane behaviours that are not considered in the model, that are less noticeable at this smaller grid size but become more apparent for the 6x10 grid sizes. Table 4 shows the percentage difference between the model and experimental Poisson's ratio for each grid size and measurement region.

Overall, the model does predict the trends of the Poisson's ratio well for the auxetic and can even provide a relatively accurate Poisson's ratio value to be expected experimentally up until the tested behaviours of the elastic range of the auxetic. Further work would be needed to understand beyond this elastic range where the auxetic shows much greater out-of-plane behaviours, more damage to the structure at the hinges, and other complex movements.

Table 4 - Percentage error between model and experimental Poisson's ratio averages for each grid size and measurement region

	3x5	**4x8**	**6x10**
1x1	3.80 %	19.2 %	10.7 %
3x1	0.10 %	23.8 %	20.6 %
3x3	1.84 %	13.7 %	20.5 %
5x1		202 %	13.8 %
5x5		55.9 %	17.3 %
6x2			15.5 %
6x8			2.40 %

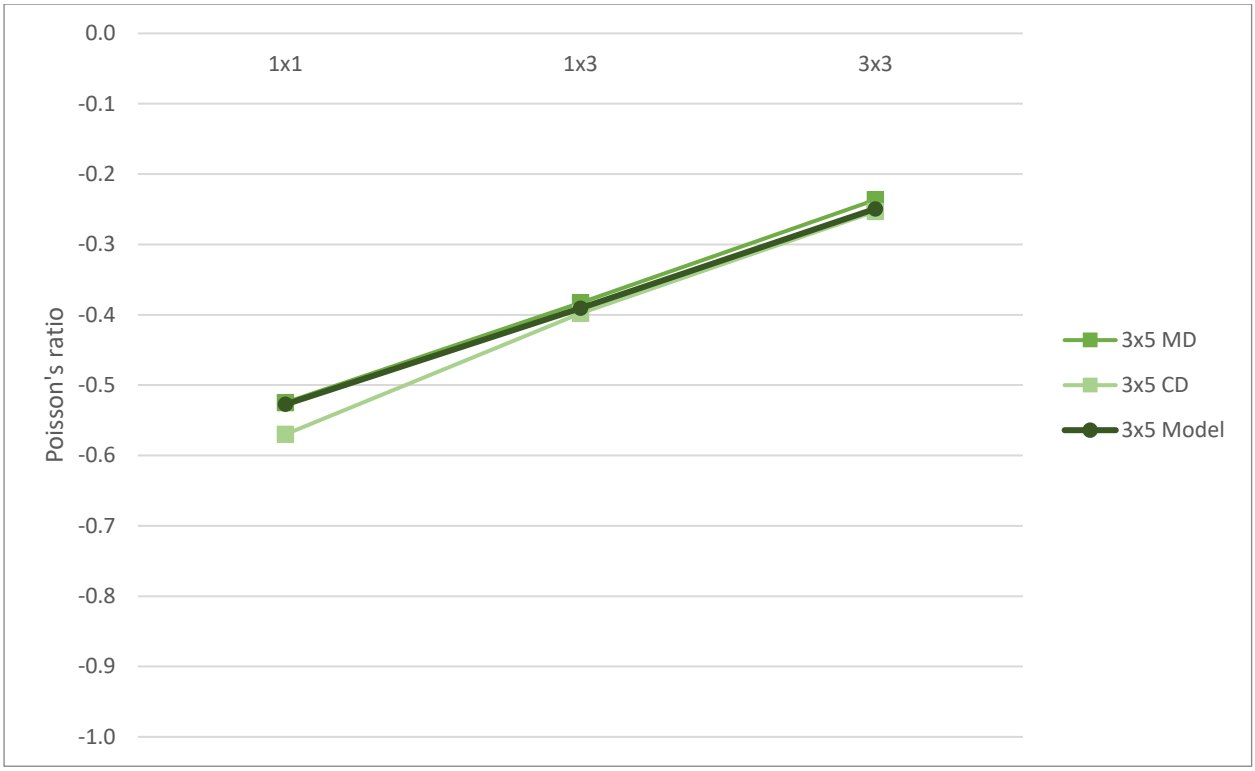

Figure 23 - Poisson's ratio of Comsol model and experimental results averages for 3x5 grid size.

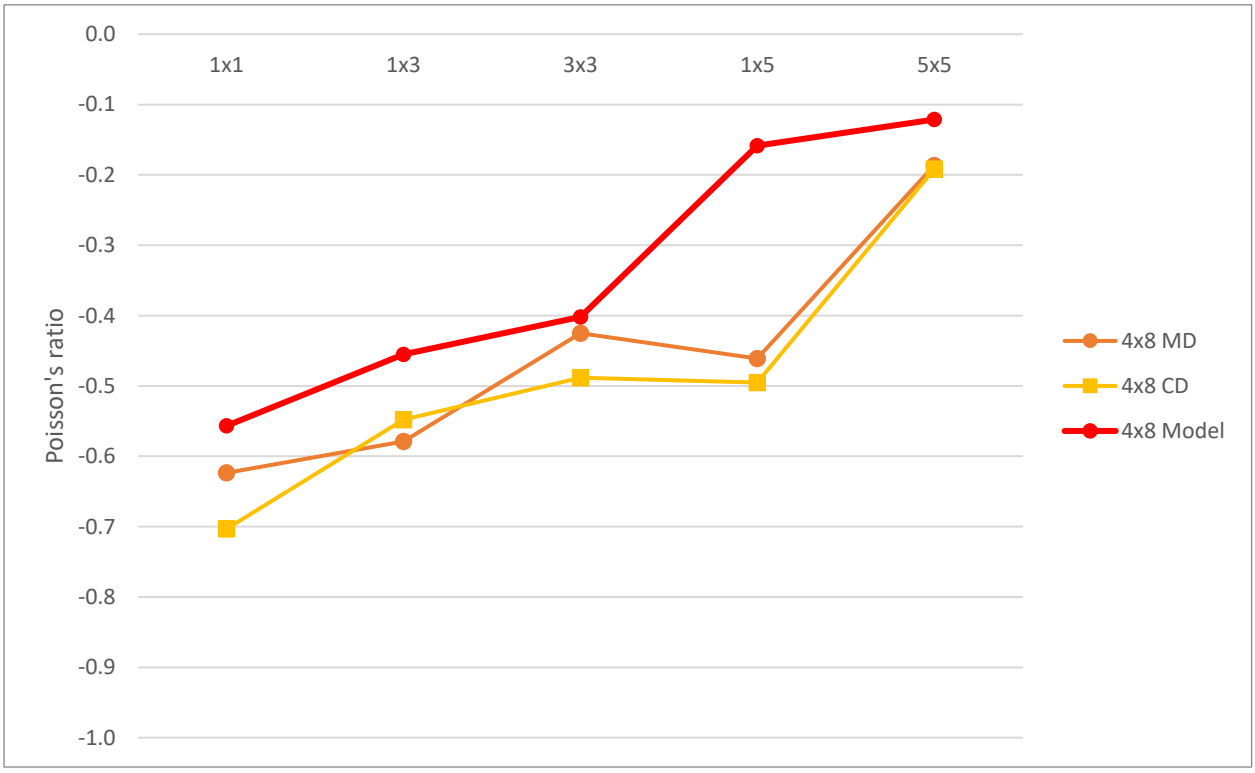

Figure 24 - Poisson's ratio of Comsol model and experimental results averages for 4x8 grid size.

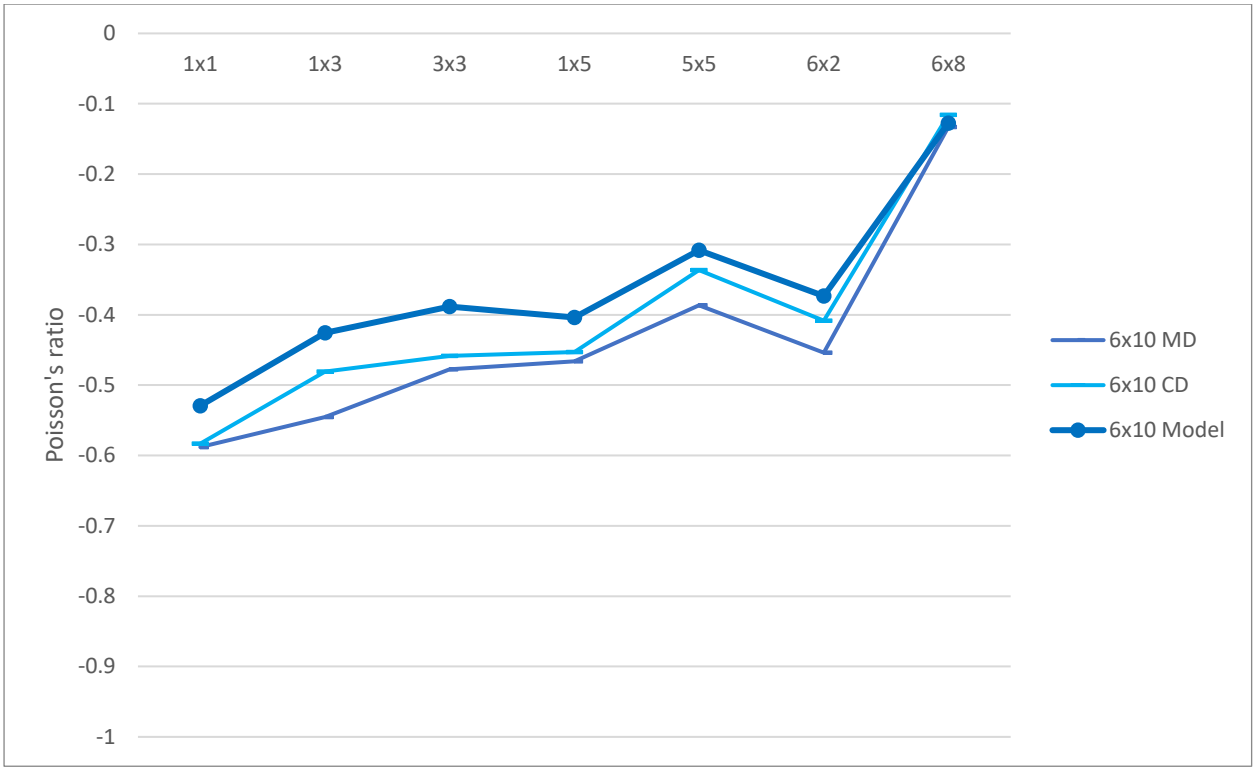

Figure 25 - Poisson's ratio of Comsol model and experimental results averages for 6x10 grid size.

4.3.2: Visual comparison between numerical and experimental results

To visually compare the numerical outputs to the experimental test results, video captures of the auxetic before and after the prescribed displacements are overlaid to understand how the model matches in expansion to the actual experimental work for all three tensile grid sizes.

When overlaying the images of the initial positions (Figures 7, 8, 9), the images fit reasonably well for all three grid sizes, with some error in matching the two images. The difference between the numerical and experimental images is due to a parallax error and possibly some lens distortion in the experimental imaging process. The specimens were placed very central of the lens to avoid distortion near the edges but there may be some parallax error. This is when the viewing angle of the image changes as you view from the centre of the image taken. So, although the image is taken facing the auxetic evenly, the viewing angle of the camera will marginally distort the view of the auxetic further out from the centre it looks. Since in the numerical approach, the extracted image is completely

straight on as if all parts are viewed at the same angle (no parallax error), the overlay of the two shows these slight discrepancies. This is also shown by the larger grid size (6x10) appearing to fit the initial overlay image much more poorly than the smaller grid size (3x5).

When comparing the images under tension the parallax error persists, but some clear conclusions can still be drawn from the differences between the model and experimental outputs. The model shows much greater in-plane expansion at the very edges of the auxetic than the experimental image after the same amount of displacement. The disparity in expansion is most notable on the lateral edges of the auxetic design where the unrestrained edges have the most motion. However, the similarity between each output is that this expansion is much greater through the centre of the auxetic than closer to the restrained tensile edges at the top and bottom of the specimen. Overall, as also noted in 4.3.1, the disparity between the experimental image and model output is much greater for the larger grid sizes than the 3x5 grid. This is a combination of the incremental errors for each element's expansion becoming more apparent at the larger sizes, but also due to a wider image required experimentally, leading to a larger parallax error.

Additionally, this much greater lateral expansion is due to the lack of out-of-plane expansion accounted for in the model (as mentioned in 3.3.4). As found experimentally, the path of least resistance naturally leads to the buckling of hinges causing this out-of-plane movement. The model, which only accounts for 2D movement, leads to the auxetic to continue to expand in-plane, leading to a different expansion path than observed experimentally. This does, however, show the potential for a more complex model construction which can account for out-of-plane deformation to provide a better understanding of the movement of the auxetic.

Figure 26 - Overlay of Comsol model (black overlay) and experimental images (background) for 3x5 grids at 0 mm displacement (left), and 2 mm displacement (right).

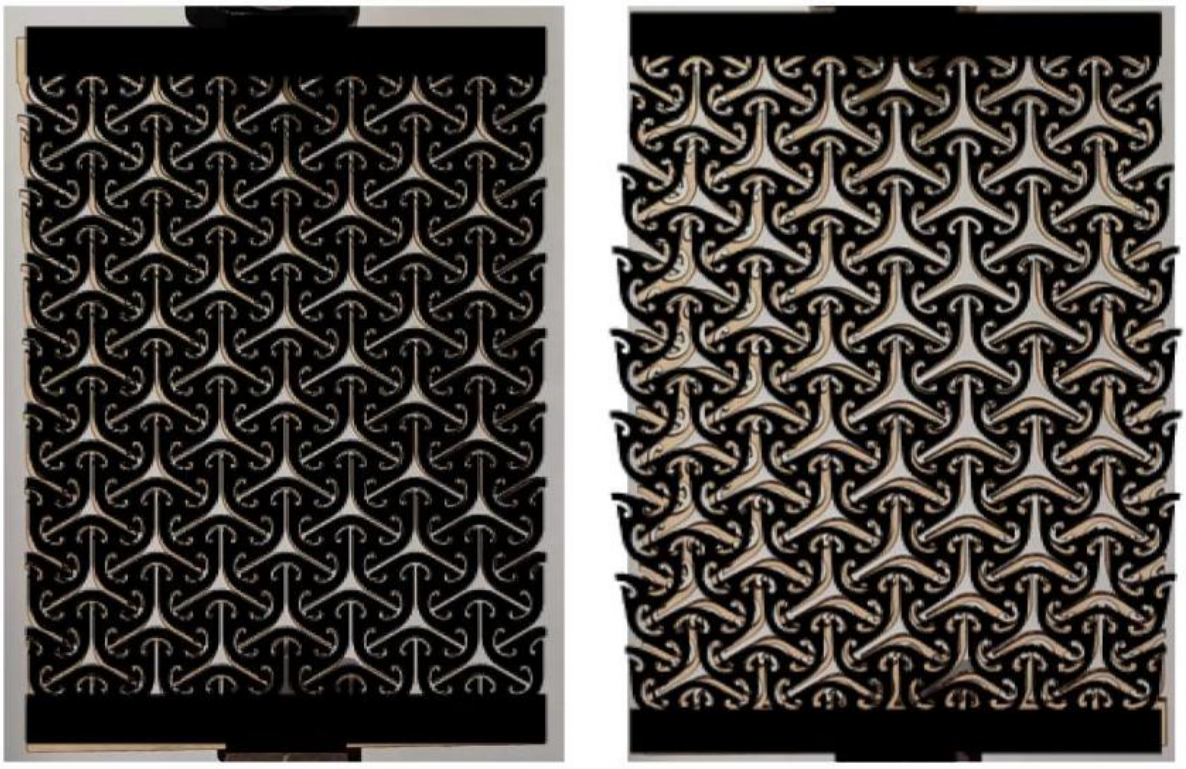

Figure 27 - Overlay of Comsol model (black overlay) and experimental images (background) for 4x8 grids at 0 mm displacement (left), and 3 mm displacement (right).

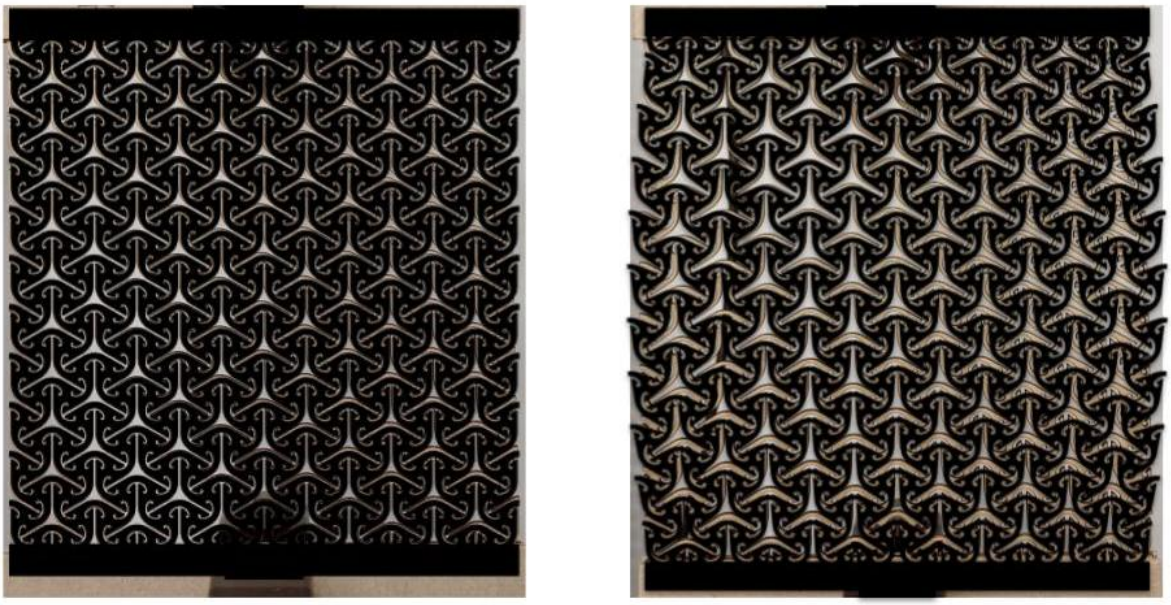

Figure 28 - Overlay of Comsol model (black overlay) and experimental images (background) for 6x10 grids at 0 mm displacement (left), and 4 mm displacement (right).

4.3.3: Stress distribution, Von Mises stress, and understanding material failure points

Understanding the stress distribution within the auxetic structure provides key insights into its mechanical response under uniaxial tension. While the exact stress magnitudes are influenced by modelling assumptions, the overall distribution patterns can reveal critical regions of high stress concentration, potential failure points, and load transfer mechanisms. This section examines the spatial variations in stress, highlighting trends that align with the expected deformation behaviour of auxetic materials.

The Comsol study of the uniaxial tensile test was conducted and used to generate stress contour plots that show the stress distribution across the auxetic structure. These contour plots show some key trends across different levels of the structures that make up the whole auxetic specimen.

At the individual element level, the stresses are distributed across the hinge (Figure 29 and Figure 30). The stresses at the hinges are highest at the narrowest point between elements, where the material is most flexible, but the distribution of the stresses is

influenced by the mangopare's smooth curve geometry that makes up the hinge distributes the forces more evenly than allowing for a higher stress concentration at a corner. These responses are similar to studies by Khare et. al (2018) and Meena & Singamneni (2019) where the curved hinges were found to reduce incidence of damage at the hinge damage and improved distribution of stress across the hinges, leading to reduced overall stress across the hinges, increased strain before failure, and more negative Poisson's ratios.

Across the whole structure, the stresses are lowest and equally distributed across centre hinges (Figure 29 and Figure 30) and gradually becoming higher towards the edges, both at the unrestrained edges in the x-direction, and the restrained edges by the top and bottom of the tensile specimen in the y-direction. This is because the restrained elements near the centre of the structure are connected on all sides, allowing it to move with the auxetic and distribute forces evenly on all side of the element. Whereas for the unrestrained edges, the expansion at these elements is greater, which leads to more twisting at these hinges, leading to a larger stress on these hinges. Hinges near this boundary experience stresses 1.3 to 1.5 times that than the hinges near the centre of the structure, while still distributing the forces across the hinge in the same way. For the restrained edge elements, the opposite effect occurs. The side of the elements connected to the ends of the specimen are unable to expand with the structure while the hinges restrained to other elements then take the stresses across the whole element into half of the hinges available, leading to higher stresses in these hinges. These hinges experience 1.1 to 1.3 times the stresses at the hinge than hinges near the centre. The stress distribution is also noted to be more skewed towards the ends of the mangopare radius of the auxetic element as opposed to more centralised with the central and unrestrained edge elements. This is shown across all tensile grid sizes but is most obvious with the 6x10 grid size as the difference between the edges and central elements is much greater.

Because of these slightly higher stresses across the outside of the auxetic specimens, it would be expected that the failure points are on the outside hinges in most cases. Although, this is only slightly higher, thus, with material inhomogeneity it would be

expected to have a distribution with some failures near the centres as well. These highest stress points are shown in Figure 29 and Figure 30.

In comparison to the experimental fracture patterns shown in 3.3.5 (Figure 17, Figure 18, and Figure 19) the fracture points appear to occur closer to the edges of the auxetic than near the centre which is consistent with the stress distribution of the model although the experimental fracture points are not conclusive due to the small sample size for a study purely on this. Overall, the model appears to predict the higher stress regions well, however, as mentioned previously, an improved model that accounts for the out-of-plane movement of the auxetic could help identify regions of higher stress more accurately to further the understanding of the kōwhaiwhai auxetic. Additionally, this could lead to models to predict the later stage tensile behaviour of the samples (shown in Chapter 3) to predict the actual failure of the auxetics. Understanding stress distribution provides valuable insights into the auxetic to suggest potential areas for geometric modifications that enhance durability and dissipating impact forces.

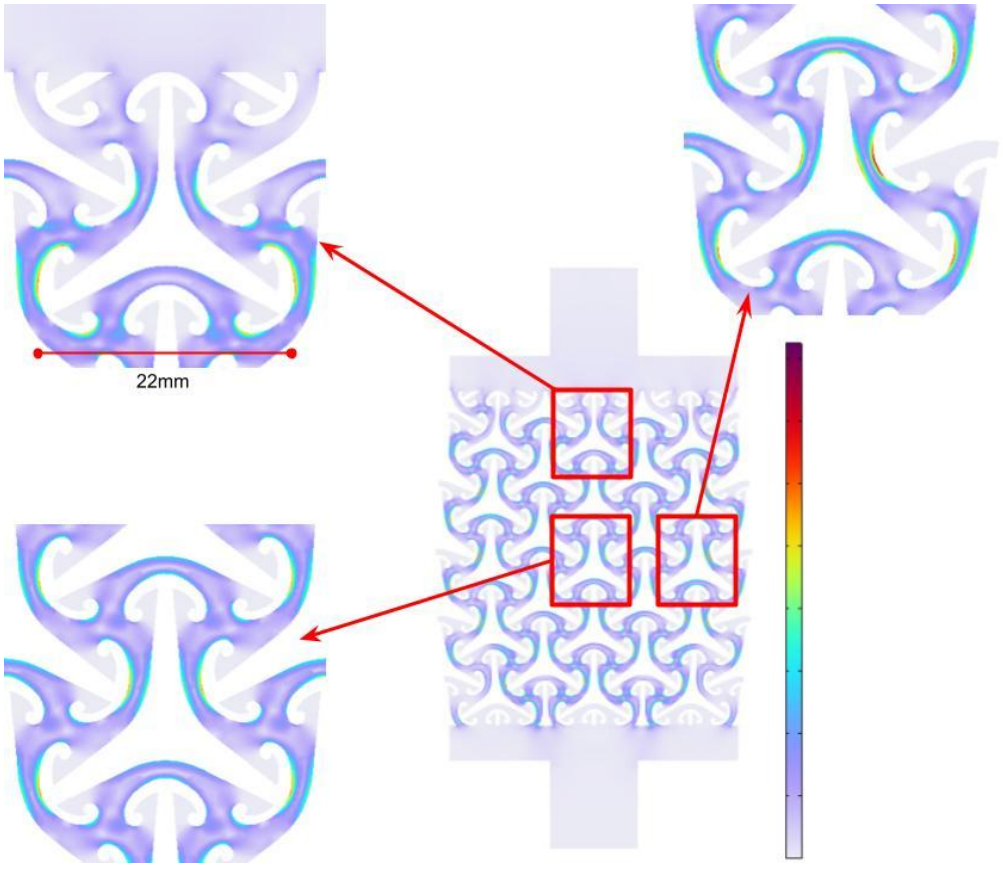

Figure 29 - 3x5 grid size element stress displacement at central element (bottom left), top edge of specimen (top left), and at the side edge of specimen (top right).

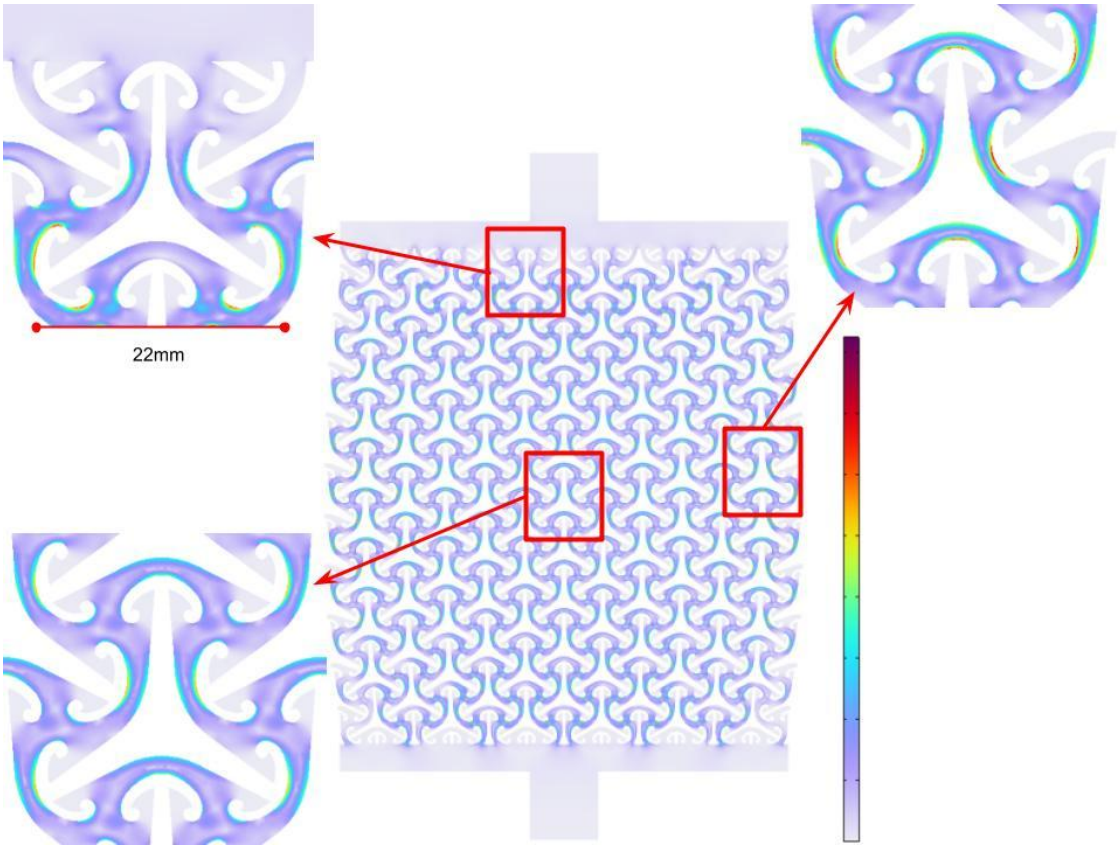

Figure 30 - 6x10 grid size element stress displacement at central element (bottom left), top edge of specimen (top left), and at the side edge of specimen (top right).

4.4: Conclusions

The FE model predicted the trend of the Poisson's ratio in relation to tensile grid size and measurement region reasonably well with differences between experimental groups in the model at 20 % error or less. Unlike the experimental situation shown in Chapter 3, the 1x1 measurement region was the most accurate region across all grid sizes for the model and the 3x5 grid size had a maximum error of 3.8 % across the three regions.

For the visual analysis of the Comsol model overlayed onto the experimental images at the same displacements, it was hard to make clear conclusions due to small errors in the imaging with parallax errors. The images matched the model reasonably well but the smaller errors become most obvious with the largest grid size. A better camera and lens system, that provides more options for controlling the image processing, could have been used to produce a more realistic comparison of the model to the actual experimental work by mitigating the parallax errors and lens distortion from the experimental images.

Stress distribution analysis showed several key trends of how the auxetic distributes stresses. At the auxetic element level, the most central hinges distributed stresses evenly across the hinge, and overall experienced reduced stresses than the outer-most auxetic elements due to boundary effects.

In comparison to experimental fracture points in the auxetic specimen tested, it was inconclusive if the model could accurately predict fracture patterns due to the reduced sample size but appeared to match the fracture pattern well from what was shown.

Overall, the model appears to provide a reasonable prediction of the trends of auxetic tensile tests and represents a sound basis for exploration of how changes in the auxetic, such as parameter changes, can be followed to optimise design choices to better understand the kōwhaiwhai auxetic used. The work could also be expanded upon further for out-of-plane models to fully show the shock absorbing ability of the auxetic material. Although this would require much deeper understanding of the mechanisms in place to maintain accuracy.

Chapter 5: In-Plane Tension of Kowhaiwhai Auxetic Structure Under Variable Humidity

5.1: Introduction

The protection of perishable goods in the supply chain is a key to reducing waste. Given the mechanical and environmental stresses packaging is exposed to, testing of the material under various conditions is important to assess performance. Additionally, understanding how different parameters influence design can help to optimise the design for key aspects of performance.

The properties of hygroscopic materials such as cardboard and other paper-based materials is greatly influenced by moisture content. Coffin (2009) writes that the mechanical response of paper materials is time, moisture, and temperature dependent. More specifically, there are significant alterations to the material's properties above 70% relative humidity (RH) (Allaoui et al., 2009; Fadiji et al., 2017). A study on relative humidity's effect on three different types of board by Strömberg (2016) found that at 90 % relative humidity, the tensile stiffness of the materials dropped to about half of the original stiffness measured at 50 % relative humidity. De Ruvo et. al. (1976) saw similar results for various handsheets tested at 90 % relative humidity. Carson (1944) also shows that the tensile strength at failure of eleven different fibre-based materials dropped by 30 % at 85 % relative humidity.

Auxetics are mechanism-based metamaterials that consist of an array of repeating elements created through the connection of a series of flexible hinges in between the elements that allow for low-energy motion within the auxetics elastic state. These elements have high tunability that allows for the optimisation for various beneficial properties. Whether the changes allow the elements to exhibit bistable properties for deployability (Chen et. Al., 2021), dispersing hinge stress concentrations through s-shaped hinges (Khare et. al, 2018; Meena & Singamneni, 2019) or simply changing internal angles and hinge sizes of the elements to obtain greater material stiffness (Cheng et. Al., 2019; Gu et. Al., 2020), auxetics have continued to show this tunability across many different element designs.

For packaging solutions, this tunability can be used to adapt packaging materials to the varying conditions encountered throughout the supply chain. The kōwhaiwhai auxetic design on corrugated board explored in this study provides an opportunity to examine how such materials perform under humid conditions. While it is expected that fibre-based auxetics would be affected by high humidity, existing literature has not described the behaviour of these designs in such environments. Given the proven effectiveness of tuneable parameters in other auxetic designs for influencing tensile properties, the kōwhaiwhai design could potentially be optimised to achieve a desired stiffness under humid conditions.

Additionally, work completed in Chapter 3 showed how the kōwhaiwhai auxetic was largely unaffected by change in board orientation, which normally shows a clear mechanical difference in corrugated board (Allaoui et al., 2009). If an auxetic can alter the behaviour of the material such that key parameters of the material itself become insignificant, could this also be true for external variables that are known to impact the material such as moisture and humidity?

This chapter aims to investigate the influence of humidity on the properties of the kōwhaiwhai auxetic cellulose based materials. When testing the auxetic tensile specimens, conclusions can be drawn to show how the fibre-based auxetic strength decreases under high humidity as would be expected with fibre-based materials (Allaoui et al., 2008; Fadiji et al., 2017). However, using the auxetic tensile specimen in previous chapters will show both the effect of humidity on the auxetic geometry and the material the auxetic is cut into. To best differentiate between two different tensile testing specimens, one must consider the impact of various design choices.

For example, varying gauge length of standard tensile dog bone specimens will impact the apparent properties of the material. A shorter gauge length will give higher elongation readings, and the necking region will occupy a much larger proportion of the specimen. This will impact the tensile energy absorption and tensile strength of the specimen at and around the maximum force reached until failure, but strain will remain uniform during the elastic deformation stage. In a similar way, the width of the tensile specimen effects the necking region and elongation measurements past the maximum force during tension (TAPPI T494, 2022b). For the purposes of the present study, this will become less

impactful as properties are only observed during the elastic range. Overall, to best compare the effects of humidity on the auxetic specimens, dog bone specimens will also be used to show how the material itself is affected by a change in humidity and compared.

There is currently a paucity of published data quantifying how humidity impacts the performance of an auxetic structure applied to paper-based materials. If auxetics are to be used in packaging, it is critical to understand how these materials are affected under various humidities as packaging is often subjected to a range or humidities across the supply chain. Therefore, the objective of this study was: (a) to show the tuneable parameters of the auxetic and how they affect the tensile properties; and (b) to examine the relationship between the stiffness and elasticity loss, and moisture content of different types of fibre-based auxetics; in order to (c) show if and how it may be possible to tune the auxetics parameters to counteract a reduced stiffness from high humidity environments.

5.2: Experimental Method

5.2.1: Kowhaiwhai Pūtoi Koiora Design and Specimen Manufacturing

This chapter investigates how changes in the kōwhaiwhai auxetic parameters, as seen in chapter 3, influence the tensile properties of the auxetic.

Due to the large number of specimens required to complete a full factorial exploration changing the three auxetic parameters, a partial factorial experimental design was used. This covers all high/low combinations between hinge thickness and radius at high and low scale values and using high, middle, and low scale values with central hinge thickness and radius values. A representation of the partial factorial design is shown in Table 5. This experimental design produces eleven different specimen variations. Ten replicates were tested for a total of 110 specimens.

To examine the relationship between the auxetic motif parameters and changes in humidity, and how they influence the material properties, a regression analysis on the stress-strain and image analysis data was performed using Minitab 21.3 (Minitab, LLC.,

2021). The models were evaluated for assumptions such as linearity, and normality of residuals, and appropriate transformations were applied where necessary.

Note:

Scale -1 = 70 %, 0 = 100 %, 1 = 130 %

Hinge Thickness -1 = 1.1 mm, 0 = 1.6 mm, 1 = 2.1 mm

Radius -1 = 0 rad, 0 =1.1 rad, 1 = 6 rad

Table 5 - Chapter 5 experimental design

Scale	**Hinge Thickness**	**Radius**
0	0	0
-1	-1	-1
-1	-1	1
-1	1	-1
-1	1	1
-1	0	0
1	-1	-1
1	-1	1
1	1	-1
1	1	1
1	0	0

Two different commercial fibreboards were selected for this study. The materials used in this study was manufactured from E-flute cardboard (65E CL) (CB) and solid board (SB) The corrugated board is used for both the change in auxetic parameters and change in humidity experiments while the solid board is only used for changes in humidity. Auxetic specimens were created through laser cutting the cardboard sheets using a Makerspace G640L Genesis laser cutter to produce the complex geometry of the auxetic samples. The settings used to cut CB and SB were 15 mm/s laser speed and 45 % laser power and 22.5 mm/s speed and 75 % power respectively.

5.2.2: Tensile Test of Auxetic Material

Uniaxial tensile tests were conducted using an Instron 5982 machine equipped with a 500 N load cell. The tensile tests were conducted with the bottom side of the specimen fixed with the top side moving at a constant machine crosshead speed of 25 mm/min. The study in Chapter 3 showed the change in board orientation was insignificant in changing tensile properties of the auxetic. Because of this, the tensile tests were only conducted in the cross-direction of the corrugated board.

The corrugated board and fibreboards cross-directions was chosen over the machine-direction as this is typically the board direction at which the influence of moisture content is most profound in typical tensile testing of the material (Rhim, 2010; Büyüksarı et al., 2011). Thus, if there were to be an influence of moisture content on the auxetic, it would be most significant in this direction and represent the worst-case scenario for the study.

This work investigated the elastic properties of auxetic specimens within their elastic range of deformation to determine the desired properties. Images were captured of the specimen at multiple points in the elastic range (Figure 31) and were used to determine the Poisson's ratio of the auxetic.

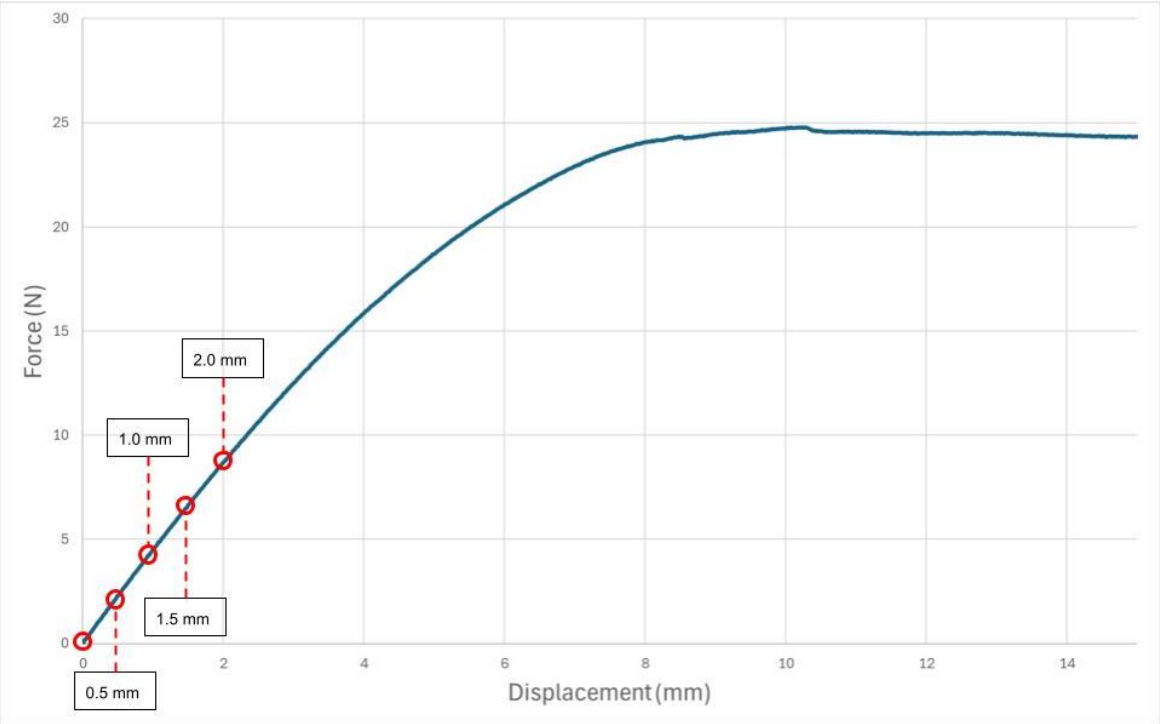

Figure 31 - Stress-strain curve of auxetic showing elastic region. Marked points showing the imaging analysis points used to calculate the Poisson's ratio.

5.2.2.1 Tensile Test of Dog Bone Specimen

Dog bone tensile specimens were produced from cardboard and solid board. Dimensions of the dog bone specimen were a 15 mm testing width with a 180 mm gauge length, and uniaxial tensile tests were conducted using both materials (CB and SB) in the two-plane directions (machine direction (MD) and cross direction (CD)) for ten replicates each (TAPPI T494, 2022b; Aboura et al., 2003).

To best quantify the change between the auxetic tensile and dog bone tensile specimen, the percentage change in stiffness when humidity was increased from 50 % to 95 % was calculated. Deviation range of the percentage change were also calculated using upper and lower quartile ranges. Despite this correlation using a percent change, the way that the auxetic reacts at the hinge level will potentially not be equivalent to the dog bone specimen. The calculation aims to provide a partially correlated comparison between the material and auxetic value irrespective of the differences in tensile specimen.

5.2.3: Pre-Conditioning Tensile Specimen

To determine how humidity affects the in-plane properties of the cardboard auxetic, the specimens were pre-conditioned such that the material was at the desired moisture content for testing. Overall, the experimental design included four different humidity variations and two material variations. Ten replicates of each were tested for a total of 80 specimen for this part.

A control (low) humidity of 50 % RH was used. The specimen was also pre-conditioned at higher humidity in a controlled chamber to reach humidities of 75 %, 85 %, and 95 % RH. All samples were conditioned to 23 ˚C. These humidities were chosen to represent a range of humidities that would be expected within the supply chain as fruit and other perishable goods are often stored at high humidities up to 95 %.

Specimens were transferred as quickly as possible from the high humidity chamber into ambient conditions to immediately conduct the tensile test. As the specimens were removed from the high humidity atmosphere for less than a minute before the completion

of the test, it was hypothesised an insignificant amount of moisture is lost (TAPPI T494, 2022b). To ensure this is loss is insignificant, sample auxetic specimens of SB and CB were measured for percentage moisture loss at regular intervals from 95 % relative humidity to ambient over a twenty-minute period.

Figure 32 shows the relative humidity of the material over time for each material. In the first minute, it is shown the effective relative humidity drops by 1.6 %. When considering the loss of moisture due to surface moisture loss and not the moisture within the main structure of the material, the difference in moisture content between replicate specimen is 5 % or greater, and that the time to test the specimen will be less than one minute. This loss of moisture is deemed to be mostly insignificant because the average RH % of the specimens will be greater than 93 % relative humidity upon completing the test. Using this principle, any specimens that took longer than 90 seconds to test were immediately removed from the dataset and replaced with another specimen.

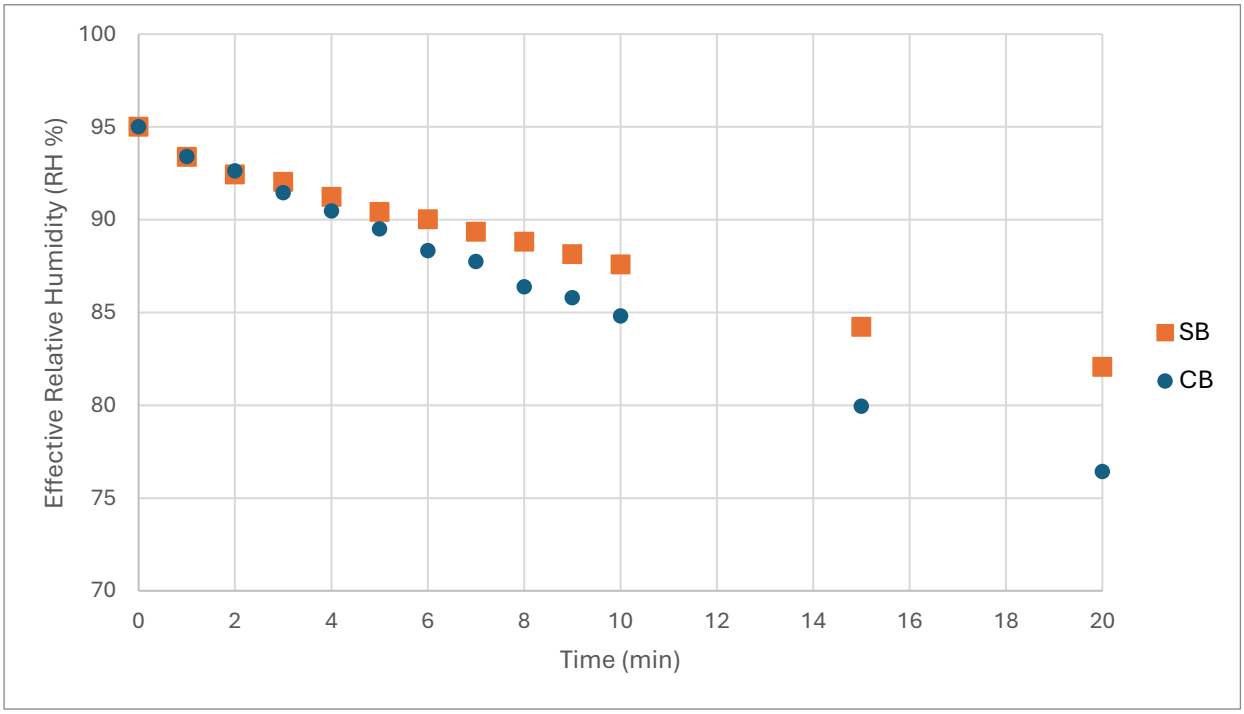

Figure 32 -Effective relative humidity percentage over 20 mins for both CB and SB

5.2.4: Image Processing Analysis

To determine the Poisson's ratio, two measurement regions, 3x3 (Yellow) and 5x5 (Blue) regions, determined in Chapter 3 and following similar methods to Yolcu and Baba

(2022), were chosen to find the most consistent Poisson's ratio within the auxetic structure. These regions were selected to include an even number of motifs in each in-plane direction and measure regions more central in the tensile specimen to avoid invalid measurements attributed to the edge of the specimen.

The measurement regions were videoed and transferred to a personal computer for further imaging analysis using Kinovea using the methods outlined in 3.2.3. The software converts a known length to a certain number of pixels in an image such that the marked target points on the specimen can be traced to determine the dimensions each marked area after testing. Then, by comparing the dimensions of the specimen at each key stage, axial and transverse strains, and the Poisson's ratio were calculated using the equations 1, 2, and 3, outlined in Chapter 3.

5.3: Results & Discussion

5.3.1: Impact of each parameter on the auxetics tensile properties

Young's Modulus

Partial factorial of changes in the three parameters (scale, hinge thickness, and radius) of the auxetic were tested at standard temperature and humidity. A boxplot (Figure 33) summarises all these variations as their respective boxplots versus Young's Modulus. The boxplots show overall a low variability within the motif design and clear changes in Young's modulus for each change in parameter. One grouping of specimens, -1.1.-1 (low scale, high hinge thickness, low radius), showed unusually high observations for Young's modulus compared to all other specimens and this was picked up in the regression model as an outlier. When excluded from the analysis, the output can account for 12 % more of the variation than when these values were included.

The linear regression model found all three parameters to have a significant impact on the output Young's Modulus with p-values <1e-12 for all parameters and t-statistics > 1.98 on the Pareto charts. Scale has an inverse relationship with Young's modulus and accounts for 21.6 % of the statistical models variation. As the size of the individual elements within the auxetic material decreases, the force to displace the same distance increases as the smaller elements must expand further for their relative size.

The hinge thickness is the parameter that most significantly affects the Young's Modulus of the auxetic material, accounting for 41.8 % of the model's accuracy and showing a linear relationship. Increasing hinge thickness increases the stiffness of each element, leading to an overall stiffer structure during expansion and contraction.

Lastly, the radius of the motif also has an inverse relationship with Young's Modulus and accounts for 13.4 % of the model's variation. The larger radius allows for greater dispersion of force along the hinge of the auxetic structure, reducing stiffness of the structure. Other studies utilising auxetics with fatigue-lowering element design (Khare et. Al., 2019; Meena & Singamneni, 2019) found that the energy dissipation not only was reduced across each hinge but also allowed for more even dissipation of the forces between elements within the whole structure, leading to more uniform expansion and contraction. Although also shown by a reduced stiffness during the tension of the auxetic,

it was also noted that the designs with the wider radius did not exhibit as much out-of-plane deformation (mentioned in 3.2.2) and appeared to expand and contract more evenly across all elements.

When highlighting the extreme values of Young's Modulus in Figure 34, -1.1.-1 and 1.-1.1 (YM = 17.70 and 0.45 respectively), the parameter values are opposite and follow with the linear regression model relationships of each parameter. The values do not appear to follow along a linear path past the central parameter value (0.0.0) and the residual plots for the model overall signify non-linearity in the material response to parameter changes, showing that the model is not completely accurate for the data. Non-linearity is common for biomaterials and should be understood for accurate model creation. Further investigation of these non-linearities is out of scope but could be beneficial in terms of creating a model to optimise such parameters for a desired output.

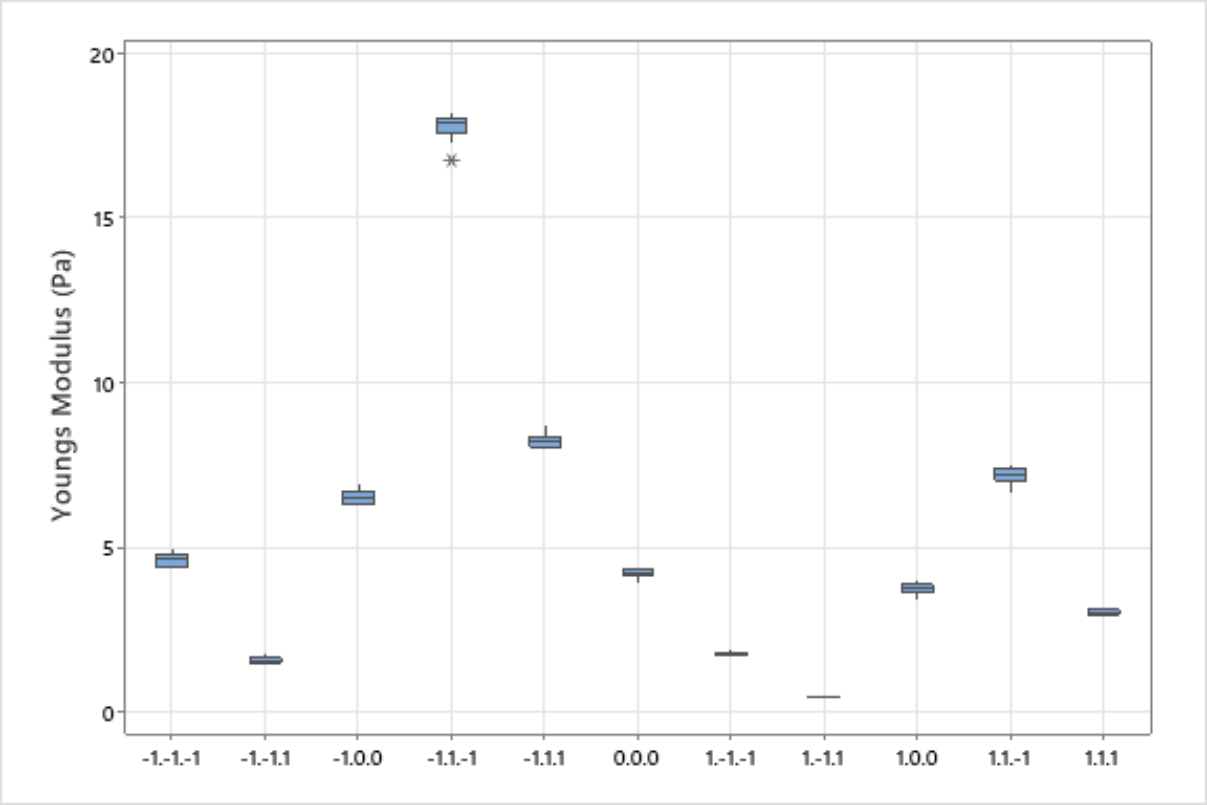

Figure 33 - Boxplots of Young's modulus versus change in motif parameters denoted by X.X.X (Scale.Hinge.Radius). See 5.2.1 for more information.

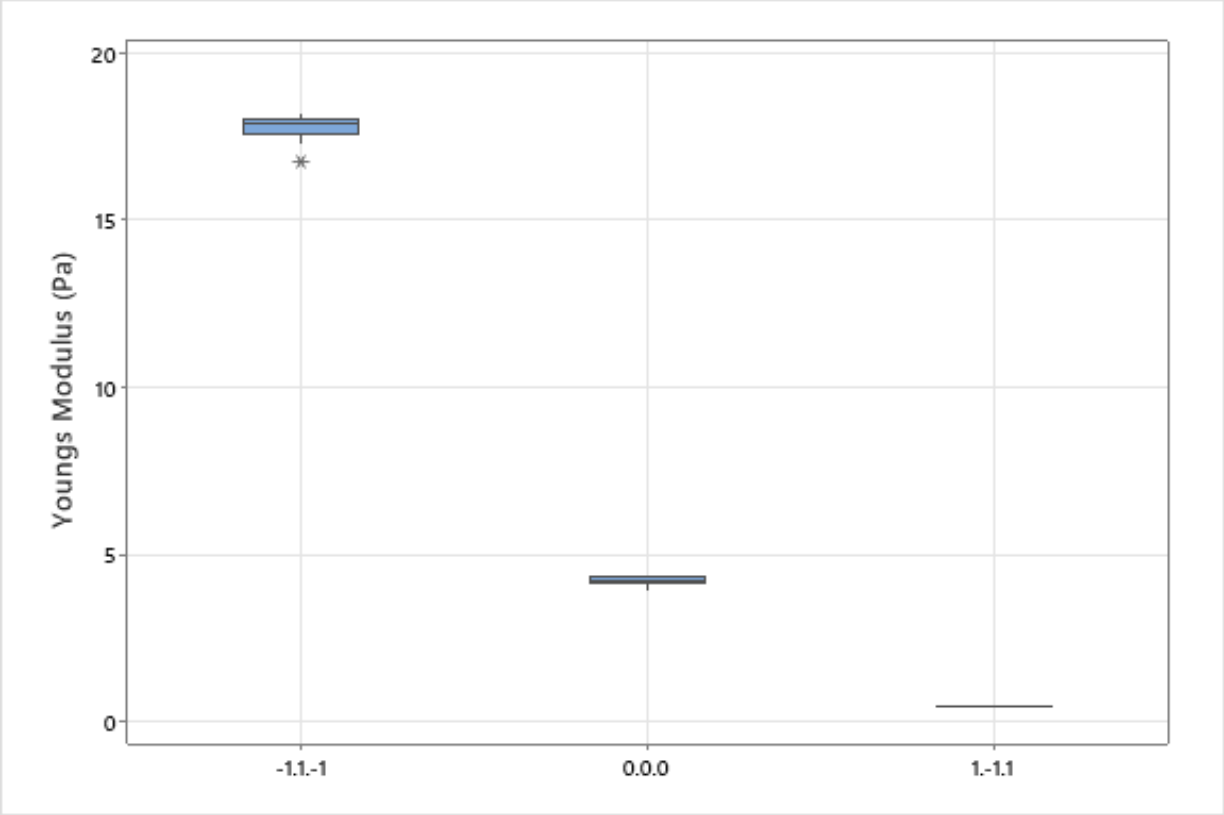

Figure 34 - Extremes of Young's modulus with motif changes. -1.1.-1 (70% scale, 2.1 mm hinge and 0 rad) showing highest modulus and 1.-1.1 (130% scale, 1.1 mm hinge and 6 rad) with lowest modulus.

Poisson's Ratio

Figure 35 describes how changes in the kōwhaiwhai motif parameters affect the Poisson's ratio of the material. The variance within a group is much greater in terms of Poisson's ratio than when comparing Young's modulus of the same specimens. This is because the error from the image analysis causing large variation in some of the Poisson's ratio measurements. Despite this higher error, the linear regression model can still draw some conclusions. It found that the scale and hinge were significant factors in the model while the radius was insignificant in effecting this measurement.

The scale of the elements has the greatest effect on the Poisson's ratio of the auxetic structure, with an inverse relationship, and accounting for 29.3 % of the variation in the model. As the scale of the elements decreases, the Poisson's ratio increases (less negative). This is partially due to a change in the microstructural effect on each individual

fibre versus the geometric shape of the whole auxetic changing. When the scale decreases, while the hinge and radius stay the same, the microstructural effect of the fibres in the hinge of the auxetic impact the individual element slightly more, leading to a slightly stiffer overall structure which reduces the amount the auxetic expands and contracts, reducing the Poisson's ratio. This will be why the effect is more significant at the lower scale than at the higher scale as at the higher scale, the effect stays more geometric than being impacted by microstructures, leading to a similar Poisson's ratio as the geometry is even throughout the material.

The hinge also has a significant proportional effect on the Poisson's ratio, accounting for 8.5 % of the model variation. The thicker hinge being less able to deform at the hinge would reduce the geometric effect of the auxetic and could be argued that the hinge is tearing before fully expanding. Thus, as the hinge thickens, the ability for the auxetic to expand is reduced and therefore marginally increasing (less negative) the Poisson's ratio.

The radius of the motif is the final parameter and is found to have no significant influence on the Poisson's ratio of the auxetic. This is because the radius is a good distributor of force but has little influence on the geometry of the individual elements, leading to no measurable influence on the Poisson's ratio.

Overall, the residual plots for the models overall do not show any significant pattern or non-linearity, showing that the model is appropriate for the Poisson's ratio data.

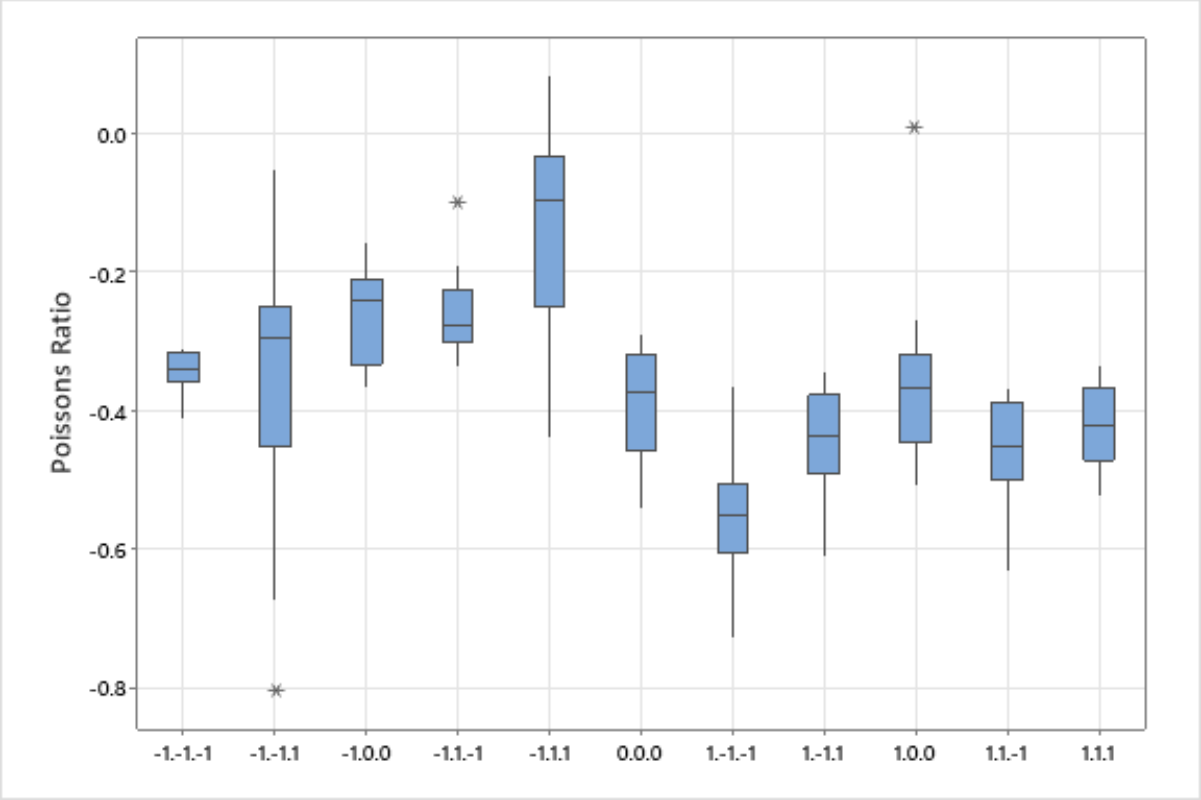

Figure 35 - Boxplots of Poisson's ratio versus change in motif parameters denoted by X.X.X (Scale.Hinge.Radius). See 5.2.1 for more information.

5.3.2: Impact of humidity on tensile properties

Young's Modulus

Young's Modulus versus a change in relative humidity for the standard element design (0.0.0) are shown in Figure 36 and Figure 37 for CB and SB respectively. The regression model shows a change in relative humidity has a significant effect on Young's Modulus of the material, with a 98.1 % and 96.8 % model fit for CB and SB, respectively.

Although the data shows a clear influence of relative humidity on stiffness, it does not decisively show whether this is due to the known influence of moisture on fibre-based materials or if the auxetic is also affected by a change in relative humidity. To directly compare the impact of humidity on a standard material test and an auxetic test is complex to quantify. However, to best quantify this change, dog bone tensile specimen of corrugated board and solid boards were produced and tested to determine the

percentage change in the stiffness of the specimen when humidity is increased from 50 % to 95 % relative humidity.

Dog bone tensile tests of the corrugated board and solid board during the elastic range of tension show consistent patterns with what would be expected. Stiffness was higher in the cross direction versus machine direction for both materials and the solid board showed a much higher stiffness than the corrugated board.

Comparison of percentage change in stiffness during the change of relative humidity for the dog bone specimen shows an average change of 58.7 % and 52.9 % for CD and MD respectively for CB with an overall average of 55.8 %. For the solid board, this is 57.7 % and 44.3 % for CD and MD respectively. Data presented by Strömberg (2016) and De Ruvo et. al. (1973) supports these findings, where across all materials tested, the stiffness was reduced by 50 % at 90 % relative humidity in the cross-direction, with slightly more stiffness retained in MD (35-45 % reduction). Although this work is done at a higher relative humidity comparison (95 %), the supporting data shows that the stiffness is greatly reduced past 90 % relative humidity and that the stiffness reductions shown in this study are reasonable. The findings also appear to be reasonable compared with theory on fibre bonding and fibre orientation with moisture. Moisture absorption causes delamination of the fibres, leading to poorer performance that would be most impactful for fibres oriented perpendicular to the force applied, the cross-direction.

In comparison to the auxetic percentage decrease of 61.9 % and 57.6 % for CB and SB respectively. This shows there is a slight difference in the calculated values for the standard material versus the auxetic at high humidities, meaning that the auxetic could be impacted by a change in relative humidity. However, Figure 38 and Figure 39 show the relationship between the auxetic and material percent change in stiffness for both materials where the deviation of each boxplot overlap, in addition to a p-value of 0.29 and 0.36 for CB and SB respectively. This shows that the percentage change from an increase in humidity is insignificant when comparing the standard material testing versus the auxetic of the same material. The auxetic is not significantly affected by a change in humidity but the if material that the geometry is a part of is influenced by this change.

From the experimental data and correlation calculations made, it can be inferred that there is reason for the insignificant change in between standard material testing and the auxetic when under higher humidity. There are many factors at play that could influence the small change, one of which may be a greater microstructural effect from more negative space within the material. The cardboard at which the auxetic is cut from, the auxetic has a far greater amount of negative space than in the solid board. The auxetic itself uses this to provide many impressive properties but also relies on the small hinges that connect the material to absorb all the strain on the material. As the negative space within the tensile specimen increases, assuming the same average fibre length and quality within the material, the stress on each fibre increases. Thus, when the auxetic is compared to the material itself, the microstructural effect at the hinge plays a larger role versus the geometrical effect of the whole tensile specimen. Therefore, when the material is under stronger environmental influence, such as an increased relative humidity, the stiffness of the structure could be impacted more.

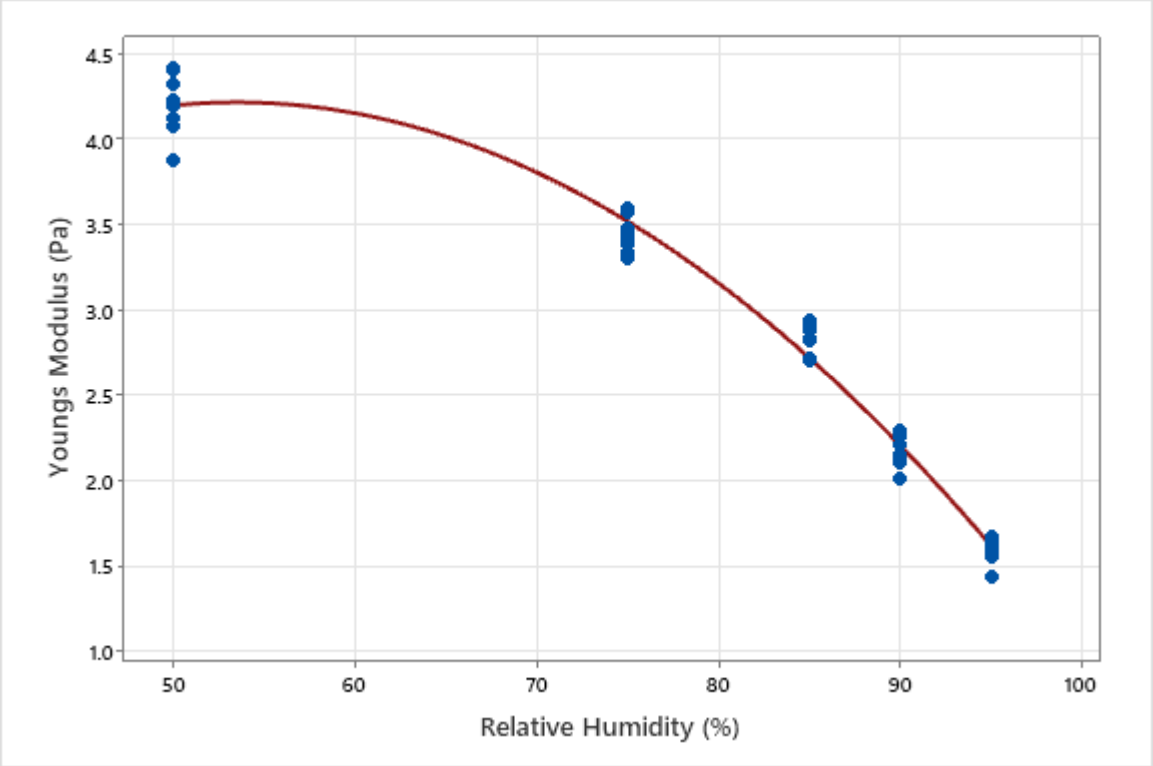

Figure 36 - Young's modulus versus relative humidity for corrugated board

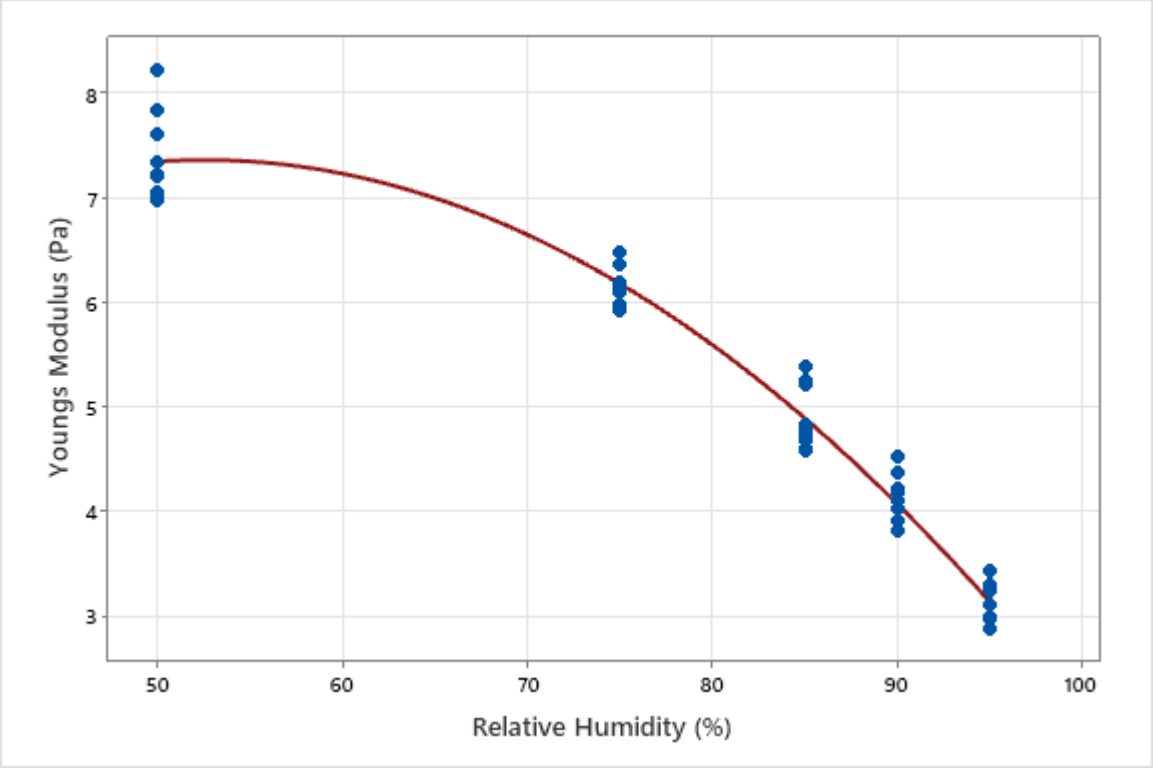

Figure 37 - Young's modulus versus relative humidity for solid fibre board

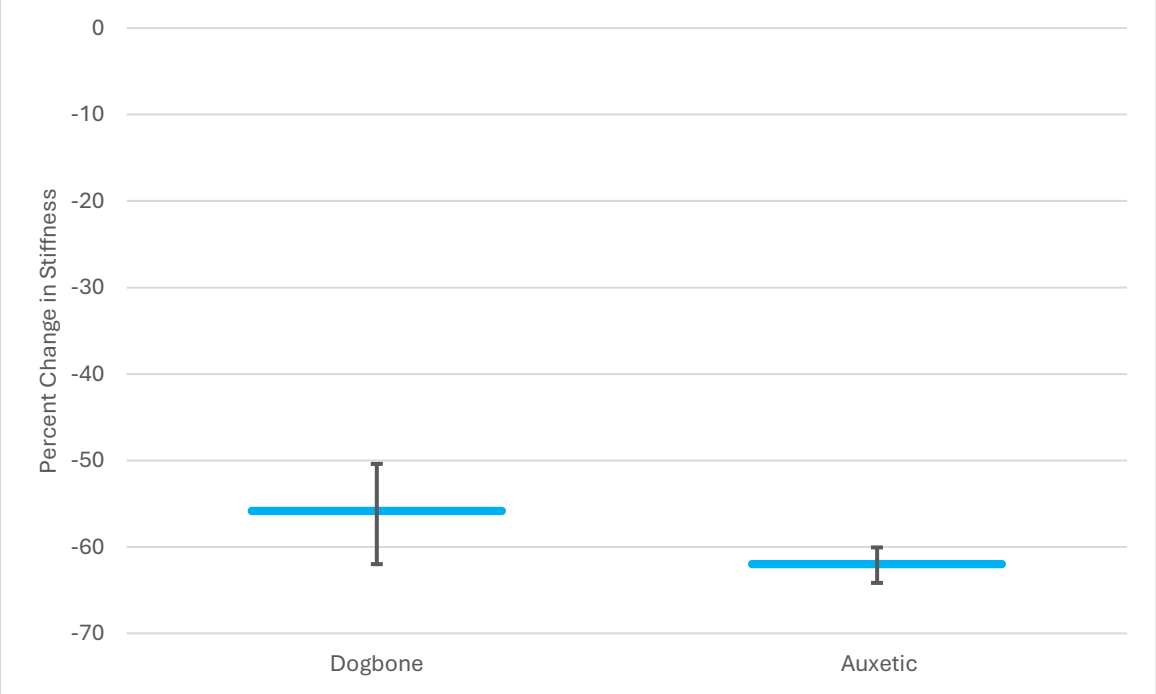

Figure 38 - Stiffness decreased percentage from 50 % Rh to 95 % RH for CB

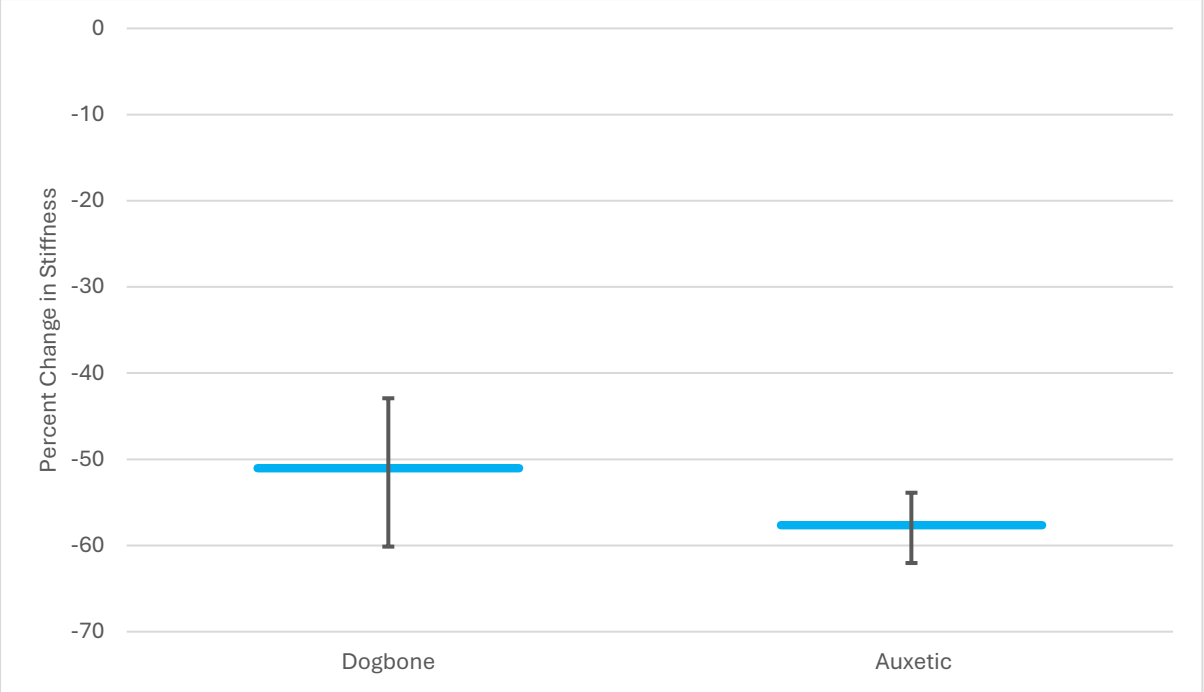

Figure 39 - Stiffness decreased percentage from 50 % Rh to 95 % RH for SB

Poisson's ratio

For the Poisson's ratio, there appears to be no clear change in Poisson's ratio as relative humidity increases for the auxetic. This is shown by the high variation between specimen and high crossover between boxplots at each increasing relative humidity. This is also signified by an insignificant p-value of 0.70 in the regression model. The residual plots for the regression model do not show any significant patterns or non-linearity, showing that the data and model are appropriate for each other. This outcome makes sense for the Poisson's ratio because as the humidity changes, the material is in equilibrium across the whole material, meaning the ratio of expansion and contraction stays constant even if the overall strength of the material is weaker.

5.3.3: Offsetting impact of humidity by changing parameters

All three parameters of the kōwhaiwhai auxetic are shown to have an influence on the stiffness of the material. Additionally, the fibre-based auxetic was shown to significantly decrease in stiffness, up to 177 %, under high humidities that would be expected during distribution through the supply chain. Despite this substantial decrease in material

stiffness at these operating humidities, an aim of the study is to show how the auxetic can be adapted to maintain the structural integrity.

The hinge thickness of the auxetic was found to be the most influential parameter of the material, accounting for 42 % of the variation in the model. To show the effect of a parameter change, just the thickness of the hinge was changed for auxetics at high humidity and compared to the standard hinge thickness of 1.6 mm at 50 % and 95 % relative humidity using the e-flute corrugated board.

Figure 40 shows the stiffness of three hinge thicknesses at 95 % relative humidity. The data follows a clear linear path and regression analysis shows high model fit with an r-squared value of 98.9 % as well as a continued high relationship with a change in hinge with a p-value < 0.05. The residual plots for the models overall do not show any significant pattern or non-linearity, showing that the model is appropriate for the data.

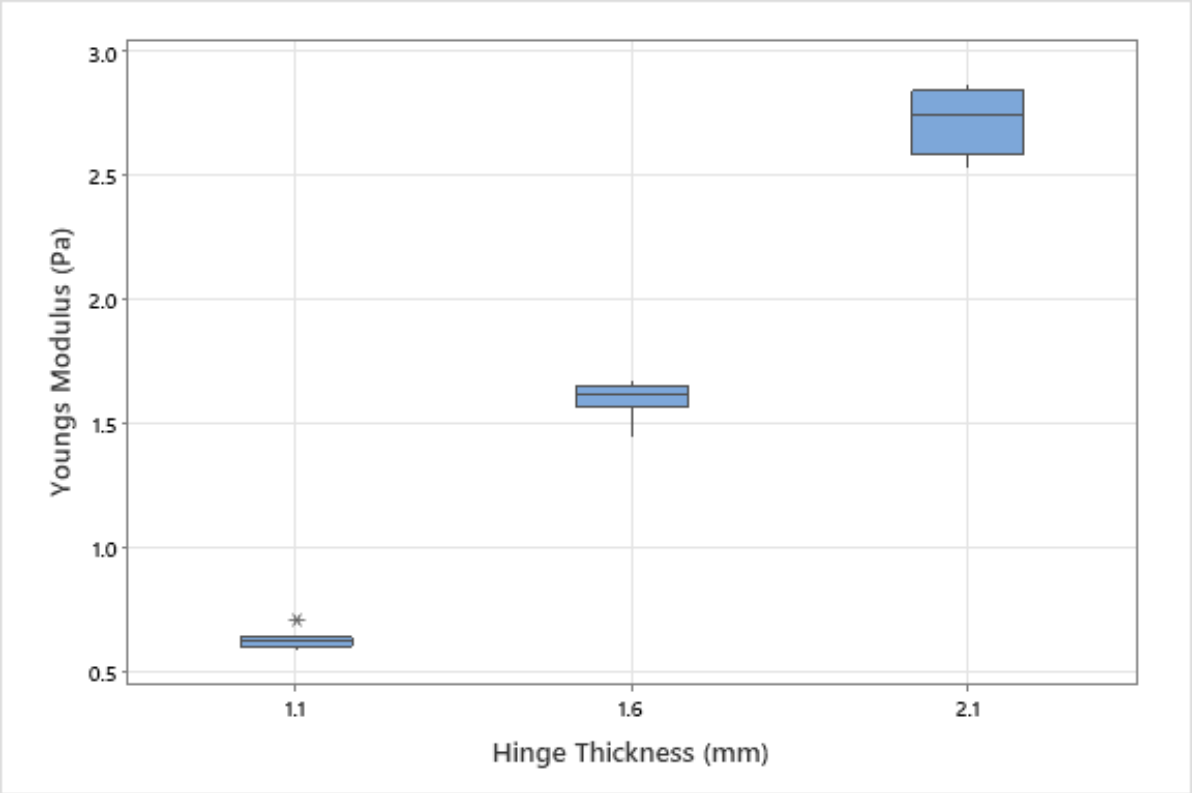

Figure 40 - Effect on Young's modulus from a change in hinge thickness @ 95 % RH

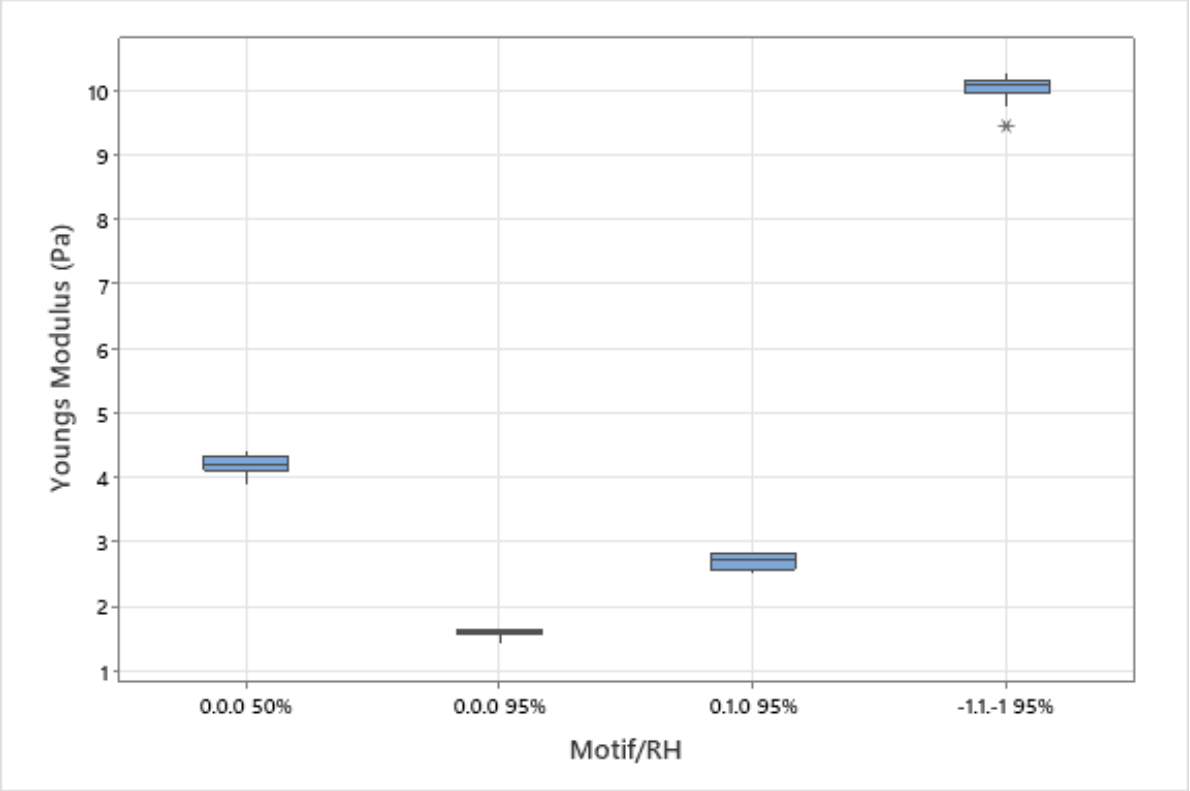

Figure 41 – Offset of thickest hinge @ 95 % RH vs standard motif @ 50 % RH.

Figure 41 shows the how humidity affected the standard element (0.0.0) design where at 95 % relative humidity the stiffness decreased from 4.21 Pa to 1.60 Pa. On the same figure, it also shows the impact of changing various parameters. When increasing the hinge thickness to 2.1 mm at 95 % relative humidity (0.1.0), the stiffness of 2.72 Pa is achieved. The regression model provides an equation that best fits the data (Equation 5). This can be used to infer beyond the tested range the hinge thickness required to maintain the stiffness of the auxetic at 95 % relative humidity compared to the standard auxetic design at 50 % relative humidity.

$$Stiffness\ @\ 95\ \%\ RH = -1.6974 + 2.0921 * \big(Hinge(mm)\big)$$

Equation 5

From the equation, to obtain a target Young's modulus of 4.21 Pa, the hinge will need to be 2.82 mm thick. This does, however, extrapolate beyond the measured data so there would be changes in the actual response.

Additionally, the radius or scale of the elements could be changed to obtain a similar stiffness without needing to change the hinge thickness as much. Data obtained in 4.4.1, where the highest Young's modulus observed by element design -1.1.-1, the Young's modulus was observed to be 17.70 Pa at 50 % relative humidity. The maximum percentage decrease calculated using data obtained from 4.4.2, the speculated stiffness of that particular design was calculated to be 10.02 Pa for 95 % relative humidity. This shows the influence of auxetic element parameter changes on the properties of the material and that the impacts of high humidity on the material can be counteracted by simple design optimisations. However, a full factorial of the variations different relative humidities should be completed to provide a more complete analysis of the interactions between each change.

5.4: Conclusions

This study looked to show the effect of parameter and humidity changes on the kōwhaiwhai auxetic design to provide a foundation of understanding to make decisions on improving the design for use in specific humid environments within the supply chain.

The analysis of the impact of key parameters on the auxetic material's tensile properties reveals significant influences of motif scale, hinge thickness, and radius on Young's Modulus. The regression model underscores hinge thickness as the most critical factor contributing to material stiffness, while scale and radius exhibit inverse relationships with Young's Modulus. The observed trends align with previous studies on auxetic behaviour, highlighting the interplay between material design and mechanical performance. The model identified that some of the parameters show non-linearity but was beyond the scope of the paper.

The Poisson's ratio analysis reveals that while the measurement is subject to higher variance due to image analysis error, meaningful trends can still be observed. The scale of the elements emerges as the most influential parameter, with a strong inverse relationship, accounting for nearly a third of the model's variation. The scales influence highlights the effect microstructural impact versus the geometric impact of the auxetic, particularly at smaller scales where microstructural stiffness plays a greater role due to

fibre quality of the material used. The hinge also has a notable impact, contributing to a less negative Poisson's ratio as it increases. Conversely, the radius is found to have no significant influence, likely due to its limited impact on element geometry. The residual plots confirm the appropriateness of the regression model, providing confidence in these conclusions despite the inherent variability.

The impact of relative humidity on Young's Modulus reveals a significant non-linear relationship for both corrugated board and solid board auxetics, with high model fit values. Through experimental work that attempted to differentiate between impact of relative humidity on the material versus the auxetic itself analysis shows this difference to be insignificant, although there is a slight trend that the auxetic may be impacted slightly more, possibly due to the increased negative space and strain concentration at hinges, which may slightly amplify environmental effects. However, the overall similarity in stiffness changes implies that the auxetic is not affected by environmental affects due to its geometry but purely based on the material at which the auxetic inhabits.

The effect of relative humidity on the Poisson's ratio indicates no significant change. The consistency of the regression model and residual plots further supports this finding. This result aligns with the expectation that while increased humidity weakens the material's overall strength, the uniform distribution of moisture ensures that the ratio of expansion to contraction remains constant, maintaining a stable Poisson's ratio.

As a final example of the benefits of the auxetic design in this chapter, it was shown and discussed how despite substantial decrease in material stiffness at high operating humidities, often found in the packaging supply chain, the auxetic can be adapted to maintain the structural integrity. The section demonstrates that the significant reduction in stiffness of fibre-based auxetics under high humidity can be mitigated through parameter adjustments. Hinge thickness, as the most influential factor, plays a pivotal role in increasing stiffness, thus, increasing this parameter (and possibly a combination of all three parameters) for the auxetic at 95% relative humidity could effectively restore stiffness to levels observed at 50% RH for the standard design. The predictive equation derived provides an insight into optimising hinge thickness and other parameters to counteract humidity-induced losses in structural integrity but does not serve as a direct conclusion as the data is extrapolated beyond its observed limits.

Adjustments to other parameters, such as the radius or scale, offer additional pathways to achieve comparable stiffness without exclusively relying on hinge modifications. For instance, a high-performance design like -1.1.-1 shows significant potential. Although not explored at high humidity, it shows the extent of improvement of how small changes in parameters can interact to provide greatly increased stiffness at 50 % relative humidity and possibly to counteract the decrease in stiffness observed at 95 % RH. These findings show versatility of auxetic designs, enabling them to withstand environmental challenges in supply chain conditions. However, a more comprehensive analysis with out-of-plane forces across varying humidities and parameter combinations is recommended to fully understand the interactions and optimise performance further for packaging materials.

Chapter 6: Conclusions

This research set out to develop an understanding of the novel kōwhaiwhai auxetic design, with tuneable parameters, on corrugated board and solid fibreboard materials. The material is designed to improve shock absorption of fibre-based packaging. In a similar way of drawing inspiration from ancient geometric motifs in other studies, this auxetic drew inspiration from traditional Māori art forms, which is ubiquitous with Aotearoa's graphic identity. Experimental and numerical analyses were combined to characterise the geometric and mechanical properties of this auxetic structure, providing a foundational understanding that can inform future optimisation efforts. The key findings from each chapter have contributed to the broader objective of evaluating the feasibility of auxetics in sustainable packaging applications.

The first stage of this research focused on characterising the Poisson's ratio of the auxetic structure experimentally. The work evaluated the importance of measurement regions and tensile specimen size on the Poisson's ratio value calculated and discussed the discrepancy between methods used in literature and thus, the uncertainty of reported Poisson's ratio values in literature. It was shown how the selected measurement region used to calculate the Poisson's ratio could vary greatly. Regions on the edge of the specimen that are restrained by the top and bottom edges of the tensile specimen increased (less negative) the Poisson's ratio as these restricted the full auxetic element movement. Elongation in the lateral direction was shown to be greatest at the centre of the specimen, causing measurement regions that incorporate an uneven number of motif's in either the lateral or longitudinal direction to affect the apparent Poisson's ratio. This study also demonstrated the interaction of the auxetic geometry in a fibre-based material. The work showed how board orientation does not significantly influence the auxetic response due to stress distribution across the hinges rather than specific locations of corrugation. Furthermore, the Poisson's ratio was observed to remain relatively stable within the auxetic elastic range, despite variations due to measurement region selection. Overall, the study highlighted the importance of standardising measurement methods for characterising the Poisson's ratio of auxetics while also providing and understanding for how auxetics behave cut into fibre-based materials.

Chapter 4 developed a finite element model to simulate the tensile behaviour of the auxetic structure. The model predicted the Poisson's ratio well for most of the measurement regions and tensile grid sizes with a maximum error for the 6x10 grid across all measurement regions of 20.6 % and 3.8 % for the 3x5 grid. The stress distribution patterns showed slightly higher stresses across the auxetics hinges near the edges of the specimen compared to the hinges near the centre. There were not enough data points to make any clear conclusions when comparing fracture points from the experimental work done in chapter 3, but they appeared to match the fracture pattern well from what was shown. Overall, the model provided a robust foundation for exploring parameter changes and optimising the design for packaging applications. This modelling approach can be further refined in future work to enhance predictive accuracy and explore additional design variations.

Chapter 5 addressed the impact of humidity and parameter changes on the performance of the fibre-based auxetic. Humidity, as expected, had a large impact on the stiffness, but the addition of the auxetic was not shown to have any more of an impact than typical fibre-based materials. Key parameters such as hinge thickness, motif scale, and radius were found to influence the material's mechanical properties, with hinge thickness being the most critical factor. The findings suggest that parameter adjustments, particularly increasing hinge thickness, could restore stiffness in high-humidity environments, making the auxetic structure viable for use in diverse supply chain conditions.

Overall, this thesis has established a fundamental understanding of the kōwhaiwhai auxetic structure and its potential as a novel packaging solution. The understanding of the auxetic properties will allow for further exploration of the specific use cases of the auxetic design, out-of-plane impact resistance, industrial manufacturing, and performance specific optimisation.

Furthermore, there is areas for further investigation to gain more understanding of the auxetic design as well as to show its efficacy as a packaging solution. The work completed in this thesis highlights the in-plane effects of the auxetic and the impact the geometric design has on the material it is cut into. However, this could be expanded upon with out-of-plane experiments and numerical models to fully show the shock absorbing ability of the auxetic material. This can be investigated using dynamic compression

testing methods such as drop tests and cyclic compression as well as the creep response of the material to show its effect under sustained stresses. These areas for further study will be necessary for showing the efficacy of the material as a packaging material.

Understanding the best manufacturing processes for these materials when used in paper materials also needs to be explored. Manufacturing auxetics from sheets of corrugated board lead to high percentage of waste and if to be done using laser cutting would introduce carcinogens and burn marks onto the surface of the goods that are packaged by the auxetics. More avenues need to be explored for these reasons if paper-based materials are used to make auxetic materials.

References:

Aboura, Z., Talbi, N., Allaoui, S., & Benzeggagh, M. (2003). Elastic behavior of corrugated cardboard: experiments and modeling. *Composite Structures*, *63*(1), 53–62. https://doi.org/10.1016/s0263-8223(03)00131-4

Alomarah, A., Masood, S. H., & Ruan, D. (2020). Out-of-plane and in-plane compression of additively manufactured auxetic structures. *Aerospace Science and Technology*, *106*, 106107. https://doi.org/10.1016/j.ast.2020.106107

Allaoui, S., Aboura, Z., & Benzeggagh, M. (2008). Phenomena governing uni-axial tensile behaviour of paperboard and corrugated cardboard. *Composite Structures*, *87*(1), 80–92. https://doi.org/10.1016/j.compstruct.2008.01.001

American Society for Testing and Materials. (2016). *Standard Test Method for Determining Poisson's Ratio of Honeycomb Cores* (ASTM D6790/D6790M – 16) https://www.astm.org/d6790_d6790m-16.html

Attard, D., & Grima, J. N. (2008). Auxetic behaviour from rotating rhombi. *Physica Status Solidi (B)*, *245*(11), 2395–2404. https://doi.org/10.1002/pssb.200880269

Attard, D., Calleja, D., & Grima, J. N. (2018). Out-of-plane doming behaviour from constrained auxetics. Smart Materials and Structures, 27(1), 015020. https://doi.org/10.1088/1361-665x/aa9e62

Balan, M. P., Mertens, J. A., & Bahubalendruni, M. V. a. R. (2022). Auxetic mechanical metamaterials and their futuristic developments: A state-of-art review. *Materials Today Communications*, *34*, 105285. https://doi.org/10.1016/j.mtcomm.2022.105285

Business Waste. (2024, February 9). *Cardboard Waste Facts and Statistics | Business waste*. https://www.businesswaste.co.uk/your-waste/cardboard-recycling/cardboard-waste-facts-and-statistics/#:~:text=The%20world%20produces%20more%20than,shipped%20in%20cardboard%20packaging%20materials

Büyüksarı, Ü., Hiziroglu, S., Akkılıç, H., & Ayrılmış, N. (2011). Mechanical and physical properties of medium density fiberboard panels laminated with thermally compressed veneer. *Composites Part B Engineering*, *43*(2), 110–114. https://doi.org/10.1016/j.compositesb.2011.11.040

Carson, F. T. (1944). Effect of humidity on physical properties of paper. *Journal of the Franklin Institute*, *237*(6), 470. https://doi.org/10.1016/s0016-0032(44)90377-7

Chang, Y., & Ma, P. (2018). Energy absorption and Poisson's ratio of warp-knitted spacer fabrics under uniaxial tension. *Textile Research Journal*, *89*(6), 903–913. https://doi.org/10.1177/0040517518758005

Charmant, J., & contributors. (2024) Kinovea (Version 2023.1.2) [Computer software]. https://www.kinovea.org

Chen, T., Panetta, J., Schnaubelt, M., & Pauly, M. (2021). Bistable auxetic surface structures. *ACM Transactions on Graphics*, *40*(4), 1–9. https://doi.org/10.1145/3450626.3459940

Cheng, X. W., Zhang, Y., Ren, X., Han, D. S., Jiang, W., Zhang, X., Luo, H. Y., & Xie, Y. (2022). Design and mechanical characteristics of auxetic metamaterial with tunable stiffness. *International Journal of Mechanical Sciences*, *223*, 107286. https://doi.org/10.1016/j.ijmecsci.2022.107286

Coffin, D. W. (2009). Developing a Deeper Understanding of the Constitutive Behavior of Paper. *Advances in Pulp and Paper Research*. https://doi.org/10.15376/frc.2009.2.841

De Ruvo, A., Lundberg, R., Martin-Löf, S., & Söremark, C. (1973). Influence of Temperature and Humidity on the Elastic and Expansional Properties of Paper and the Constituent Fibre. *Fundamental Properties of Paper Related to Its Uses*. https://doi.org/10.15376/frc.1973.2.785

Fadiji, T., Berry, T., Coetzee, C. J., & Opara, L. (2017). Investigating the mechanical properties of paperboard packaging material for handling fresh produce under different environmental conditions: experimental analysis and finite element modelling. *Journal of Applied Packaging Research*, *9*(2), 3. https://paperity.org/p/83756327/investigating-the-mechanical-properties-of-paperboard-packaging-material-for-handling

Fibre Box Association (1999). The Fiber Box Handbook. Chicago, IL. Baum, G. A., Habeger Jr, C. C., & Fleischman Jr, E. H. (1982). Measurement of the orthotropic elastic constants of paper. The Institute of Paper Chemistry, Wisconsin, USA.

Garbowski, T. (2025). Review on Numerical Homogenization of Corrugated Materials. State-of-the-art in Modelling of Corrugated Board. BioResources, 20(2).

Gaspar, N., Ren, X., Smith, C., Grima, J., & Evans, K. (2005). Novel honeycombs with auxetic behaviour. *Acta Materialia*, *53*(8), 2439–2445. https://doi.org/10.1016/j.actamat.2005.02.006

Gatt, R., Wood, M. V., Gatt, A., Zarb, F., Formosa, C., Azzopardi, K. M., Casha, A., Agius, T. P., Schembri-Wismayer, P., Attard, L., Chockalingam, N., & Grima, J. N. (2015). Negative Poisson's ratios in tendons: An unexpected mechanical response. *Acta Biomaterialia*, *24*, 201–208. https://doi.org/10.1016/j.actbio.2015.06.018

Gatt, R., Mizzi, L., Azzopardi, J. I., Azzopardi, K. M., Attard, D., Casha, A., Briffa, J., & Grima, J. N. (2015). Hierarchical auxetic mechanical metamaterials. *Scientific Reports*, *5*(1). https://doi.org/10.1038/srep08395

Grima, J. N., & Evans, K. E. (2000). Auxetic behavior from rotating squares. *Journal of Materials Science Letters*, *19*(17), 1563–1565. https://doi.org/10.1023/a:1006781224002

Grima, J. N., Alderson, A., & Evans, K. E. (2004). NEGATIVE POISSON'S RATIOS FROM ROTATING RECTANGLES. *Computational Methods in Science and Technology*, *10*(2), 137–145. https://doi.org/10.12921/cmst.2004.10.02.137-145

Grima, J. N., Alderson, A., & Evans, K. E. (2005). Auxetic behaviour from rotating rigid units. *Physica Status Solidi (B)*, *242*(3), 561–575. https://doi.org/10.1002/pssb.200460376

Grima, J. N., Gatt, R., Alderson, A., & Evans, K. E. (2005). On the potential of connected stars as auxetic systems. *Molecular Simulation*, *31*(13), 925–935. https://doi.org/10.1080/08927020500401139

Grima, J. N., & Evans, K. E. (2006). Auxetic behavior from rotating triangles. *Journal of Materials Science*, *41*(10), 3193–3196. https://doi.org/10.1007/s10853-006-6339-8

Grima, J. N., Zammit, V., Gatt, R., Alderson, A., & Evans, K. E. (2007). Auxetic behaviour from rotating semi-rigid units. *Physica Status Solidi (B)*, *244*(3), 866–882. https://doi.org/10.1002/pssb.200572706

Groufsky, J. (2019). A Local Motif; Use of kōwhaiwhai patterns in printed textiles. *Textile Society of America Symposium Proceedings*. https://doi.org/10.32873/unl.dc.tsasp.0030

Gu, L., Xu, Q., Zheng, D., Zou, H., Liu, Z., & Du, Z. (2020). Analysis of the mechanical properties of double arrowhead auxetic metamaterials under tension. *Textile Research Journal*, *90*(21–22), 2411–2427. https://doi.org/10.1177/0040517520924850

Hamilton, A. (1896). *Maori Art*. Fergusson & Mitchell, Printers and Manufacturing Stationers.

Hengsbach, S., & Lantada, A. D. (2014). Direct laser writing of auxetic structures: present capabilities and challenges. *Smart Materials and Structures*, *23*(8), 085033. https://doi.org/10.1088/0964-1726/23/8/085033

International Organisation for Standardisation. (2008). *Paper and board — Determination of tensile properties* (ISO standard No. 1924.2-2008). *Retrieved from https://www.iso.org/standard/41397.html#:~:text=41397-,ISO%201924%2D2%3A2008%20Paper%20and%20board%20%E2%80%94%20Determination%20of,method%20(20%20mm%2Fmin)&text=This%20publication%20was%20last%20reviewed,Therefore%20this%20version%20remains%20current.*

Jamsari, A. (2020). *The role of flute morphology in mechanical behaviour of corrugated fibreboard : a numerical, analytical and empirical study : a thesis presented in partial*

fulfilment of the requirements for the degree of Doctor of Philosophy in Engineering at Massey University, Palmerston North, New Zealand. https://mro.massey.ac.nz/handle/10179/16435

Khare, E., Temple, S., Tomov, I., Zhang, F., & Smoukov, S. K. (2018). Low fatigue dynamic Auxetic lattices with 3D printable, multistable, and tuneable unit cells. *Frontiers in Materials*, *5*. https://doi.org/10.3389/fmats.2018.00045

Kline, J. E. (1991). Paper and paperboard: manufacturing and converting fundamentals. Backbeat Books

Kueh, Celia Swee Li. Modelling buckling and post-buckling behaviours of corrugated paperboard structures. Diss. University of Waikato, 2012.

Lees, C., Vincent, J. F. V., & Hillerton, J. E. (1991). Poisson's ratio in skin. *Bio-Medical Materials and Engineering*, *1*(1), 19–23. https://doi.org/10.3233/bme-1991-1104

Li, X., Wang, Q., Yang, Z., & Lu, Z. (2019). Novel auxetic structures with enhanced mechanical properties. *Extreme Mechanics Letters*, *27*, 59–65. https://doi.org/10.1016/j.eml.2019.01.002

Liu, Y., & Hu, H. (2010). A review on auxetic structures and polymeric materials. *Scientific Research and Essays Vol. 5*. https://doi.org/10.5897/SRE

Lvov, V. A., Senatov, F. S., Veveris, A. A., Skrybykina, V. A., & Lantada, A. D. (2022). Auxetic Metamaterials for Biomedical Devices: Current Situation, Main Challenges, and Research Trends. *Materials*, *15*(4), 1439. https://doi.org/10.3390/ma15041439

Ma, H., Wang, K., Zhao, H., Hong, Y., Zhou, Y., Xue, J., Li, Q., Wang, G., & Yan, B. (2022). Energy dissipation in multistable auxetic mechanical metamaterials. *Composite Structures*, *304*, 116410. https://doi.org/10.1016/j.compstruct.2022.116410

Meena, K., & Singamneni, S. (2019). A new auxetic structure with significantly reduced stress concentration effects. *Materials & Design*, *173*, 107779. https://doi.org/10.1016/j.matdes.2019.107779

Minitab, LLC. (2021). *Minitab*. Retrieved from https://www.minitab.com

Mizzi, L., Azzopardi, K. M., Attard, D., Grima, J. N., & Gatt, R. (2015). Auxetic metamaterials exhibiting giant negative Poisson's ratios. *Physica Status Solidi (RRL) - Rapid Research Letters*, *9*(7), 425–430. https://doi.org/10.1002/pssr.201510178

Neich, R. (1993). *Painted Histories : Early Māori figurative painting*. https://natlib.govt.nz/records/21961536

Onwude, D. I., Chen, G., Eke-Emezie, N., Kabutey, A., Khaled, A. Y., & Sturm, B. (2020). Recent advances in reducing food losses in the supply chain of fresh agricultural produce. *Processes*, *8*(11), 1431. https://doi.org/10.3390/pr8111431

Ostlund, R. . “Mechanics of Paper Products”. 2nd ed. Pp. 33-34.

Rafsanjani, A., & Pasini, D. (2016). Bistable auxetic mechanical metamaterials inspired by ancient geometric motifs. *Extreme Mechanics Letters*, *9*, 291–296. https://doi.org/10.1016/j.eml.2016.09.001

Razbin, M., Jeddi, A. a. A., Semnani, D., & Ramzanpoor, M. (2021). A generalized method of measuring the Poisson’s ratio of warp knitted fabrics under uniaxial loading based on image processing technique. *Journal of the Textile Institute*, *113*(1), 70–79. https://doi.org/10.1080/00405000.2020.1863568

Rhim, J. (2010). Effect of moisture content on tensile properties of paper-based food packaging materials. *Food Science and Biotechnology*, *19*(1), 243–247. https://doi.org/10.1007/s10068-010-0034-x

Saxena, K., Das, R., & Calius, E. P. (2016). Three Decades of Auxetics Research – Materials with Negative Poisson’s Ratio: A Review. *Advanced Engineering Materials*, *18*(11), 1847–1870. https://doi.org/10.1002/adem.201600053

Schönwälder, J., & Rots, J. (2008). Mechanical Behaviour of Cardboard in Construction. *Cardboard in Architecture*, 131–146. https://doi.org/10.3233/978-1-58603-820-5-131

Shah, I. A., Khan, R., Koloor, S. S. R., Petrů, M., Badshah, S., Ahmad, S., & Amjad, M. (2022). Finite element analysis of the ballistic impact on Auxetic sandwich composite human body armor. *Materials*, *15*(6), 2064. https://doi.org/10.3390/ma15062064

Spadoni, A. (2011). An isotropic auxetic structural network with limited shear stiffness. *Volume 8: Mechanics of Solids, Structures and Fluids; Vibration, Acoustics and Wave Propagation*, 179–187. https://doi.org/10.1115/imece2011-64254

Spadoni, A., & Ruzzene, M. (2011). Elasto-static micropolar behavior of a chiral auxetic lattice. *Journal of the Mechanics and Physics of Solids*, *60*(1), 156–171. https://doi.org/10.1016/j.jmps.2011.09.012

Strömberg, F. (2016). Humidity’s effect on strength and stiffness of containerboard materials : A study in how the relative humidity in the ambient air affects the tensile and compression properties in linerboard and fluting mediums. *Karlstad University*. http://www.diva-portal.org/smash/record.jsf?pid=diva2:942509

Technical Association of the Pulp and Paper Industry. (2021). *Standard conditioning and testing atmospheres for paper, board, pulp handsheets, and related products* (TAPPI T402 sp-21) https://imisrise.tappi.org/TAPPI/Products/01/T/0104T402.aspx

Technical Association of the Pulp and Paper Industry. (2022a) *Sampling and accepting a single lot of paper, paperboard, containerboard, or related product* (TAPPI T400 sp-22) https://imisrise.tappi.org/TAPPI/Products/01/T/0104T400.aspx

Technical Association of the Pulp and Paper Industry. (2022b). *Tensile Properties of Paper and Paperboard (using constant rate of elongation apparatus)* (TAPPI T494 om-22) https://imisrise.tappi.org/TAPPI/Products/01/T/0104T494.aspx

Uzun, M. (2012). Mechanical Properties of Auxetic and Conventional Polypropylene Random Short Fibre Reinforced Composites. *Fibres & Textiles in Eastern Europe*. http://fibtex.lodz.pl/2012/5/70.pdf

Veronda, & Westmann, R. (1970). Mechanical characterization of skin—Finite deformations. *Journal of Biomechanics*, *3*(1), 111–124. https://doi.org/10.1016/0021-9290(70)90055-2

Wang, H., Lu, Z., Yang, Z., & Li, X. (2018). A novel re-entrant auxetic honeycomb with enhanced in-plane impact resistance. *Composite Structures*, *208*, 758–770. https://doi.org/10.1016/j.compstruct.2018.10.024

Wang, Z., Luan, C., Liao, G., Liu, J., Yao, X., & Fu, J. (2020). Progress in Auxetic mechanical metamaterials: structures, characteristics, manufacturing methods, and applications. *Advanced Engineering Materials*, *22*(10). https://doi.org/10.1002/adem.202000312

Wang, Z., Poh, L. H., Zhu, Y., Dirrenberger, J., & Forest, S. (2019). Systematic design of tetra-petals auxetic structures with stiffness constraint. *Materials & Design*, *170*, 107669. https://doi.org/10.1016/j.matdes.2019.107669

Wang, Z., Hu, H., & Xiao, X. (2014). Deformation behaviors of three-dimensional auxetic spacer fabrics. *Textile Research Journal*, *84*(13), 1361–1372. https://doi.org/10.1177/0040517514521120

Wang, H., Zhang, Y., Lin, W., & Qin, Q. (2019). A novel two-dimensional mechanical metamaterial with negative Poisson's ratio. *Computational Materials Science*, *171*, 109232. https://doi.org/10.1016/j.commatsci.2019.109232

Wang, M., Wu, H., Yang, L., Chen, A., Chen, P., Wang, H., Chen, Z., & Yan, C. (2022). Structure design of arc-shaped auxetic metamaterials with tunable Poisson's ratio. *Mechanics of Advanced Materials and Structures*, *30*(7), 1426–1436. https://doi.org/10.1080/15376494.2022.2033890

Yolcu, D. A., & Baba, B. O. (2022). Measurement of Poisson's ratio of the auxetic structure. *Measurement*, *204*, 112040. https://doi.org/10.1016/j.measurement.2022.112040

Zhang, J., Lu, S., Yang, Y., Liu, Y., Guo, Y., & Wang, H. (2024). Efficacy of auxetic lattice structured shoe sole in advancing footwear comfort—From the perspective of plantar pressure and contact area. *Frontiers in Public Health*, *12*. https://doi.org/10.3389/fpubh.2024.1412518

Zhang, J., Lu, S., Lin, Y., Wang, Y., Yi, X., & Fang, W. (2024). Pressure-Reducing design of 3D-Printed diabetic shoe midsole utilizing auxetic lattice structure. *Applied Sciences*, *14*(12), 5291. https://doi.org/10.3390/app14125291

Zulifqar, A., Hua, T., & Hu, H. (2017). Development of uni-stretch woven fabrics with zero and negative Poisson's ratio. *Textile Research Journal*, *88*(18), 2076–2092. https://doi.org/10.1177/0040517517715095

Appendices

Appendix A - Chapter 3:

MD vs CD of all tested specimen in Chapter 3:

Figure A1: All 3x5 tensile grid specimens tested. Machine-direction in blue and cross-direction in orange.

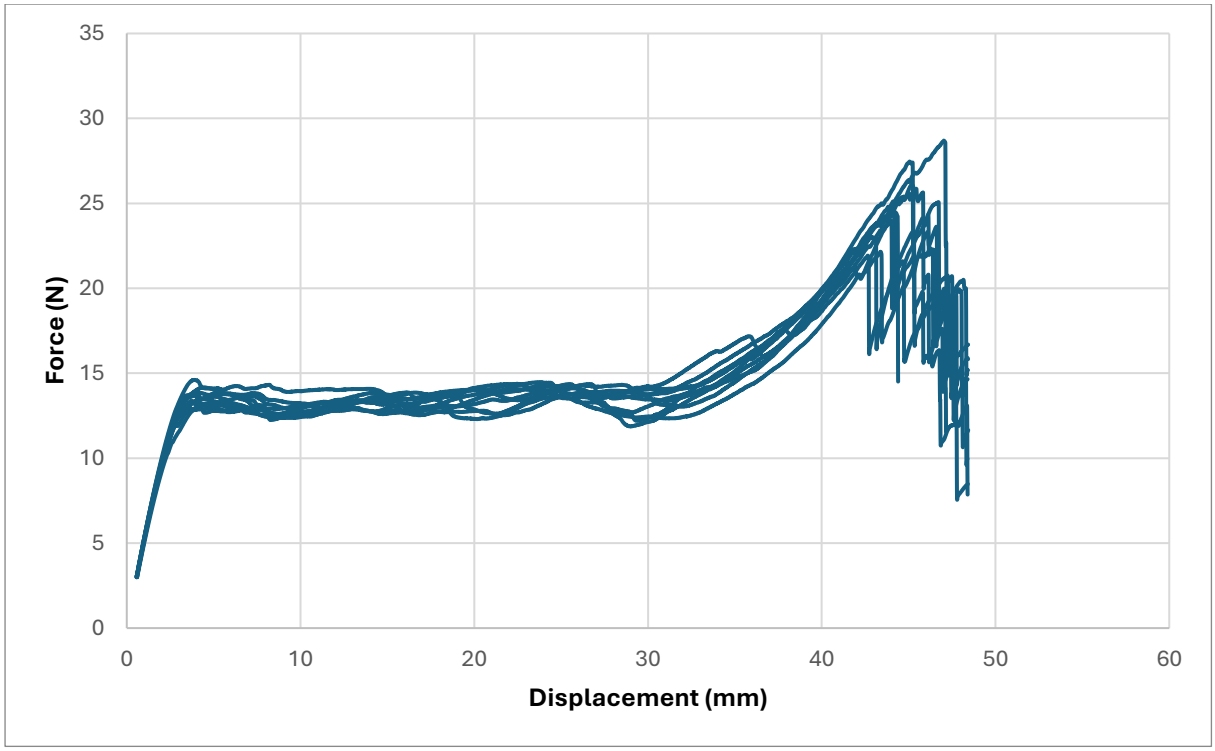

Figure A2: All 4x8 tensile grid specimens tested. Machine-direction in blue and cross-direction in orange.

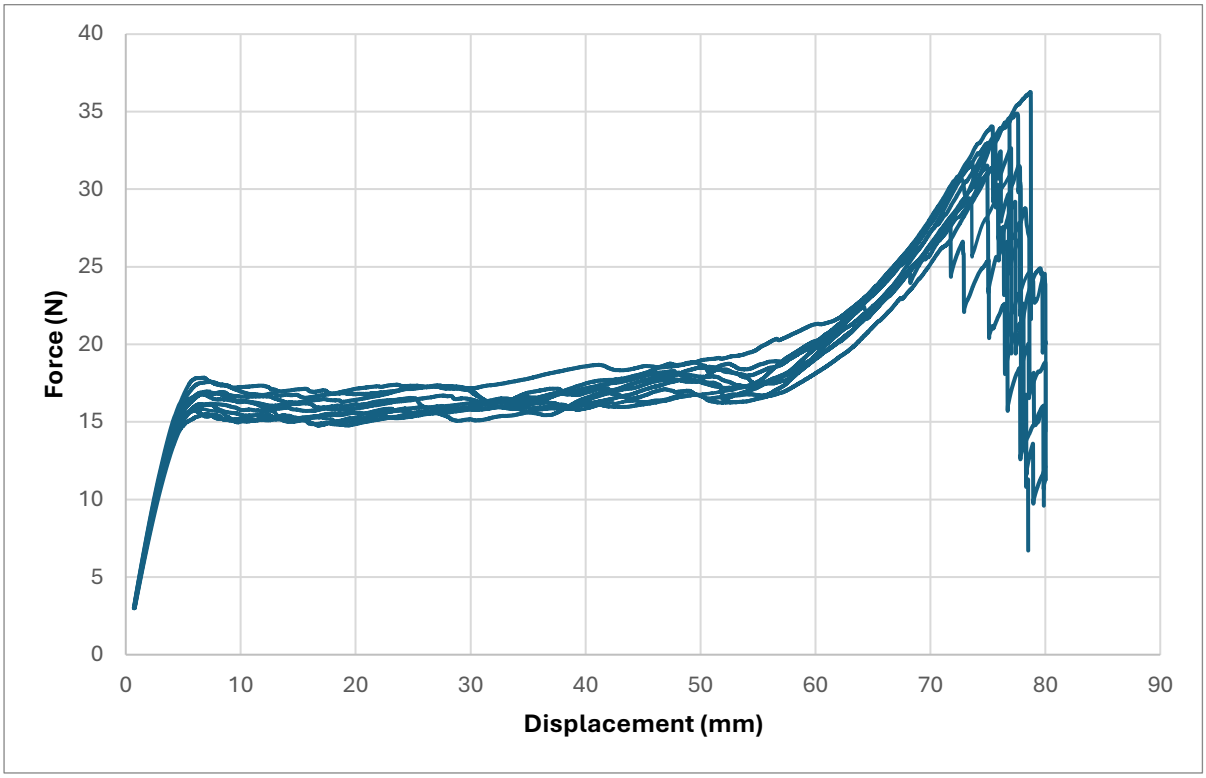

Figure A3: All 6x10 tensile grid specimens tested. Machine-direction in blue and cross-direction in orange.

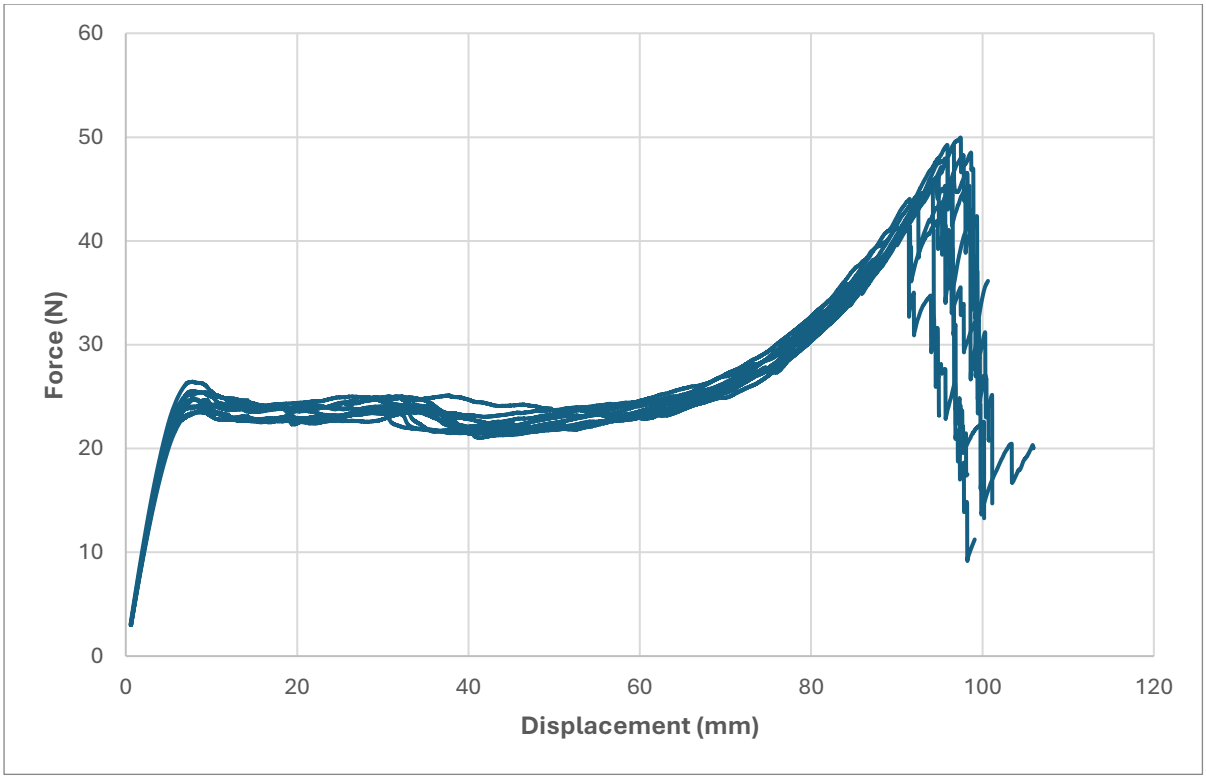

Appendix B – Chapter 5:

Young's modulus with changes in motif parameters:

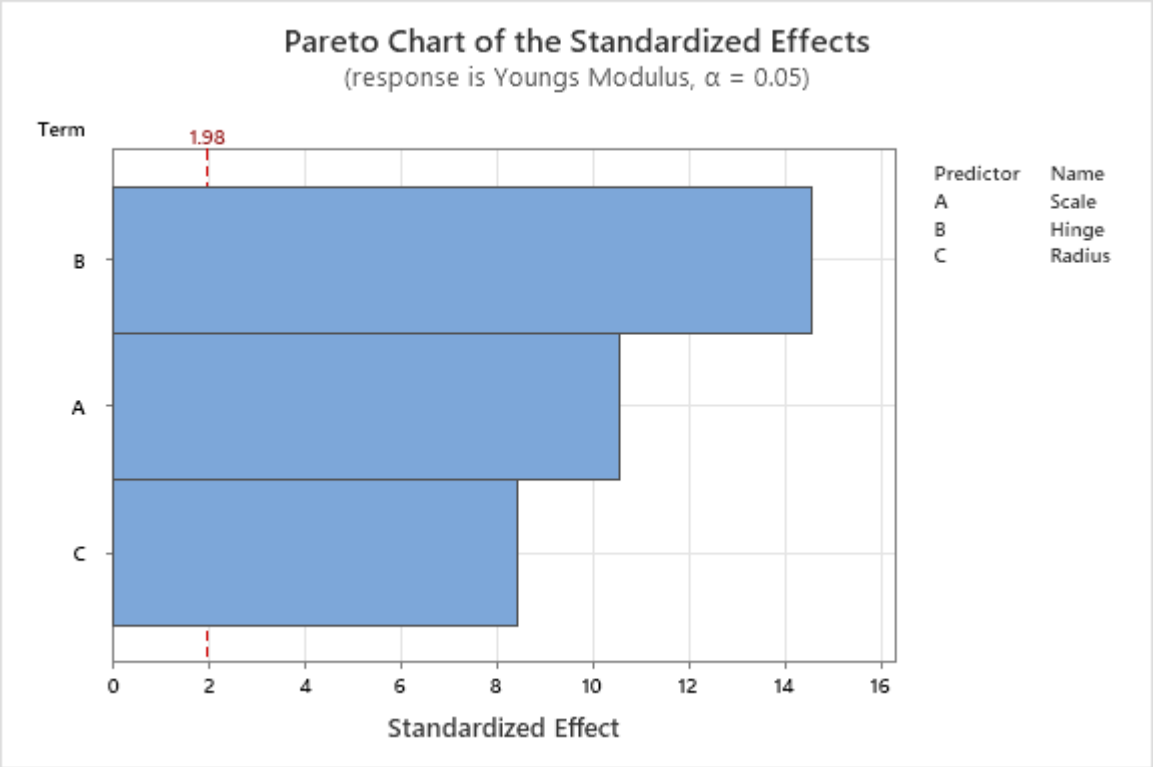

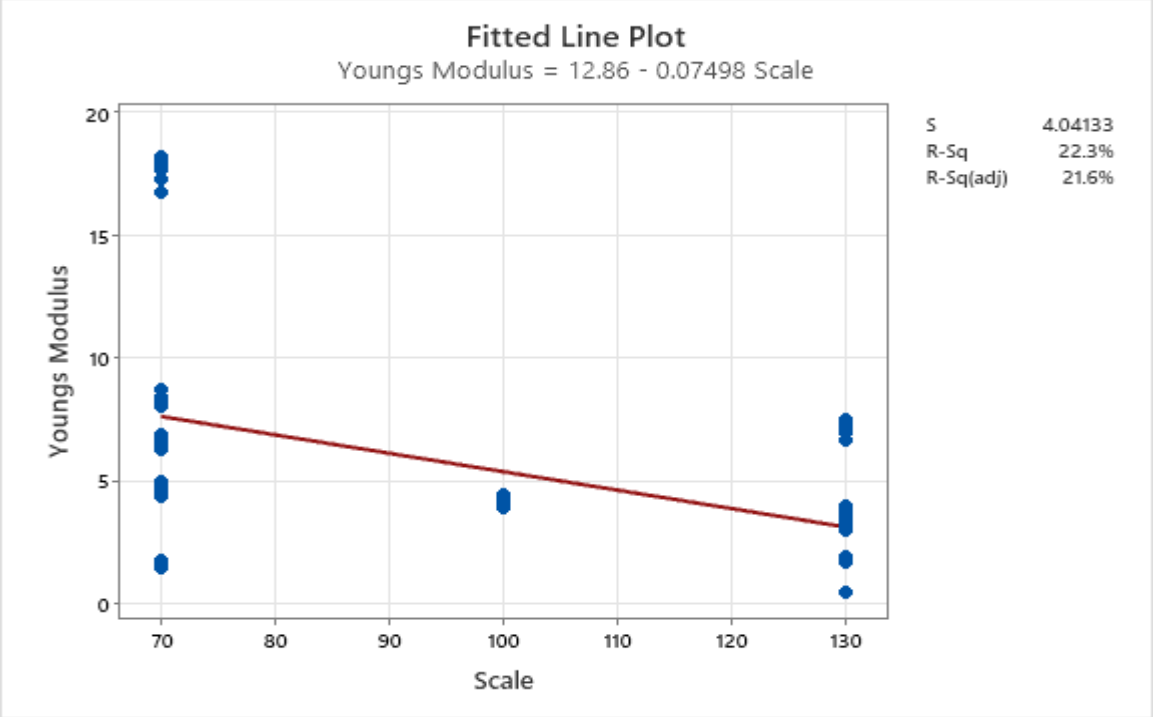


Fitted Line Plot
Youngs Modulus = - 5.731 + 6.932 Hinge
S 3.48129
R-Sq 42.3%
R-Sq(adj) 41.8%
Youngs Modulus
Hinge
0
5
10
15
20
1.0
1.2
1.4
1.6
1.8
2.0
2.2

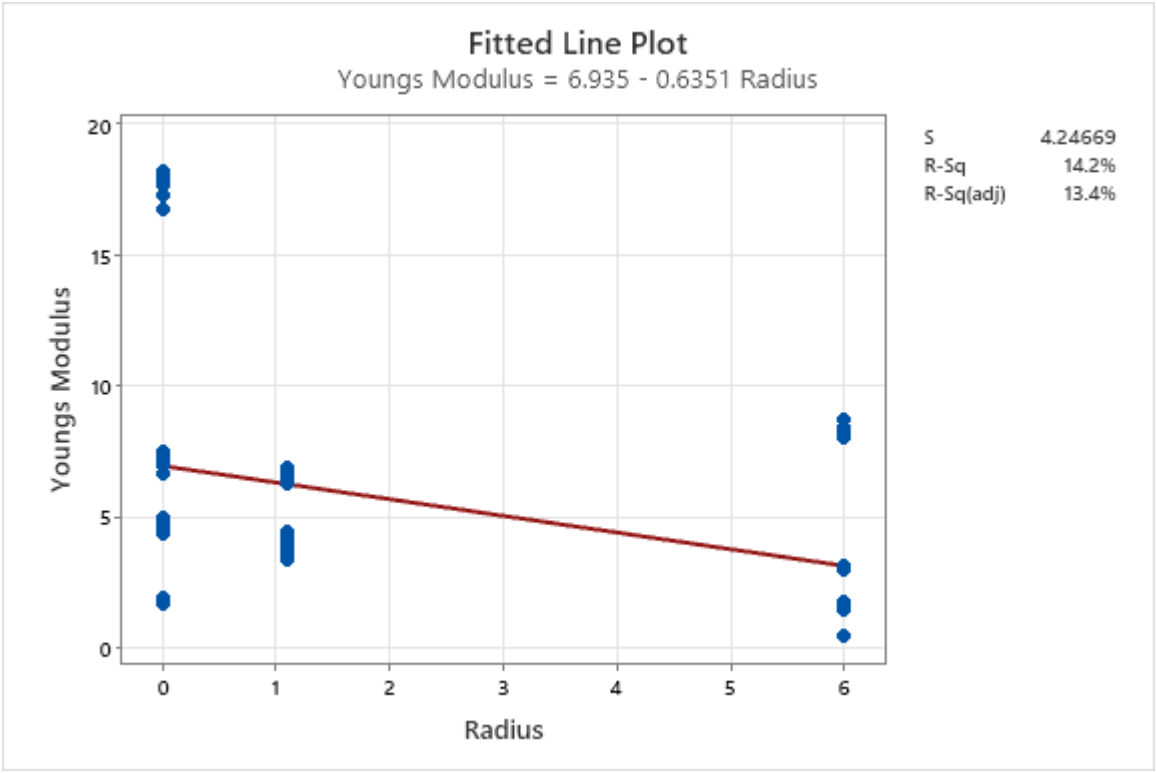
Fitted Line Plot
Youngs Modulus = 6.935 - 0.6351 Radius
S 4.24669
R-Sq 14.2%
R-Sq(adj) 13.4%
Youngs Modulus
Radius
0
5
10
15
20
0
1
2
3
4
5
6

Poisson’s ratio vs motif change:

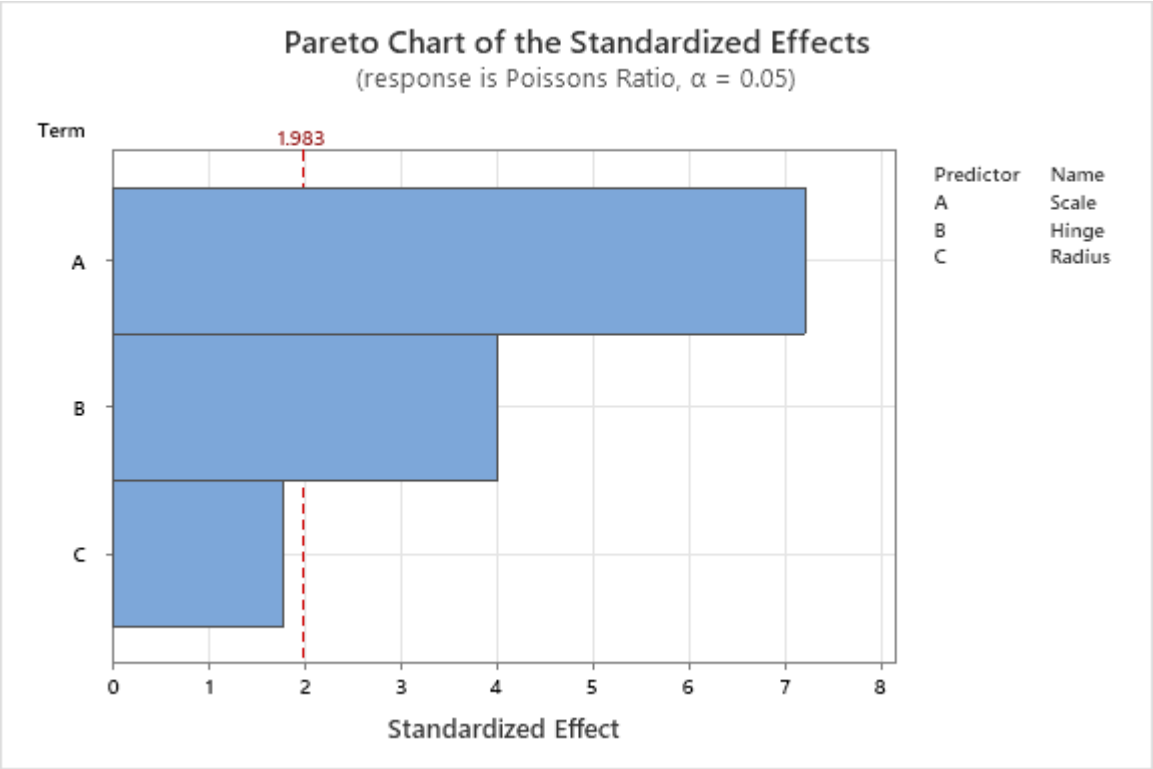

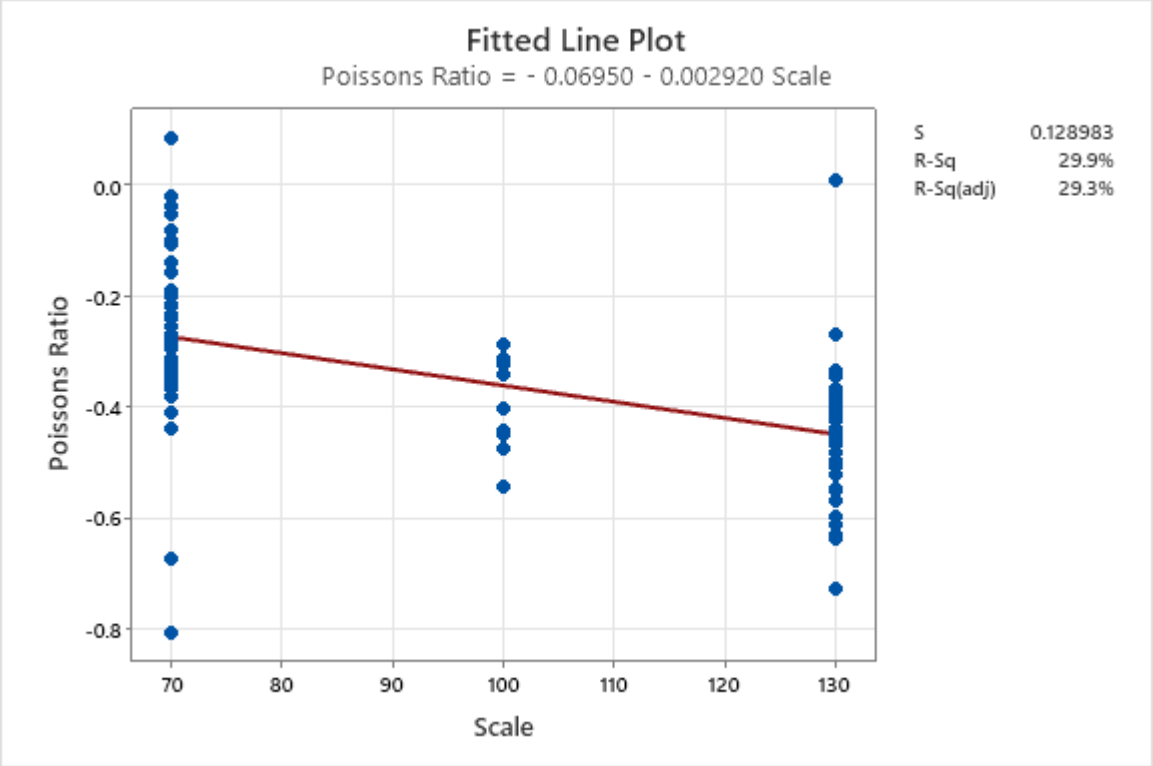

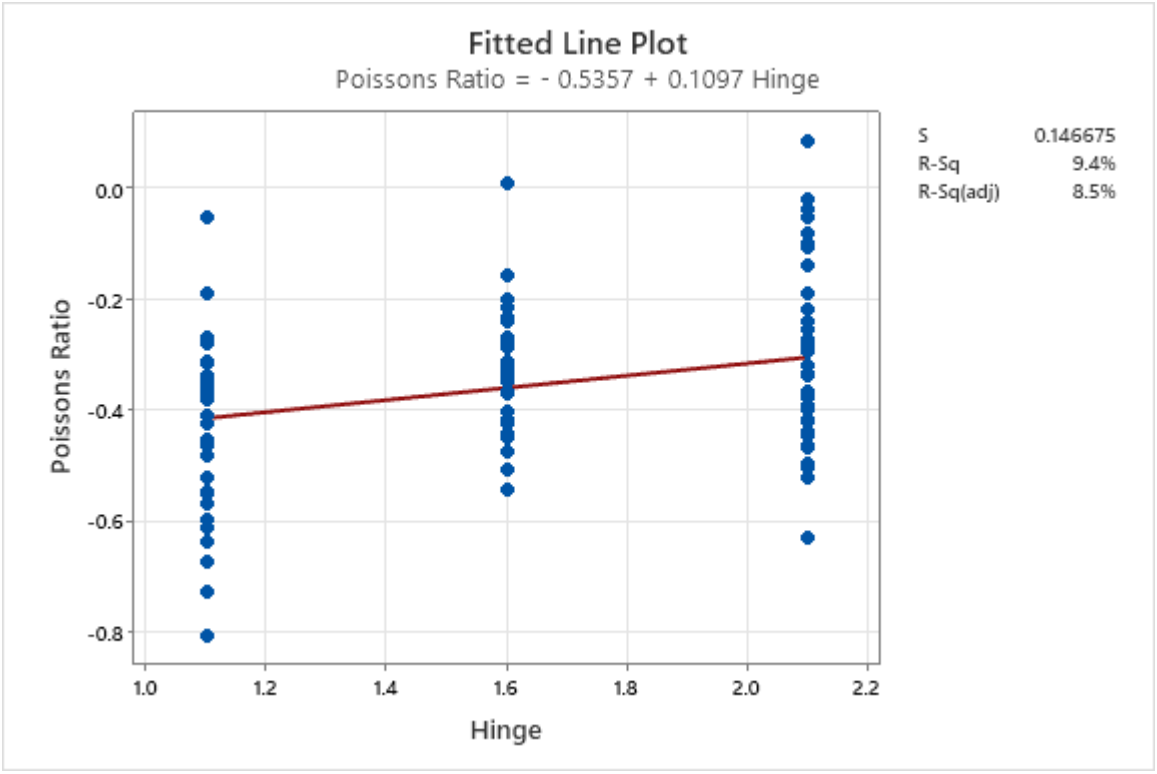
Fitted Line Plot
Poissons Ratio = - 0.5357 + 0.1097 Hinge
S 0.146675
R-Sq 9.4%
R-Sq(adj) 8.5%
Poissons Ratio
0.0
-0.2
-0.4
-0.6
-0.8
1.0
1.2
1.4
1.6
1.8
2.0
2.2
Hinge

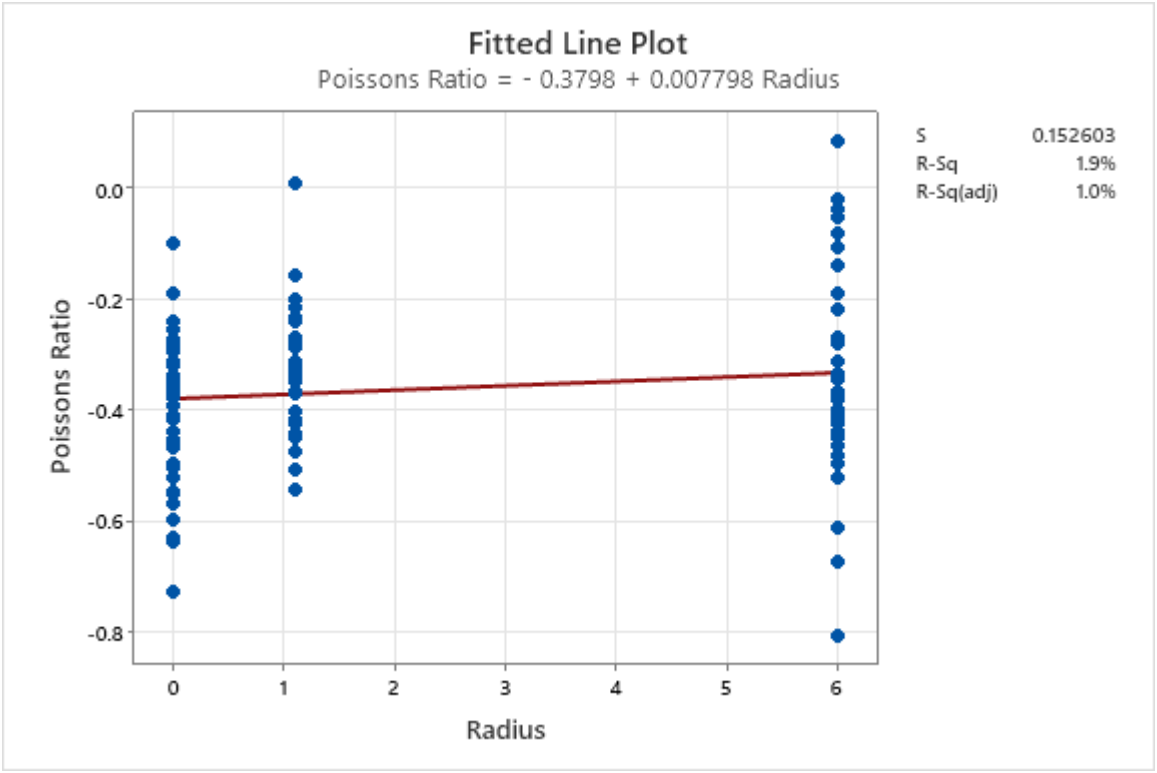
Fitted Line Plot
Poissons Ratio = - 0.3798 + 0.007798 Radius
S 0.152603
R-Sq 1.9%
R-Sq(adj) 1.0%
Poissons Ratio
0.0
-0.2
-0.4
-0.6
-0.8
0
1
2
3
4
5
6
Radius